Investigation of crown wall stability on top of rubble mound structures with OpenFOAM®

Nikolaos Sigalas

Delft University of Technology | Van Oord

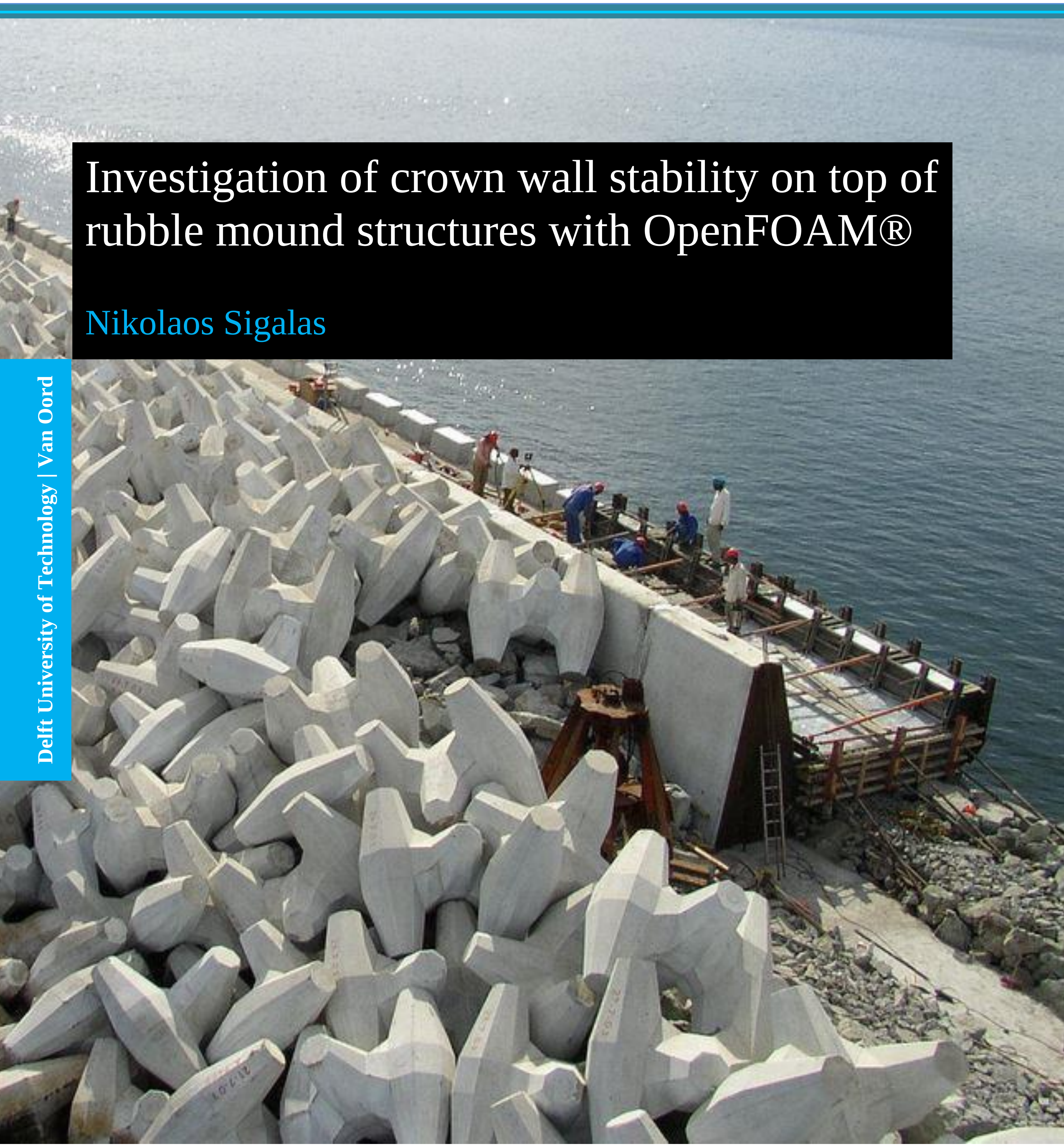

ERASMUS +: ERASMUS MUNDUS MOBILITY PROGRAMME

Master of Science in

COASTAL AND MARINE ENGINEERING AND MANAGEMENT

CoMEM

INVESTIGATION OF CROWN WALL STABILITY ON TOP OF RUBBLE MOUND STRUCTURES WITH OPENFOAM®

Technische Universiteit (TU) Delft
17 July 2019

Sigalas Nikolaos

The Erasmus+: Erasmus Mundus MSc in Coastal and Marine Engineering and Management is an integrated programme including mobility organized by five European partner institutions, coordinated by Norwegian University of Science and Technology (NTNU).

The joint study programme of 120 ECTS credits (two years full-time) has been obtained at two or three of the five CoMEM partner institutions:

- Norges Teknisk- Naturvitenskapelige Universitet (NTNU) Trondheim, Norway
- Technische Universiteit (TU) Delft, The Netherlands
- Universitat Politècnica de Catalunya (UPC). BarcelonaTech. Barcelona, Spain
- University of Southampton, Southampton, Great Britain
- City University London, London, Great Britain

During the first three semesters of the programme, students study at two or three different universities depending on their track of study. In the fourth and final semester an MSc project and thesis has to be completed. The two-year CoMEM programme leads to a multiple set of officially recognized MSc diploma certificates. These will be issued by the universities that have been attended by the student. The transcripts issued with the MSc Diploma Certificate of each university include grades/marks and credits for each subject.

Information regarding the CoMEM programme can be obtained from the programme coordinator:

Øivind A. Arntsen, Dr.ing.
Associate professor in Marine Civil Engineering
Department of Civil and Environmental Engineering
NTNU Norway
Mob.: +4792650455 Fax: + 4773597021
Email: oivind.arntsen@ntnu.no

CoMEM URL: https://www.ntnu.edu/studies/mscomem

CoMEM Thesis

This thesis was completed by:
Sigalas Nikolaos

Under supervision of:

Chairman:	*Dr. Ir. B. Hofland,*	*TU Delft*
Supervision:	*Dr. Ir. A. Antonini,*	*TU Delft*
Supervision:	*Ir. G.M. Smith*	*TU Delft / Van Oord*
Daily Supervision:	*Ir. A. Zoon*	*Van Oord*

As a requirement to attend the degree of
Erasmus+: Erasmus Mundus Master in Coastal and Marine Engineering and Management (CoMEM)

Taught at the following educational institutions:

Norges Teknisk- Naturvitenskapelige Universitet (NTNU)
Trondheim, Norway

Technische Universiteit (TU) Delft
Delft, The Netherlands

University of Southampton,
Southampton, Great Britain

At which the student has studied from August 2017 to July 2019.

In collaboration with:

Keywords: crown wall stability, crown wall loading, uplift pressure, freeboard, time lag, phase lag, numerical modelling, waves2Foam, wave impacts.

Front cover: Crown wall element on Fujairah breakwater under construction. Source: De Graauw, A. 2019. Ancient Port Structures An engineer's perspective. Proceeding of PortusLimen Conference, Rome

Preface

This thesis was written to fulfil the graduation requirements for obtaining my MSc degree in Coastal and Marine Engineering and Management (CoMEM), in the track of Coastal Engineering, at the Technical University of Delft. During this program, three universities were visited, the Norwegian University of Science and Technology (NTNU), Delft University of Technology (TU Delft) and the University of Southampton. The thesis work has been conducted in collaboration between the Technical University of Delft and the Dutch marine contractor Royal Van Oord. I would like to express my gratitude to all those who supported me during the demanding process of my graduation.

First of all, I would like to thank my graduation committee members for their valuable guidance throughout the research and writing, which helped further developing my skills in scientific research. Bas Hofland thank you for taking my ideas further and your enthusiasm, Alessandro Antonini for your guidance on numerical modelling and wave analysis and Greg Smith for proposing this interesting topic, giving me the opportunity to do this research at Van Oord and your attention to detail. Special thanks to my daily supervisor Arthur Zoon for always finding time whenever this was needed and providing useful comments and organizational guidance.

Besides the committee, my gratitude goes out to Van Oord that supported my research with computational capacity, valuable advice and excellent workspace. I would also like to thank Jeroen Bekker for providing his dataset and his help with its interpretation. Furthermore, I want to thank Sander de Vree of the hydraulic laboratory of TU Delft for his help with acquiring data and post processing it, as well as my fellow student Piet Zaalberg for his introduction to the numerical tool used.

On a personal note, these two unforgettable years of traveling and studying in different countries and universities has been the most special experience of my life. It would not have been the same without the wonderful friends that I made during this journey. To this beautiful mix of people that is my fellow CoMEM students, thank you for your friendship and amazing moments together.

Last but not least, I would not have been able to complete this journey without the continuous support of my parents and sister. I am grateful for always believing in me, being there in difficult times and your immense love.

N. Sigalas

Delft, July 2019

Summary

In the present study the stability of crown wall elements on top of a rubble mound breakwaters is investigated. Crown walls are concrete superstructures which gain stability from their own weight and are usually implemented to achieve the required structure height, reduce wave overtopping and enable access along the breakwater.

The first step was to conduct a thorough literature review on the topic, in order to identify knowledge gaps. It was found that current design methods do not take the freeboard of the crown wall base into account when calculating the vertical force on the crown wall. Recent research has established that when the freeboard is increased, the vertical force is reduced and has indicated that the portion of the crown wall base that is wet is reduced as well, linking these two parameters. However, there have been different approaches to increasing the base freeboard, that could lead to different effects on the loading. Moreover, it was found that parametric investigations regarding the vertical force were very limited. Furthermore, the currently used design formulas assume that the maximum horizontal and vertical forces occur simultaneously. Previous research suggests however that there is a time lag between these two maxima.

Based on the knowledge gaps, the goals of the study were defined. The first goal of this research is to gain insight in the influence of different methods of increasing the base freeboard on the loading and the crown wall base saturation. A second goal is to define the shape of the uplift pressure distribution, as recent research proposed that it deviates from the previously assumed triangular distribution. The next goal is to examine the time lag between the horizontal and vertical forcing and its effects. The final goal is to study the effects of breakwater slope parametrization on the crown wall loading and uplift distribution shape for which no previous research was found.

In order to achieve these goals numerical model simulations were prepared and ran. Simulations for which the base freeboard was varied with two different approaches, as well as simulations with varied breakwater slope were performed, whereas the wave height, wave period and other geometric parameters remained unchanged. The selected CFD numerical model is OpenFOAM® making use of the waves2Foam toolbox, implementing the volume of fluid (VOF) method. A dataset from physical model tests was acquired, on which the simulations were based. An effort to validate the model with this dataset was made but significant discrepancies were found both between the simulated results and the dataset, but also between the dataset and calculated loadings with prominent empirical methods. For that reason, the investigation is based on comparison of the simulated results to a reference base case.

By analysing the results, it is found that the currently used empirical methods of (Pedersen, 1996) and (Nørgaard et al., 2013) fail to predict the changes in loading for increasing base freeboard, resulting in overestimation, as suggested by previous research. It is found that for an increasing base freeboard, less part of the base becomes wet and that the vertical force, as well as the critical weight calculated for sliding failure are reduced. On the other hand, the horizontal force was found to increase.

It is concluded that when increasing the base freeboard by means of lowering the water level results in lower loading compared to an increase of freeboard by elevating the crown wall element. Additionally, for the latter approach, a larger portion of the base slab is wet. Also, it was confirmed that a recently proposed reduction coefficient by (Bekker et al., 2018) for calculating the uplift pressures can be used to provide more accurate results in the case of freeboard increase by lowering the water level. However, in the case of freeboard increase by crown wall elevation, there is no existing method that provides accurate results and hence it is recommended to perform scale model tests to gain insight on the stability when designing with that approach.

When the uplift pressure distributions were examined, it was found that for a zero base freeboard the pressure distribution follows an S-shaped profile, which with increasing base freeboard converts into a reversed polynomial shape. An interesting finding is that, due to the wave-structure interactions at the point where the

front and bottom faces of the crown wall meet and the entrapped air, the peak pressure is found to be located slightly inwards instead of the most seaward end of the base slab and is followed by a reverse peak. However, in order to propose a generally applicable profile shape more data is required, including cases with varying wave conditions.

The results also indicate the presence of a time lag between the maximum horizontal and vertical force which for some cases becomes significant. This time lag results in quite lower critical loading on the structure than when assuming simultaneous maxima. Thus, the widely used stability criterion of (CIRIA et al., 2007) for sliding is overestimating. Nonetheless, further research is necessary as these findings are a result of only one wave condition and specific geometry.

An unexpected finding which contradicts the predictions made with the empirical methods of (Pedersen, 1996) and (Nørgaard et al., 2013) is that gentler breakwater slopes resulted in higher loading on the crown wall, especially the vertical force. This is considered to be a result of an increased internal set-up that was observed for gentler slopes.

Further research is recommended, especially on tests with varying wave conditions and geometries, which should make these conclusions more generally applicable.

Contents

List of Tables

List of Figures

1 Introduction

Breakwaters are broadly used around the world. Such structures are constructed to fulfil various functions. Mainly, they are designed for the protection of vessels entering or harboured within ports, as well as the various port facilities from wave action and tidal currents. Often however, they are used to protect beaches from erosion, channels against siltation and valuable habitats that are threatened by the destructive forces of the sea (van den Bos and Verhagen, 2018). An example of a breakwater and its function is shown in Figure 1. Waves arrive from the seaside and impact the two breakwaters which protect the harbour basin from the waves.

Figure 1. Completion of breakwaters for Portarlington harbour redevelopment project. Source: (Maritime, 2017).

In this chapter the thesis is introduced by giving an outline of the motivation that led to this research and by presenting the structure of the report.

1.1. Research motivation

Recent studies (Van Heemst, 2014, Bekker, 2017, Jacobsen et al., 2018) have shown that the existing empirical methods for calculating the stability of crown wall elements on top of rubble mound breakwaters result in large overestimations when the freeboard of the base of the element increases. This means that the existing design formulae result in crown walls that are too heavy, resulting in additional cost.

These overestimations emerge from the fact that the previous empirical methods were based on tests with zero base freeboard, as well as assumptions regarding the shape of the uplift pressure distribution that could be incorrect. The investigations that have been conducted so far for increased base freeboard, propose different approaches of increment which is hypothesised that have different effects on the loading exerted on the crown wall. Additionally, there have only been detailed parametric investigations on the horizontal and not the vertical forces exerted on the crown wall.

Thus, the current study focuses on investigating the effect of varying base freeboard with different methods to the stability of the crown wall, as well as some parametric investigations. According to (Pedersen, 1996), the vertical (uplift) pressures acting on the base of the crown wall are hard to determine in small scale flume tests because of strong scale effects related to the flow inside the porous mound. This was one of the reasons for choosing numerical modelling with the use of OpenFOAM for the investigation. This model can simulate with fairly good accuracy the flow inside the rubble mound and the pressures exerted on the crown wall element from the wave action.

1.2. Report Outline

This section provides a brief overview of what is treated in the following chapters of this report.

<u>Chapter 2: Theoretical Background</u>

In this chapter the basic theoretical background is given on rubble mound breakwaters, crown wall elements and their stability, as well as numerical modelling using the volume of fluid method. It also provides a brief overview of the main physical and hydraulic parameters used throughout the report.

<u>Chapter 3: Crown Wall Loading</u>

In this chapter a detailed overview of the existing wave load calculation methods is given. The methods are described and critically analysed.

<u>Chapter 4: Findings from literature and Study Approach</u>

In this chapter the findings that are most relevant to the investigation from chapter 3 are discussed and knowledge gaps from literature are identified. Following, the methodology followed is provided and the research questions are defined.

<u>Chapter 5: Numerical Analysis</u>

This chapter briefly describes the physical experiment on which the simulations are based, followed by a detailed description of the setup of the numerical model, the sensitivity analysis, calibration and validation, as well as the cases (simulations) prepared for the investigation.

<u>Chapter 6: Results and Analysis</u>

In this chapter the results and findings of the investigation are given. These results are analysed, compared to the existing empirical methods and conclusions are drawn.

<u>Chapter 7: Conclusions and Recommendations</u>

The main conclusions of the investigation are outlined followed by recommendations for further research into this subject.

2 Theoretical Background

This chapter provides the basic background for the readers on rubble mound breakwaters, the forces acting on crown wall elements and numerical modelling using the volume of fluid method. The first section gives a brief description of the functions of breakwaters and the layout of rubble mound breakwaters, while the second section describes the crown wall element and its stability. Following, the third section specifies the major physical and hydraulic parameters that are used throughout this study. Finally, the fourth section introduces the volume of fluid method of numerical modelling along with the basic mathematical model incorporated in OpenFOAM which will be used for the investigation.

2.1. Rubble mound breakwaters

There are many different types of breakwaters such as rubble mound types, monolithic (caisson) types, composite types and various special (unconventional) types of breakwaters (van den Bos and Verhagen, 2018). Some typical cross-sections of different types of breakwaters can be observed in Figure 2.

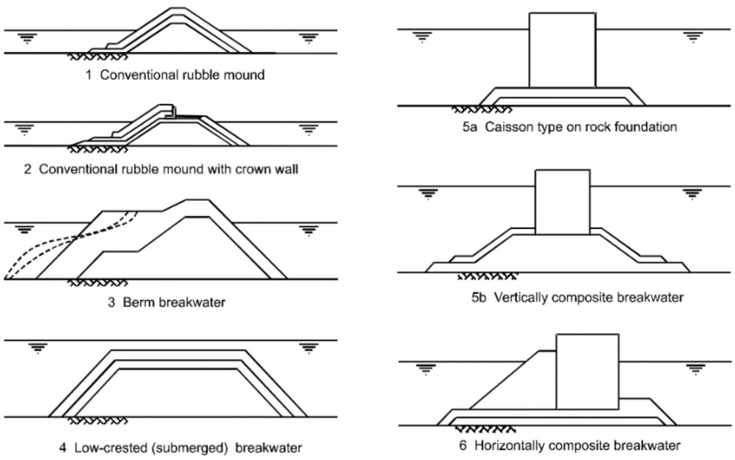

Figure 2. Typical cross-sections of various types of breakwaters. Source: (CIRIA et al., 2007).

The selection of preferred breakwater type for each situation depends on factors such as cost, constructability, local availability of materials and the preference of the owner. For example, rubble mound breakwaters have better wave energy dissipation properties than vertical breakwaters and as such are often preferred in order to reduce wave reflections, especially in situations where quarry material is easy to obtain at a low cost. However, as the material quantities for a rubble mound increase significantly with increasing depth, caisson type breakwaters are often preferred in deeper water (CIRIA et al., 2007).

The present investigation focuses on conventional rubble mound breakwaters with a crown wall on top. A typical cross section with its main elements and their functions can be observed in Figure 3. These coastal structures are mainly used for port protection and the geometry depends on the function of the breakwater, the required access, the use of the lee side, the crest elevation requirements and cost considerations or repair requirements (CIRIA et al., 2007). The main body is comprised of the core (usually built of gravel, quarry run or dredged material), one or more under (filter) layers, and the cover or armour layer. As such, they are permeable, and water can flow through the structure.

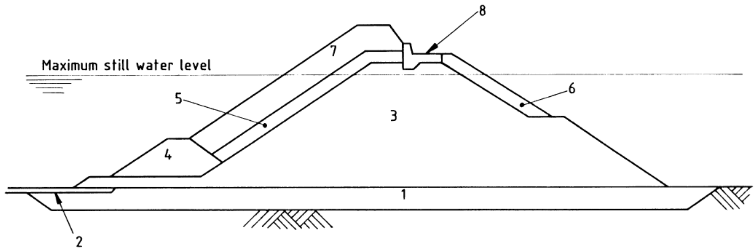

Element	Function
1 Foundation improvement (if necessary)	Provides embankment stability
2 Scour protection apron	Prevents erosion
3 Core	Provides bulk of structure and reduces wave transmission
4 Toe mound	Supports the main armour
5 Underlayer	Contains the core and provides foundation for armour
6 Rear face armour	Protects core from overtopping waves. Provides wave protection inside harbour
7 Main armour	Provides wave protection
8 Concrete crest structure (with key or cut-off toe)	Provides access and reduces overtopping (Key prevents sliding failure)

Figure 3. Elements and functions of typical rubble mound breakwaters with crest element. Source: (British Standards Institution, 1991).

The outer armour layer is subjected to direct wave attack and protects the whole structure from failure. To withstand these heavy loads it is usually comprised of heavy armour stones (quarried rock) or concrete armour units. (CIRIA et al., 2007). According to (van den Bos and Verhagen, 2018), generally the heaviest fraction of the quarry yield curve with a narrow grading is used for the outer armour. In recent years, special designed heavy concrete elements like X-blocks which increase the interlocking between elements, are being used as well. The stone size of the filter layers is usually smaller than the armour layers because it is protected from direct wave attack and also needs to prevent the core material from washing out of the structure. Additionally, a toe is commonly built to support the armour layer. In many cases scour protection is also used to prevent scour of the adjacent sea bed, which could affect breakwater stability (CIRIA et al., 2007).

Breakwaters can be massive structures in which a large amount of stones are used with a great cost. In order to achieve the required crest height more cost efficiently (as breakwater width is reduced), a crown wall or crest element is often used.

2.2. Crown Wall

A crown wall is a gravity based concrete superstructure placed on top of a rubble mound breakwater, which sometimes is casted in one piece and sometimes it consists of two pieces, a vertical wall and a base slab. The performance of a rubble mound breakwater against run-up and overtopping is significantly improved by the use of a concrete crown wall, as the crest level to be considered for overtopping is the crest of the crown wall. Thus, the dimensions of this element are usually a function of the allowed overtopping and required resistance to sliding (CIRIA et al., 2007, British Standards Institution, 1991). A sketch of a profile of the Bilbao breakwater which incorporates a crown element is given in Figure 4.

Rubble mound breakwaters often sustain some damage and access along the breakwater is required for repairs. So, the crown element often incorporates a roadway that allows access along the breakwater for inspection and maintenance, port operations (such as ship mooring or storage areas) or for recreation (British Standards Institution, 1991, CIRIA et al., 2007). In such cases, a minimum width of 2 m for pedestrian access or 4 m for vehicles (single-lane) is generally required (CIRIA et al., 2007). When there are berthing takes place immediately behind a breakwater, the crown wall often carries facilities for cargo loading and unloading, pipelines, conveyor, electrical and water supply systems (CIRIA et al., 2007). Another benefit of crown walls is that a parapet can lead to a substantial reduction in the amount of required armour stone compared to a conventional design with the same crest height.

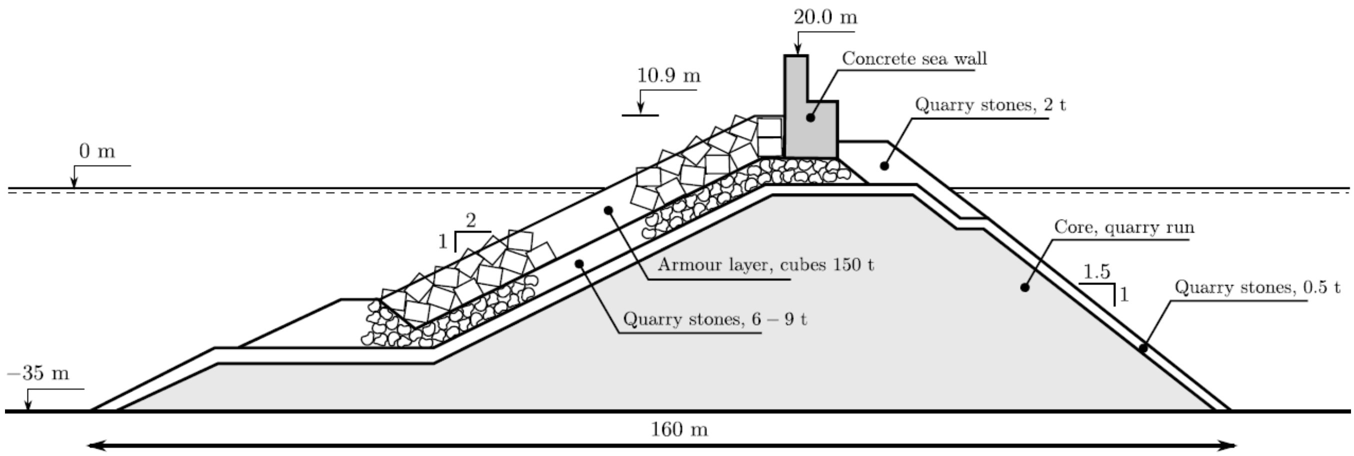

Figure 4. Sketch of the Bilbao breakwater profile. Source: (Jensen, 1984a).

The circulation of water and pore pressure beneath the crown wall should also be considered, either impermeable materials should be used to prevent contact with the underside of the crown wall or highly permeable materials to allow free drainage (CIRIA et al., 2007). Design guidelines for crown walls suggest that it is preferable to place the crown wall on the core and not on the underlayer, in order to avoid the higher penetration of uplift pressures under the wall (in contrast with the Bilbao breakwater of Figure 4). According to (CIRIA et al., 2007): “The bottom of the crown wall should be kept sufficiently above still water level to reduce uplift forces to acceptable values to ensure stability of the crown wall section”.

The position of the crest structure on the top of the armour layers needs consideration. “A berm of secondary armour on which primary armour is placed, seaward of the crest wall, is preferred in order to reduce forces on the wall and to provide enhanced stability of the top of the primary armour slope against wave turbulence caused by reflections from the wall. In all cases a horizontal berm of underlayer sufficient for at least two armour units should be provided in front of the crest structure” (British Standards Institution, 1991).

Underneath the front side of the base slab a key (downstand, skirt) can be implemented which penetrates the rubble mound base, anchoring the crown wall. A key increases the resistance against horizontal displacement (sliding) of the entire crown wall element (Pedersen, 1996, British Standards Institution, 1991, CIRIA et al., 2007). Typical crest structures are shown in Figure 5. For reasons of simplicity, in this research an L-shaped crown wall without a key (downstand) is investigated.

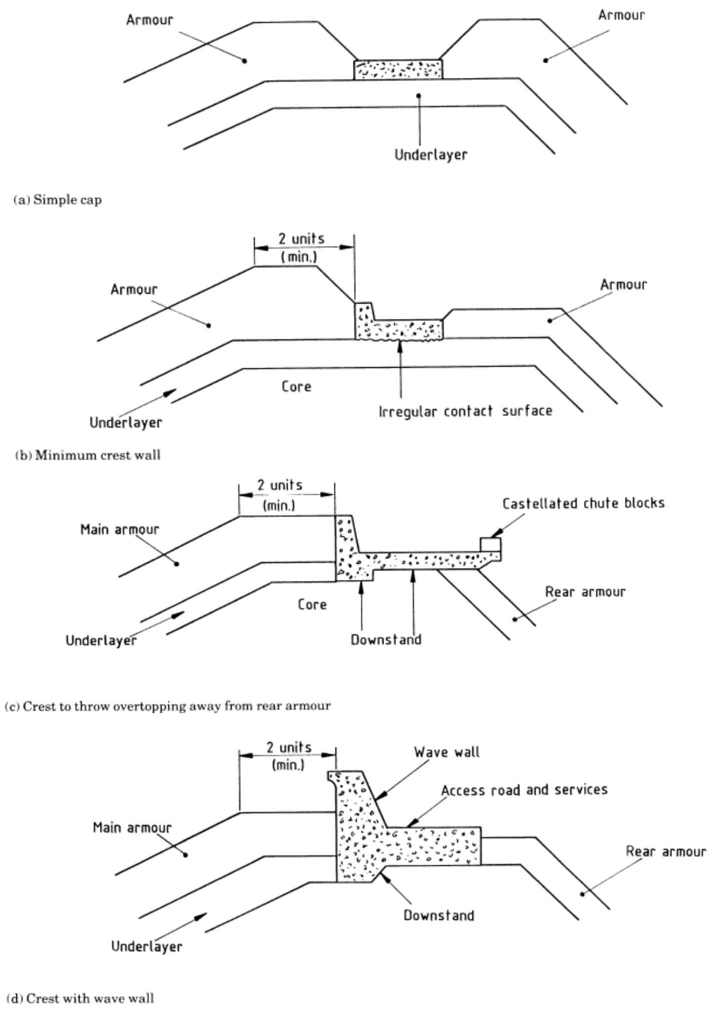

Figure 5. Typical crest structures for rubble mound breakwaters. Source: (British Standards Institution, 1991).

As already mentioned, in order to reduce overtopping, the wall is extended upwards to increase the total crest of the breakwater. However, the tendency to increase the height of the wall in order to reduce the volume of armourstone can lead to very large wave impact forces on this wall. For the forces acting on the superstructure to be minimised, the crown wall should not extend above the level of seaward armour (CIRIA et al., 2007). On the other hand, a wall which protrudes above the berm is less expensive than placing rubble mound up to the same level as the top of the wall. Thus, the selection of the crest wall height can be optimized during design taking into account the overtopping limits, the resistance to wave induced loads and economic factors. In the case that the armour protrudes above the crown wall, the maximum height of the armour above the wall should be 0.3 times the armour layer thickness, as otherwise there is a risk of tilting of units on to the crown wall (CIRIA et al., 2007).

Crown Wall Stability

The focus of the present study is the stability of a crown wall on top of a rubble mound breakwater under wave loading. Here, the failure modes and forces that determine the stability are briefly outlined. According to (Pedersen, 1996), the stability of the crown wall is essential since a failure of this structure might lead to a total breakdown of the whole rubble mound breakwater. The balance between the stabilizing and the destabilizing forces determine the stability of a crown wall. The stabilizing force is produced by the mass of the superstructure, while the destabilizing force is generated by the waves induced forces (CIRIA et al., 2007). When the wave loading on the crown wall becomes too large the structure can move or break, leading to failure of the crown wall (Pedersen, 1996). The crown wall behaviour is very different than that of the armour layer. While the armour layer is progressively damaged by wave attack, the crown wall can suddenly fail due to large destabilizing forces without any previous damage (Molines, 2016). Failure can occur in different modes, from which the most common are depicted in Figure 6. These can be grouped into those depending on the strength of the superstructure (such as cracking/breakage) and those depending on the interaction with the underlying structure (such as sliding and overturning) (CIRIA et al., 2007). The second group becomes relevant in this study.

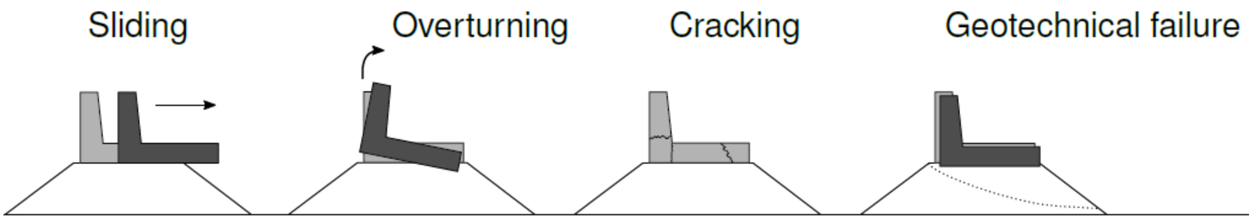

Figure 6. Crown wall failure modes. Source: (Pedersen, 1996).

When the stability of the rubble mound base is insufficient, geotechnical failure can occur because the rubble mound base does not provide a stable foundation for the wall. When the strength of the crown wall is insufficient the structure may break (cracking failure mode). In Figure 7 sliding and overturning failure that accrued at the port of Bermeo are shown. Sliding is the most common reason for failure of crown walls (Pedersen, 1996). The current investigation focuses on the sliding failure mode which causes displacement of the entire structure due to wave loading. The forces investigated can be used to also calculate the moments for the overturning criterion. However, as the current study also investigates the pressure distributions, further on will be shown that these vary significantly, which as a consequence makes the point where the forces are applied a perplexing issue. This point is required in order to calculate the moments. Thus, calculating the moments would require assumptions that would increase the uncertainty of the results greatly.

The loads on crown walls are a function of the attacking waves but are also strongly depended on the geometry of the armour layer near the crest and of the crown wall itself. The main force is exerted on the front (vertical) face of the wall. This horizontal force is either a dynamic load (short-duration impact force caused by the wave front, where the load is time dependent and for which inertial effects cannot be ignored) or a quasi-static load (where the acting force is "slow" enough such that inertial effects can be ignored) resulting from the overtopping water. This horizontal force will be resisted by the weight of the crown wall and by the friction force between the underside of the crown wall and the armourstone layer on which it sits. Depending on the elevation of the underside of the crown wall, the materials directly underneath it may or may not be saturated. In the case that the area underneath the crown wall is saturated, the wave forces and flows through the rubble mound led to an increase in pressure on the underside of the crown wall causing uplift forces (CIRIA et al., 2007).

Figure 7. Port of Bermeo, Biscay (northern Spain). Slide failure and overturning in 2010. Source: (Negro Valdecantos et al., 2013).

Stability against sliding and overturning of the crown wall can be assessed with the following criteria 2.1 and 2.2:

Stability against sliding

The crown wall is a gravity based structure. Stability is obtained when the resistance against sliding is larger than the horizontal force exerted on the element. This resistance is produced by the weight of the element, reduced by the uplift force. A sketch of a crown wall which is loaded in horizontal and vertical direction is given in Figure 8. The horizontal and vertical (uplift) pressure distributions are simplified as concentrated forces and the stability criteria for sliding is presented.

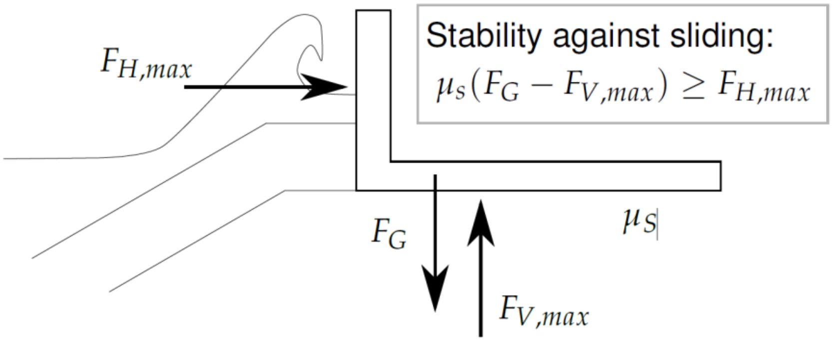

(2.1)

Figure 8. A simplification of wave loads acting on a crown wall for the criteria of stability against sliding. Source: (Bekker, 2017).

The stability against sliding equation given by (CIRIA et al., 2007) in Figure 8 will be treated as equation 2.1, where:

- $F_{H,max}$ in N/m is wave-induced horizontal force.
- F_G in N/m is the (buoyancy-reduced) weight of the crown wall element, $(M_{cw} – V_{cw}\rho_w)g$, where M_{cw} and V_{cw} are the mass and the volume of the crown wall.
- $F_{V,max}$ in N/m is the wave-induced uplift force.
- μ_s is the dimensionless (static) friction coefficient.

The value of the friction coefficient μ_s is determined by the amount of friction between the rubble mound base and the crown wall and has a value between 0 and 1. A value close to zero corresponds with very low friction between both surfaces. It is generally assumed to be around 0.5. With the use of a substantial key into the underlayer, higher values can be assumed. According to (CIRIA et al., 2007), these values assume that the crown wall is cast in place directly on the core or on to an underlayer. Precast elements, or elements cast in situ on to finer material, will provide lower values of the friction coefficient.

Stability against overturning

This criterium is given by the equation:

$$M_G - M_V \geq M_H \tag{2.2}$$

Where:

- M_G is the stabilizing moment due to the weight of the crown wall in Nm.
- M_V is the overturning moment due to the uplift force in Nm.
- M_H is the overturning moment due to the horizontal force in Nm.

These moments are generated by the forces shown in Figure 8.

2.3. Physical and hydraulic parameters

Forces on crown walls are the result of waves that reach sufficient run-up to hit the crown wall and even overtop it. Therefore, crown wall stability is closely related to the same variables that affect wave overtopping such as the crown wall freeboard, crest berm width and type of armour. Crown wall stability must consider not only wave attack but also the effect of pressure within the armour and filter layers (Molines, 2016). Several parameters are used for the design of a coastal structure such as a rubble mound breakwater and a crown wall. These can be distinguished into physical (geometrical conditions) and hydraulic parameters (wave conditions). In this section, the most important parameters that are used in this study are explained.

Physical parameters

Figure 9 shows a typical cross section of a rubble mound breakwater with a crown wall. It defines the governing physical parameters and symbols used to describe them according to (CIRIA et al., 2007). In Table 1 an overview of these parameters is given.

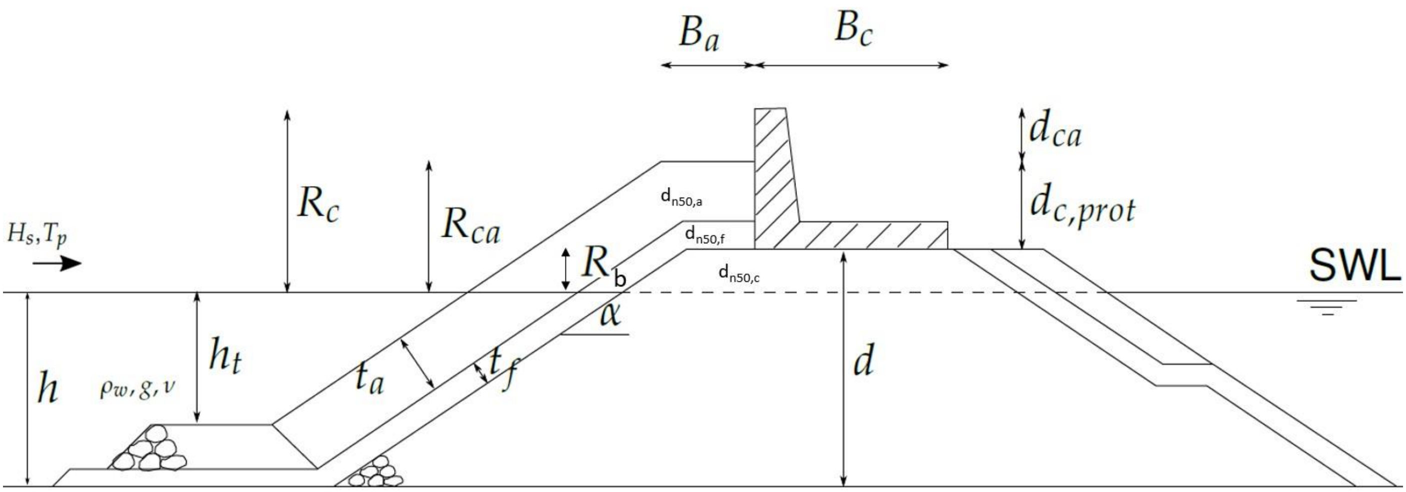

Figure 9. Governing parameters related to the structure, breakwater cross-section with a crown wall on top. Modified figure from(CIRIA et al., 2007).

Table 1. Physical Parameters

Symbol	Parameter Description	Unit
h	Local water depth	m
h_t	Water depth above the toe	m
R_C	Crown wall crest freeboard above still water level (SWL)	m
R_{CA}	Armour crest freeboard above SWL (many times found as A_c)	m
R_b	Base freeboard (distance of crown wall base slab to SWL)	m
t_a and t_f	Thickness of the armour and filter layers (usually≈$2\times d_{n50}$)	m
α	Slope angle of the breakwater	°
$d_{n50a, f, c}$	Nominal grain diameter for the armour (a), filter (f) and core (c)	m
B_a	Armour berm width	m
B_c	Width of the crown wall	m
d	Height of the rubble mound breakwater	m
d_{ca}	Unprotected crown wall height (from armour crest to crown wall crest)	m
$d_{c,prot}$	Protected crown wall height (from crown wall base to armour crest)	m

Hydraulic parameters

Following, the most significant hydraulic parameters for the current study are described.

- Wave height (**H**, **H_s,H_{m0}**): The wave height is usually defined as the average of the highest one third of the waves (significant wave height Hs) $H_{1/3}$, or the spectral wave height H_{m0} (Bosboom and Stive, 2015, van den Bos and Verhagen, 2018). The wave height that is exceeded by 0.1% of the waves

(2.3)

$H_{0.1\%}$ is also used in the following chapters. For the calculation of a wave height with a probability of exceedance P, (Bosboom and Stive, 2015) present the following equation:

$$H_P = 2\sigma\sqrt{2\ln(1/P)}$$

However, in most experimental cases that this wave height was used, the authors used a number of waves equal or more than 1000 waves and picked the largest values as $H_{0.1\%}$.

- Wave period (**T**, **Tp, Tm**): The most frequently used wave periods are the average period T_m and the peak period T_p (taken from the wave spectrum).

- Wavelength (**L, L_{0p}, L_{0m}**): In deep water the wavelength is defined as:

$$L_0 = \frac{gT^2}{2\pi} \tag{2.4}$$

When the peak deep water wavelength L_{0p} is considered Tp must be used whereas Tm is used for the mean deep water wavelength L_{0m}.

- Wave steepness (**S_0**): Wave steepness is defined as the ratio of wave height to wavelength H/L. For this study the fictitious steepness in deep water based on the peak period is relevant which is indicated by $S_{0p} = H_s/L_{0p}$. Generally, a steepness of 0.01 indicates a typical swell wave and a steepness of 0.04 to 0.06 indicates a typical storm wave.

- Breaker (Iribarren) parameter (**ξ**): This parameter indicates if waves are breaking on a slope and the kind of breaking/impact that can be expected. It is defined as the ratio of slope steepness to wave steepness as follows:

$$\xi = \frac{\tan a}{\sqrt{\frac{H_0}{L_0}}} \tag{2.5}$$

Where:

- tana is the steepness of the slope in sexagesimal degrees.
- H_0 is the deep water wave height in m.
- L_0 is the deep water wavelength in m.

For irregular waves the Iribarren parameter is often computed using Hs and L_{0p} based on Tp. Breaking waves can be distinguished between spilling plunging and surging breakers depending on the value of the Iribarren parameter, as show in Figure 10. The shown values are indicative and the transition between the type of wave breaking is gradual (Bosboom and Stive, 2015).

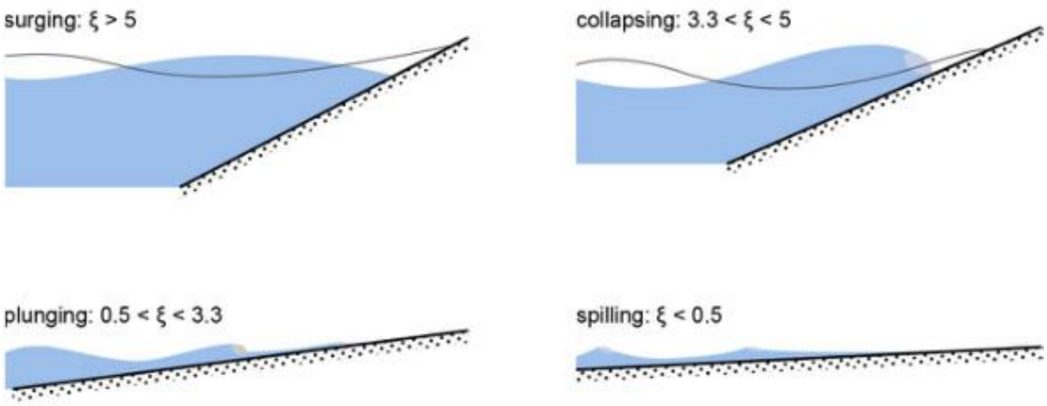

Figure 10. Breaker types in relation to the Iribarren parameter. Source: (Bosboom and Stive, 2015)

- Water density (ρ_w): For seawater is around 1025 kg/m^3 while for lab experiments usually water with density of around 1000 kg/m^3 is used.

- Run up (R_u): Is the ascent of the sheet of water on the slope. There are many proposed methods for calculating it (most include the Iribarren parameter). It is used in many of the design formulations for calculating the wave loads on a crown wall, as each author uses a different method to calculate the run-up, it will be treated separately within each section.

2.4. CFD Numerical modelling with OpenFOAM®

This section provides a brief introduction to Computational Fluid Dynamics (CFD) numerical modelling, followed by the description of the basic principles of the numerical model Open Field Operation and Manipulation (OpenFOAM) used in the investigation, where the governing processes, the assumptions and the equations that form the basis of the model are treated.

Studying viscous free surface flow under breaking waves is an exceptionally challenging topic, however the results may provide valuable insight to more detailed mechanisms. The development of numerical methods capable of predicting solutions to flow problems with a moving free surface separating two segregated fluids are of great interest for the civil and coastal research and engineering communities (Ingram et al., 2004). The model can be used as a numerical wave flume, where the same tests as in a physical wave flume are performed by a computer. By doing a numerical simulation, geometrical changes are easier and less costly to implement and scale effects can be avoided. This is the main advantage of using a numerical model over a physical scale model test. A schematic of a generic CFD numerical wave flume is shown in Figure 11, depicting the main features included in the numerical model.

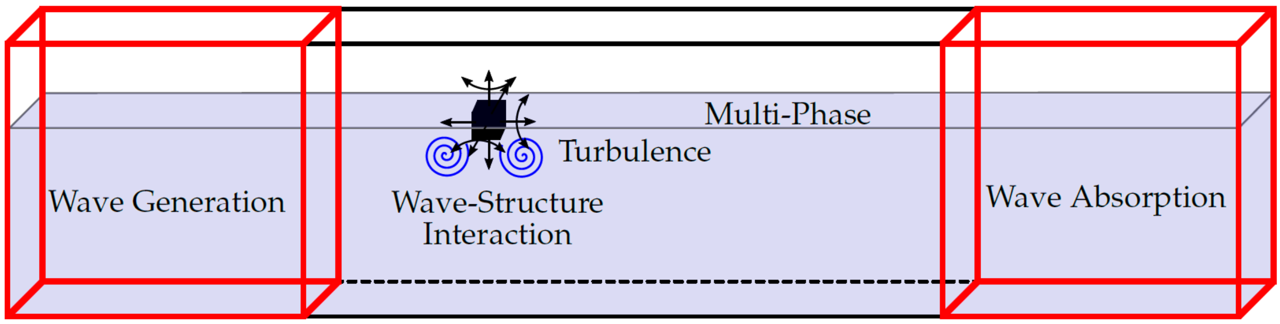

Figure 11. Generic CFD-based numerical wave tank schematic, depicting the main features to be included in the numerical model. Source: (Windt et al., 2019)

Numerical models can be potential flow based, implementing the Laplace equation, where the velocity potential and free surface elevation are the only unknown variables and require minimal computational cost. However, they are only accurate in limited conditions, e.g., small incident waves and small body motions (Zhang, 2018). Or they can be viscous based (like CFD), that have the advantage of capturing relevant hydrodynamic non-linearities, such as complex free surface elevation (including wave breaking), viscous drag and turbulence effects.

These models can deliver accurate results in high resolution, which is particularly useful for the investigation of specific flow phenomena around coastal and offshore structures, but they are more computational expensive. Generally, only the initial location and geometry of the free surface are known. "Since the free surface is determined as part of the solution, gross topological changes that occur during the processes of merging and break-up and which amplify wave-structure coupling problems must be handled" (Ingram et al., 2004). Thus, powerful numerical tools are necessary for handling arbitrarily shaped interfaces naturally. With the rapid development of high performance computing technology, the use of CFD tools is becoming increasingly widespread in engineering design work (Chen et al., 2014, Windt et al., 2019, Zhang, 2018). Another technique that is gaining interest within the scientific community is the smoothed particle hydrodynamics approach (SPH) which uses using the Lagrangian approach, representing the fluid domain by a set of particles instead of a computational mesh and where the equations are expressed as interaction forces between the particles. However, most of these models are still under development and quite computationally intensive.

CFD models can be based on the non-hydrostatic Euler or Navier-Stokes equations and can be implemented in two ways. First, by solving the equations for the fluid domain assuming that the free surface is described by a single-valued function of the horizontal coordinates. In that way the effects of the wave breaking process can be included, but overturning waves cannot be modelled. It is clear however that the movement of both the air and water are important in determining the flow physics and should therefore be fully accounted for in the solution (Ingram et al., 2004). So, the second way is by using a mesh covering both the water domain and a layer of air above the water surface, where the equations of motion are solved for the water. For each cell of the mesh a variable describing the fraction of water is used, the so-called volume of fluid (VOF) free-surface tracking method, where the free surface can attain arbitrarily complex geometries. A transport equation is solved to move the VOF with the flow. This technique can model detailed processes, amongst others wave overturning and breaking, overtopping and slamming forces on structures (CIRIA et al., 2007). Some successful VOF models are: SKYLLA, VOFbreak, COBRAS, IHFOAM, IH2-VOF, IH3-VOF, Flow-3D, EdgeCFD and ComFLOW. In this study OpenFOAM, which is a free, open-source C++ library for continuum-mechanics problems and has already been applied to a variety of problems in coastal and offshore engineering is used, along with the waves2Foam toolbox developed by (Jacobsen et al., 2012).

OpenFOAM® and waves2Foam toolbox

The open-source CFD library OpenFOAM contains a method for solving free surface Newtonian flows using the three-dimensional Reynolds averaged Navier–Stokes (RANS) equations for two incompressible phases using a finite volume discretisation and the VOF method. Reynolds averaging is the decomposition of the flow velocity and pressure into a time averaged component and a turbulent component. This way, the Navier-Stokes equations become time averaged (Van Heemst, 2014).This has been extended with a generic wave generation and absorption method termed 'wave relaxation zones' and a method that imposes the velocity field directly at the boundary with a Dirichlet type boundary condition into the waves2Foam toolbox by (Jacobsen et al., 2012). This latter method "applies a mixed Dirichlet/ Neumann boundary condition for the indicator function of the volume of fluid field according to (Higuera et al., 2012)" (Jacobsen et al., 2015). The effect of the flow resistance due to the presence of a permeable core is included through the Darcy–Forchheimer approximation. The ability to use OpenFOAM for the modelling of waves and their interactions with porous structures has been validated by (Jacobsen et al., 2012, Jacobsen et al., 2015, Jacobsen et al., 2018, Chen et al., 2014, Jensen et al., 2014b, Higuera et al., 2014b, Jacobsen et al., 2017, Hu et al., 2016) and others.

The numerical framework is OpenFOAM version foam-extend-3.1. The hydrodynamic model is based on the RANS equations, which describe the conservation of mass and momentum, in a Volume-Averaged (VARANS) form that accounts for permeable coastal structures proposed by (Jensen et al., 2014b). This considers the porous material to be a continuous media characterized by its macroscopic properties, eliminating the need for a detailed description of their complex internal geometry (Losada et al., 2016). It is thus a spatial filter that results in the averaged flow behaviour inside porous zones. The process is depicted in Figure 12 and a more detailed explanation is given in (Jensen et al., 2014b, Losada et al., 2016).

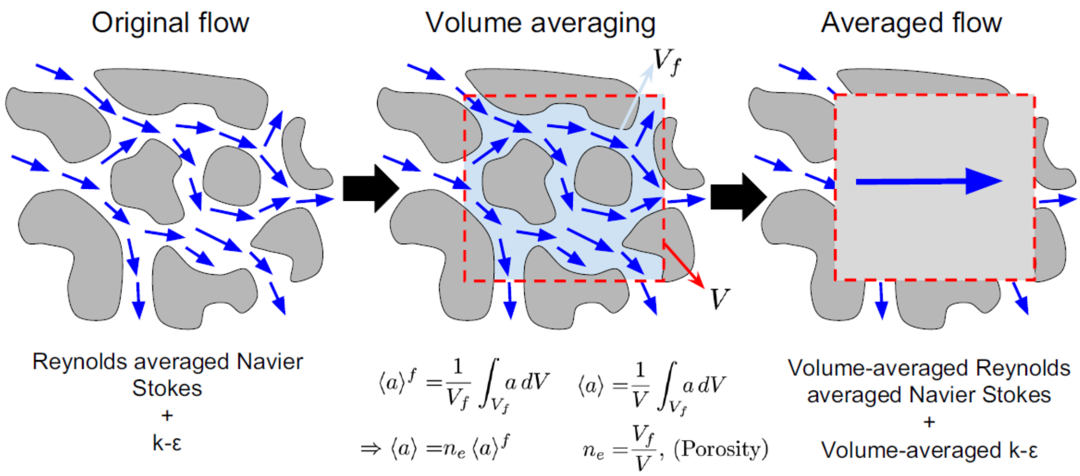

Figure 12. The Volume Averaging process. Source: (Losada et al., 2016)

The VARANS equation which use the filter velocity is given as:

$$(1 + C_m)\frac{\partial}{\partial t}\frac{\rho \mathbf{u}}{n_p} + \frac{1}{n_p}\nabla\cdot\frac{\rho}{n_p}\mathbf{u}\mathbf{u}^T = -\nabla p^* + \mathbf{g}\cdot\mathbf{x}\nabla\rho + \frac{1}{n_p}\nabla\cdot\mu_u\nabla\mathbf{u} - \mathbf{F}_p \tag{2.6}$$

Where:

- Cm is the added mass coefficient.
- u is the filter velocity vector in Cartesian coordinates.
- n_p is the porosity of the permeable structure.
- p* is an excess pressure defined as p* = p-ρg·x, where p is the total pressure.
- x = [x, y, z] is the Cartesian coordinate vector.
- μ_u is the dynamic viscosity of the velocity field.
- F_p is the resistance from the permeable structure described by the Darcy-Forchheimer resistance formulation.

The added mass term is given by:

$$C_m = \gamma_p \frac{1-n}{n} \tag{2.7}$$

Where γ_p = 0.34 is an empirical coefficient.

The resistance term is given by:

$$\mathbf{F}_p = a\rho\mathbf{u} + b\rho\|\mathbf{u}\|_2\mathbf{u} \tag{2.8}$$

Where a and b are closure coefficients that are evaluated based on:

$$a = \alpha\frac{(1-n_p)^2}{n_p^3}\frac{\nu}{D_{n50}^2} \quad \text{and} \quad b = \beta\left(1+\frac{7.5}{KC}\right)\frac{1-n}{n^3}\frac{1}{D_{n50}} \tag{2.9}$$

In which:

- v is the kinematic molecular viscosity.
- D_{n50} is the nominal diameter of the permeable layer.
- KC is the Keulegan-Carpenter number.
- α= 1,000; β= 1.1 are common closure coefficients, affected by stone grading and shape.

The system of equations is closed with the incompressible continuity equation:

$$\nabla \cdot \mathbf{u} = 0 \tag{2.10}$$

According to (Chen et al., 2014), the Navier–Stokes equations are first integrated over the time domain and the whole solution domain and followingly are discretized into a number of cells and timesteps, respectively. Dependent variables and other properties then can be denoted by the values at the centroids. The cells need to be continuous, which means they do not overlap with each other and fill the whole computational domain. The main control over timestep is the Courant number, which represents the portion of a cell that the flow will transverse due to advection effect in one timestep. The Courant number has the following form:

$$Co = \frac{\delta t |U|}{\delta x} \tag{2.11}$$

Where:

- δt   is the maximum timestep.
- δx   is the cell size in the direction of the velocity.
- |U| is the magnitude of the velocity at that location.

In order to improve accuracy and ensure the stability of the model, the Courant number should not exceed the value of be 1 throughout the domain.

The tracking of the free surface is performed with the standard advection algorithm of OpenFOAM and the advection equation takes the form:

$$\frac{\partial F}{\partial t} + \frac{1}{n_p}[\nabla \cdot \mathbf{u}F + \nabla \cdot \mathbf{u}_r(1 - F)F] = 0 \tag{2.12}$$

Where:

- u_r is a relative velocity introduced to keep a sharp interface.
- $\frac{1}{n_p}$ is a factor introduced by (Jensen et al., 2014b) to ensure the conservation of mass, when the fluid passes through a permeable structure. This term is required, since water and air can only occupy the pore volume (Jacobsen et al., 2018)
- F   is the indicator function of the VOF field defined as the quantity of water per unit of volume in each cell. If F= 0, the computational cell is filled with air and if F= 1 with water. A value of F between these two refers to a cell located at or close to the free surface.

To evaluate the spatial variation of any of the properties of the fluid at each cell the indicator function is used. For example, the fluid density and the dynamic viscosity of the cell are computed as:

$$\rho = F\rho_1 + (1 - F)\rho_0 \quad \text{and} \quad \mu_u = F\mu_{u,1} + (1 - F)\mu_{u,0} \tag{2.13}$$

The waves2Foam toolbox generates and absorbs surface water waves with the use of the relaxation zone technique. In the present study, fully nonlinear waves are used, in a first attempt computed with the wave transformation model OceanWave3D which is coupled to OpenFOAM (Paulsen et al., 2014, Engsig-Karup et al., 2009) and allows for accurate transformation of the waves from the offshore boundary to the vicinity of the coastal structure with less computational expense (Jacobsen et al., 2018). The input to OceanWave3D is given by means of a paddle signal used in the laboratory experiments of (Bekker, 2017). In the final setup of the model the waves were generated by the use of a JONSWAP wave spectrum.

One key concern for the accurate modelling of wave loads is the entrapment of air between the water surface and structural elements (Jacobsen et al., 2015, Jacobsen et al., 2018). It was observed that waves in closed cavities filled with air exert much larger forces on than when the air is able to escape and re-enter. Even a small amount of openness of the cavity can reduce the vertical force under a structure by a factor of three (Jacobsen et al., 2018). The solution developed for this problem is a ventilated boundary condition that allows for air ventilation, while enforcing a predefined head loss characteristic developed by (Jacobsen et al., 2018), which is used for the crown wall surface boundary in the current investigation.

In the permeable (ventilated) boundary condition essentially the pressure drop over the structural element is given by a classical head loss relationship known from hydraulic engineering. The boundary condition is effectively infinitely thin, comparable to the description of head losses over membranes and at its simplest form is given by:

$$p_b^* = p_{ref}^* + \frac{\rho}{2}\xi_p |u_p^\perp| u_p^\perp \qquad (2.14)$$

Where:

- P_b^* is the pressure at the boundary (taken equal to the atmospheric pressure).
- P_{ref}^* is the pressure in the imaginary reservoir on the backside of the structural element.
- $u_p^\perp$ is the pore velocity of the fluid in the gap(s) through the structural element.
- ξ_p is a loss coefficient.

In Figure 13 a sketch of the notion of the ventilated boundary condition can be observed.

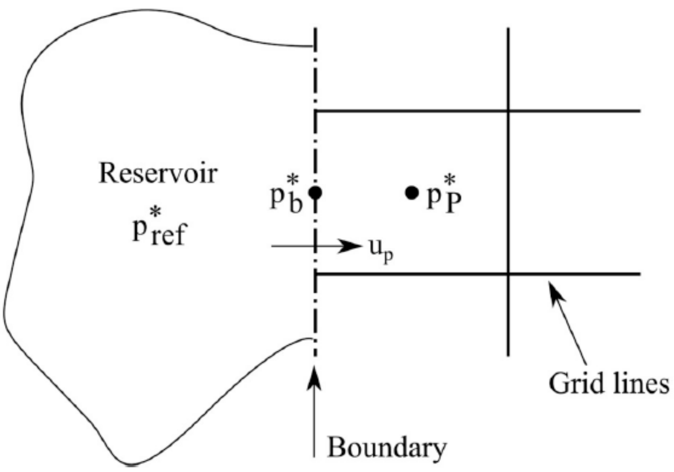

Figure 13. The ventilated boundary condition on a discrete level. P_P^* is the pressure in the cell centre of the cell adjacent to the boundary. Source: (Jacobsen et al., 2018).

As mentioned, the formulation of the VARANS equations is based on the filter velocity. By expressing the ventilated boundary conditions in filter velocities and replacing them by the discretised normal pressure gradient from the discretised normal momentum equation to ensure stability (the full derivation can be seen in (Jacobsen et al., 2018)), results in the final boundary condition:

$$\frac{\rho}{2}\frac{\xi_p}{e_p^2}\frac{|u^{\perp}|}{A_{D,f}}\nabla_b^{\perp} p_b^* + p_b^* = p_{ref}^* + \frac{\rho}{2}\frac{\xi_p}{e_p^2}|u^{\perp}|u^{\perp *} \tag{2.15}$$

Where:

- $u^{\perp} = e_p\, u_p^{\perp}$.
- e_p is the degree of openness of the structural element. Note that the scaling $1/e_p^2$ is in the range of 1 -10^6 for e_p between 100% and 0.1%.
- $u^{\perp *}$ is an explicit source term.
- $A_{D,f}$ is the diagonal coefficient in the discretised momentum equation.
- $\nabla_f^{\perp}$ is the normal derivative over the boundary.

The left part of the equation is treated implicitly, while the right part only contains explicit source terms. For stability reasons, connected to the explicit update of the nonlinear coefficient $|u^{\perp}|$, $|u^{\perp}|$ is updated each pressure iteration and not just each time step (Jacobsen et al., 2018).

It was shown by (Jacobsen et al., 2018) that compared to the previous technique for handling the issue, by introducing small meshed tubes through the structure, the resulting forces magnitude is quite similar but this method gives a 95% reduction in the number of time steps required (for an openness of 1.1%), resulting in a similar reduction in the total simulation time. This boundary condition was validated by (Jacobsen et al., 2018) against results from previous physical model test and new data sets from new experimental tests that they conducted for integrated wave loads on crest wall elements.

3 Crown Wall Loading

As discussed in the previous chapter, in order to access the stability of a crown element, the wave loads must be determined. This chapter aims at giving a comprehensive overview of the calculation methods currently used to convert wave conditions into forces and pressures acting on the superstructure as a function of its physical properties. Firstly, the available methods are briefly described, with more details given for the most commonly used, followed by a critical analysis of the various methods.

Wave forces on a crown wall structure under the action of irregular waves are of a stochastic and thus very complicated nature. The imposed loads on a crown wall depend both on the characteristics of the waves and the geometry of the structure, including permeability and roughness of the rubble beneath and in front of the superstructure (British Standards Institution, 1991). As discussed in the previous chapter, the wave loads on the superstructure can be distinguished in the horizontal wave force and the overturning moment which results from it, as well as the uplift pressure on the base of the element. As the up-rushing water travels faster on the outside of the armour than inside the porous layers, the pressure loading on the wall is expected first to take place in the region just above the crest of the armour (Pedersen, 1996).

According to (Pedersen, 1996), during wave attack "A solid water impact in the form of a water hammer impinges on the upper unprotected part of the wall." This impact exerts a large horizontal force and overturning moment to the element. The secondary uplift pressure depends on the porous flow, as it is generated when the water level moving up and down inside the core and layers of the breakwater reaches the slab of the superstructure (Pedersen, 1996). Since water pressure is isotropic, when the wall base is wet, the vertical pressure will cause loads on the crown wall with the same magnitude as the horizontal pressure at the base of the element. This solid water impact however occurs in a very short duration, the water moving through the porous layers has not enough time to reach the bottom of the slab, which results in low uplift pressures. This indicates a lag between the horizontal and vertical loads, a phenomenon that was further investigated by (Bekker, 2017) with inconclusive results. For simplicity, in the current investigation the maximum horizontal and vertical forces will be assumed to be occurring simultaneously for the stability calculations, which will provide a slightly overestimated required weight of the crown wall. Following, this "water hammer" is reflected from the wall leading to a decrease on the loading. Subsequently, the wave that is still progressing fully covers the wall, the pores in the armour and sublayers are filled with water, which results in large values for both forces (and a slightly smaller overturning moment compared to the one during the initial impact) (Pedersen, 1996).

As mentioned in the previous chapter, the time evolution of the horizontal wave force component can be described by the peak force (dynamic load) and the more slowly varying (quasi-static load or reflecting) part of the impact (Pedersen, 1996). As the wave pressure varies along the crown wall, a pressure distribution is formed. By integrating this pressure distribution, the wave force is calculated. In Figure 14 the pressure distributions from the experiments of (Martin, 1999) are shown, where the dynamic pressures are indicated in A with higher pressures on the unprotected part of the wall and the quasi static load in B where the armour has less influence. According to (Martin et al., 1999), "when the wave impinges the crown wall after breaking in the armour slope, the first peak is generated during the abrupt change of direction of the bore front due to the crown wall, while the second peak occurs after the instant of maximum run-up and is related to the water mass down-rushing the wall".

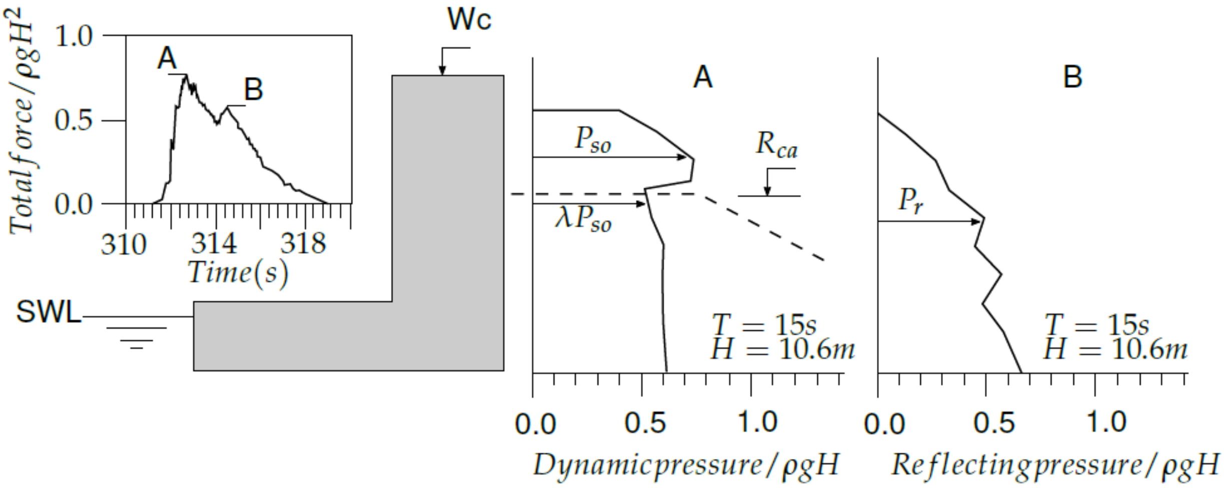

Figure 14. Experimental dynamic and reflecting pressure distributions for broken waves. Source: (Martin et al., 1999).

The maximum load situation that is most critical for the stability of the wall depends on the type of wave breaking and configuration of the armour (Pedersen, 1996). Usually, the first pressure peak is the largest and the secondary peak is smaller but lasts longer. However, in some cases (when H_s/R_{ca} is small and, or, B_a/L is large), the reflecting pressure peak can be larger than the dynamic pressure peak (Martin et al., 1999).

Two situations can be distinguished depending on the breakage or not of the waves on the armour slope. Due to breaking in front of the crown wall a lot of wave energy is already dissipated before hitting the superstructure (van den Bos and Verhagen, 2018). For a breaking wave impact a rapid rise of wave pressures on the upper part of the wall is registered, whereas the lower part, which is protected by the armour units situated in front of the structure, has not yet experienced any increase in pressure from the up-rushing wave, as mentioned. Shortly after, the full height of the wall is exposed to wave pressures. For a non-breaking (surging) wave impact, the pressure rise is more gentle and a clear difference between wave loading on the upper unprotected and the lower armour protected part of the wall is not present (Pedersen, 1996). An example of the pressure distributions in case of breaking and non-breaking waves can be observed in Figure 15.

The breaking of waves depends on their steepness. With increasing steepness, the likelihood of waves breaking on the breakwater slope and causing a dynamic impact also increases. When the wave steepness is low, a standing wave with quasi-static impact can be formed. “The most frequently used breakwater slopes are in the range $1.5 < \cot an(\alpha) < 2.5$. For rough seas, large wave height and period, or swell conditions, large wave period and moderate wave height, this range of slopes produces essentially collapsing wave breaking” (Martin et al., 1999). A characteristic of this type of breaker is that wave breaking occurs around the SWL. As a result, the waves hit the crown wall as broken waves if $R_{ca} > 0.8 \sim 0.9H_s$. In this case, the wave breaks on the slope, and hits the crown wall during the run-up process (Martin et al., 1999).

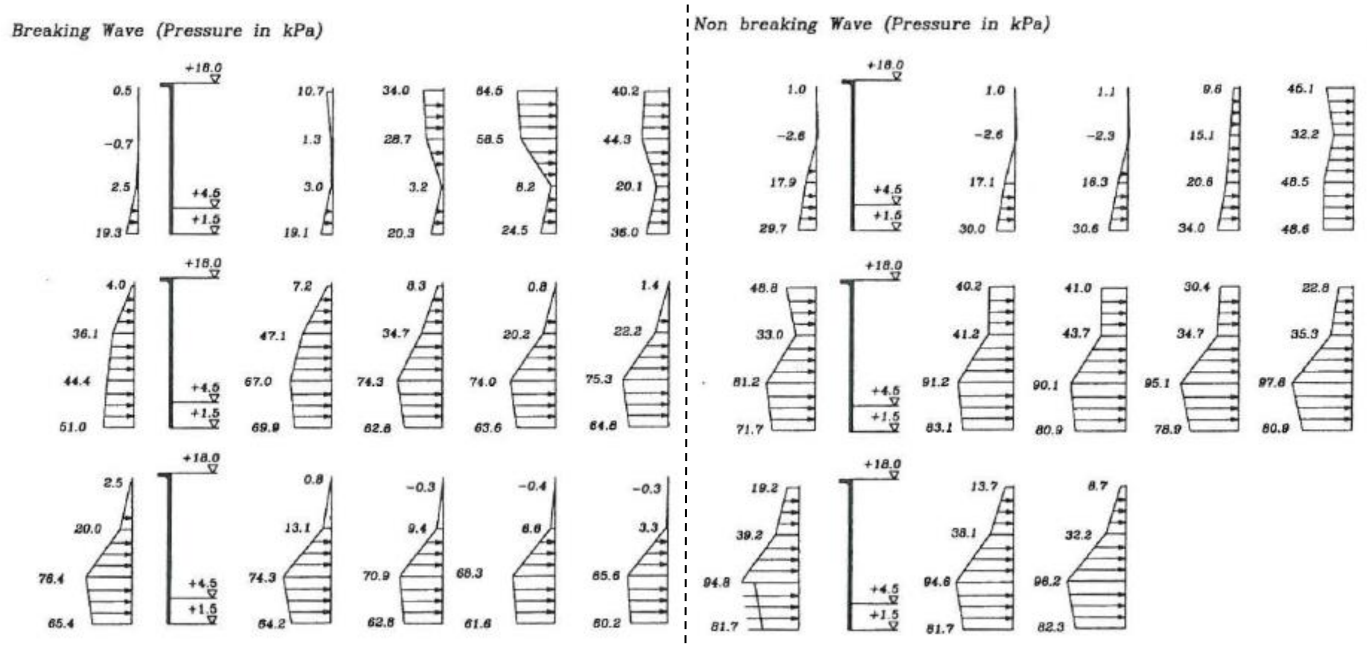

Figure 15. Examples of measured pressure distributions. Prototype scale. All levels in m. Time lag between recordings: flt = 0.37s. Wave incidence angle: f3 = 20°. Armour crest is located in level +14.0 m. Source: (Burcharth et al., 1995).

Concerning the uplift forces and their distribution on the slab of the crown wall, little knowledge is available. A reason for that according to (Pedersen, 1996) is the difficulty of measuring upward pressures in small scale flume tests because of strong scale effects related to the flow inside the porous media. In most of the existing formulations for its calculation a distribution of the wave pressure is assumed that acts over the full length of the crown wall base and equals the horizontal pressure value at the bottom of the wall from where it decreases linearly to zero at the end of the slab. This assumption is proven to provide results that are too conservative, especially in cases with an increasing freeboard, where not all of the material under the slab is saturated (Van Heemst, 2014, Molines, 2016, Bekker, 2017, Jacobsen et al., 2018). Recent investigations by (Bekker, 2017) and (Jacobsen et al., 2018) show that by increasing the freeboard between the bottom of the slab and the SWL, leads to decrease of the uplift forces. However, there are several knowledge gaps concerning the influence of several parameters like changes in the wave characteristics, breakwater slope, armour type and permeability, armour crest berm width and others to the magnitude and distribution of the uplift forces.

The crown wall is usually partly protected by the armour layer which due to the randomly placed armour elements is not uniform. That, along with the stochastic nature of the wave attack, results in the pressure distribution not being similar along the length of the crown wall. Thus, the forces are determined empirically, with the use of some assumptions. There are several semi-empirical methods available to calculate the magnitude of the wave force on the crown wall, which are treated in the following sections of this chapter.

3.1. Current design methods for calculation of pressures and forces

The various formulations available for calculating the wave forces on a crown wall were developed by performing scale model tests in wave flumes and making a fit of the data obtained, thus determining the wave forces and pressures distributions in an empirical way.

Eight different methods (and two extensions) for wave wall calculation are currently available and are presented in chronological order. The notation used by the authors themselves in their respective papers has been retained and is defined in the text following the equations associated with each method. Some of them provide pressures and others give forces as can be seen in Table 2. Each one is briefly addressed with its basic formulation and assumptions.

Table 2. Available design methods for the calculation of wave pressures or forces and their distribution.

Method	Output
Iribarren and Nogales (1954)	Pressure
Günback and Göcke (1984)	Pressure
Jensen (1984)	Force
Bradburry et al. (1988)	Force
British Standard -Maritime Structures (1991)	Pressure
Pedersen (1996)	Force
Martin et al. (1995 & 1999)	Pressure
Berenguer and Baonza (2006)	Force
Nørgaard et al. (2013)	Force
Bekker et al. (2018)	Pressure

The Rock Manual (CIRIA et al., 2007), which according to (van den Bos and Verhagen, 2018) is sometimes seen as a de facto informal design standard for breakwaters, includes the methods of Jensen (1984) and Bradbury et al (1988), the method of Pedersen (1996) and the one from Martin (1999). The method of Pedersen (1996) is a further refinement of the method proposed by Bradburry & Allsop (1988), which is an extension of the work of Jensen (1984) and was later extended by (Nørgaard et al., 2013) and (Bekker et al., 2018). In the following paragraphs the methods by Pedersen 1996 and Martin et al. 1999 are described in more detail as the most broadly applicable method and the one that best represents the physical problem, respectively. The method by Iribarren and Nogales is not investigated in more detail in this study because it the oldest and less accurate method and is based on only one breakwater geometry. The geometry is atypical and therefore it is not recommended to apply it to a different breakwater design (Negro Valdecantos et al., 2013). In addition, the method does not address the uplift pressure, which is of concern in this study. The method by Berenguer and Baonza 2006 is interesting as it gives a detailed calculation for the uplift forces that includes the structure geometry and the freeboard, however the type of armour layer units and its porosity are not addressed, and it is only applicable for non broken waves, which is rarely the case in such structures (Martin et al., 1999).

Iribarren and Nogales 1954

The first to give a definition for the forces exerted on a crown wall on top of a rubble mound breakwater were (Iribarren and Nogales, 1954). The method only applies to the specific geometry that they recommended and assumes that the waves are broken before arriving at the superstructure (Negro Valdecantos et al., 2013). According to their findings, they provide a pressure diagram as shown in the following Figure 16.

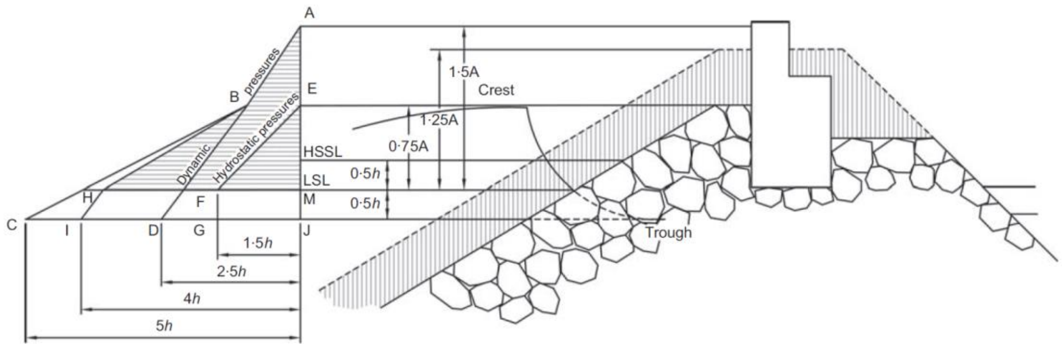

Figure 16. Pressure distribution according to Iribarren and Nogales. HSSL is the high still sea level, LSL the low sea level. Wave height equals 2h. Source: (Negro Valdecantos et al., 2013).

The representative height of the pressure at the wave crest and trough (according to Figure 16) are given by equations 3.1 and 3.2 respectively, the sum of them both results in the total horizontal pressure.

$$EB = 2\frac{V_h^2}{2g} = h \tag{3.1}$$

$$JC = 2\frac{V^2}{2g} = 5h \tag{3.2}$$

Where h is the wave amplitude. According to the authors, the friction factor between the base of the crown wall and its foundation was assumed to be 0.5.

There are a few shortcomings of this method which is to be expected as it is the first and oldest one. Firstly, it does not address the uplift pressures at all. Secondly, the method does not asses the influence of the width of the protection berm located facing the crown wall, or the number of armour units in front of the wall, on reducing pressure (Iribarren and Nogales, 1954, Negro Valdecantos et al., 2013). Moreover, it does not indicate the wave height to be considered in the calculation. According to (Martin et al., 1999), this method is known to result in a quite conservative design.

Günback and Göcke (1984)

After failures of several rubble mound breakwater with crown walls between 1970 and 1981, such as the ones in Antalya and Tripoli, (Günback and Göcke 1984) performed a study to investigate the reason for the total breakdown of the Antalya breakwater in 1971 (Günback and Ergin, 1983, Günback, 1985, Van Heemst, 2014). The investigation is based on scale model tests, where eight different geometries were tested under the action of regular waves that break before reaching the crown wall.

Günback and Göcke (1984) proposed a method for assessing the wave pressure on a crown wall based on physical interpretation of the run-up process and its interaction with the structure. They considered that the maximum force is caused by an impact pressure, exerted by the water hitting the wall (they called it shock pressure P_m), and by a hydrostatic pressure (P_h), induced by the maximum water level reached by the wave run-up (Pedersen, 1996, Camus and Flores, 2004b, Günback and Göcke 1984). In that way, they separated the action of the waves on the vertical wall into two simultaneous distributions: a rectangular one (linearly reduced to 50% at the base of the crown wall because of the presence of the protective layer), which is associated with the kinetic energy of the wave and a hydrostatic one extended up to the end of the wedge run-up (Negro Valdecantos et al., 2013, Molines, 2016). Also, they proposed a triangular distribution for the up-lift forces, as shown in Figure 17, where the assumed pressure distributions are outlined. They used the described procedure to analyse the Tripoli and Antalya breakwater failures (Günback and Ergin, 1983, Günback, 1985), and found in both cases that the crown wall would fail under the given circumstances (Pedersen, 1996).

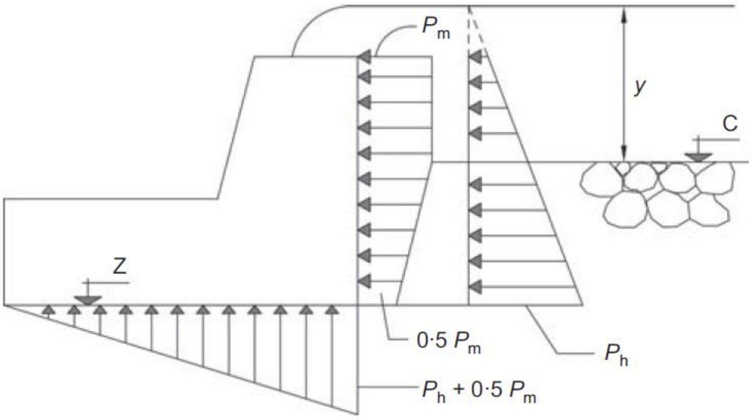

Figure 17. Pressure distribution according to the method of Günback and Göcke. Source: (Negro Valdecantos et al., 2013).

In order to calculate the pressures P_m and P_h a triangular wave run-up wedge is assumed on the breakwater slope, which can be observed in Figure 18. The fictitious run-up height R_u is calculated as if the structure had an infinitely long slope, according to equations (3 .3) and (3.4) (Pedersen, 1996, Negro Valdecantos et al., 2013).

$$R_u = 0{\cdot}4\xi H \quad \text{if } \xi < 2{\cdot}5 \tag{3.3}$$

Or

$$R_u = H \quad \text{if } \xi > 2{\cdot}5 \tag{3.4}$$

In which:

$$\xi = \sqrt{\frac{g}{2\pi H}}T \cdot \tan\alpha$$

Where:

- H is the wave height in m.
- g is the acceleration due to gravity in m/s^2.
- T is the wave period in sec.
- α is the angle of the armour layer’s slope to the horizontal in sexagesimal degrees.

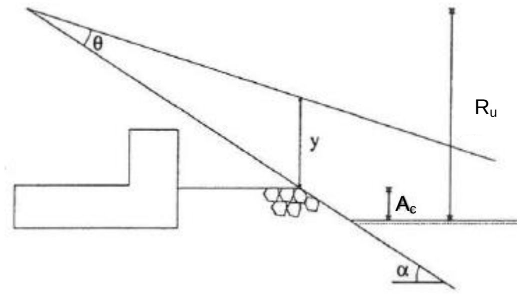

Figure 18. Triangular wave run-up wedge is assumed on the breakwater slope by Günback and Göcke. Source: (Pedersen, 1996).

The apex angle (θ) of the run-up wedge is assumed to be 15°. The vertical distance (y) over which to calculate the hydrostatic pressure component can be calculated as:

$$y = \frac{(\mathrm{R}_u - \mathrm{A}_c)}{sin\alpha}\frac{sin\theta}{\cos(\alpha - \theta)} \tag{3.5}$$

Where:

- y is the distance between the berm's crown and the end of the run-up in m.
- A_c is the height of the protection berm in m.
- R_u is the fictitious run-up height (height of the liquid vein) in m.
- α is the angle of the armour layer's slope to the horizontal in sexagesimal degrees.
- θ is the angle the liquid vein forms (Günback gives it a value of 15 sexagesimal degrees).

For calculating the pressures:

$$P_m = \frac{g\rho_w y}{2} \tag{3.6}$$

And

$$P_h = g\rho_w(y + s) \tag{3.7}$$

Where:

- ρ_w is the specific weight of the water in kN/m^3.
- S is the stretch of crown wall protected by the armour layer in m.

The total pressure is calculated by adding the hydrostatic pressure to the impact pressure. The maximum force occurs at the moment that the run up is the highest (Van Heemst, 2014).

Günback and Göcke also addressed the uplift pressure for the first time. They assumed it is equal to the local horizontal pressure at the bottom of the front side of the crown wall. This assumption is physically correct when dynamic effects are ignored, because the water pressure is isotropic, which means that the water pressure acting at a location is equal in all directions (Van Heemst, 2014). From the front side of the crown wall it reduces linearly to zero at the end of the slab as can be seen in Figure 17.

There are shortcomings in this method as well, as for example, the formulation requires a wave height as an input that is not specified, which also applies for the location the Iribrarren number refers to. Additionally, the range of application of the method is not clearly stated by the authors however they vaguely indicate that the methods can be applied to Mediterranean ports. Also, they consider that the armour berm in front of the wall gradually reduces the pressure at the protected part by 50%, but for that there should be at least three armour units in front of the crown wall. As the width of the layer is not included in the calculation, it must always be equal to the length equivalent to three units of the armour layer for the method to be applicable (Negro Valdecantos et al., 2013). Furthermore, they did not including a number of structural parameters (e.g. the berm width) and aside from some calculation examples of crown wall structures that had failed, they did not validate their method (Pedersen, 1996). Even for those examples, the eight cross-sections that the authors tested had all the same slope of 1:2, while the actual ports that the results where contrasted to (Tripoli and Antalya) had slopes of 1:1.5 and 1:2.5.

However, it must be recognized that they are the first to address the uplift pressures and that the theoretical approach that they developed, linking the wave pressure to a fictitious run up height, is still followed by most of the recent methods.

Jensen (1984)

Jensen (1984) studied the influence of variations in wave height (Hs), wave period (Tp) and sea water level on the maximum wave force per meter wall for 1000 waves ($F_{h_{0.1\%}}$). By analysing cite specific model tests, (Jensen, 1984a) concluded that with an increase of wave period, there is an increase in wave forces and that the influence of sea water level variations can be expressed through the crest freeboard. Thus, the wave force is directly proportional to $\frac{H_s}{A_c}$ (Jensen, 1984a, Molines, 2016, Molines et al., 2018). This correlation between crown wall crest freeboard and pressures is later used by more recent methods, however it still fails to include the influence of the freeboard of the base of the crown wall. He proposed the following expressions for estimating the horizontal ($F_{h_{0.1\%}}$) and vertical ($F_{v_{0.1\%}}$) wave forces per meter width on a crown wall, which are easy to apply but depends on calibrating two coefficients (A1 and A2). The expressions are:

$$F_{h_{0.1\%}} = \left(A1 + A2\frac{H_s}{A_c}\right)\rho g C_h L_{0p} \tag{3.8}$$

$$F_{v_{0.1\%}} = \left(A1 + A2\frac{H_s}{A_c}\right)\rho g C_b L_{0p} 0.5 \tag{3.9}$$

Where:

- A1, A2 are fitted dimensionless coefficients which depend on the armour slope, wave obliquity, core permeability and crown geometry.
- H_s is the significant wave height at the toe of the structure in m.
- A_c is the armour crest in m.
- ρ is the water mass density in kN/m^3.
- g is the gravity acceleration in m/s^2.
- C_h is the crown wall height in m.
- L_{0p} is the deep water wavelength associated to Tp in m.
- C_b is the length of the crown wall base in m.

The above equations are derived from only a limited range of parametric variations and structural layouts, as such, they should only be used within that range, which is given in Table 3. The equation can be used only in situations with moderate overtopping due to the influence of the wall height (Pedersen, 1996). According to (Martin et al., 1999), this method is not reliable because the influence of the armour geometry in reducing wave loading has not been addressed, the influence of the wave period is not represented adequately and, therefore, calculated wave forces deviate from measurements up to ±30%.

Table 3. Jensen 1984 method validity range. Source: (Camus and Flores, 2004b).

Parameter	Range / Value
A_c	5.6 – 10.6
H_s/A_c	0.76
H_s/L_{0p}	0.016

Bradbury et. al. (1988)

Bradbury et. al. (1988) investigated the effect of the slope on the loads over the superstructure, by performing experiments with five different rock slope configurations under irregular wave attack but did not draw clear conclusions about its influence. They fitted their own coefficients to equations 3.8-9 by (Jensen, 1984a) with good results, however these are only useful for geometries very close to the ones they tested (CAMUS and FLORES, 2004a, Molines, 2016, Pedersen, 1996). Specifically, the coefficients a and b by (Bradbury et al., 1988) had to be fitted for each geometry, and they obtained different coefficients than Jensen even for a similar structure (Pedersen, 1996). For cases which do not match the cross-sections indicated, new coefficients need to be obtained (Negro Valdecantos et al., 2013). The configurations used, as well as the coefficients for each can be seen in Figure 19.

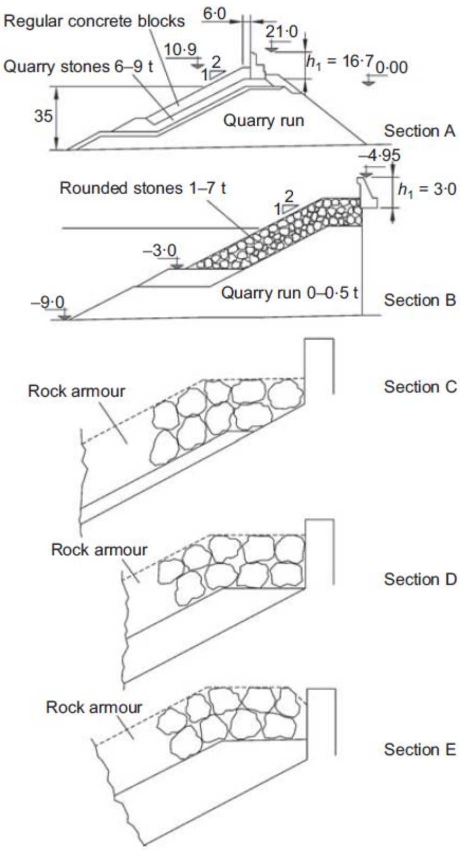

Section	Coefficients in equation a	Coefficients in equation b
Section A	0·054	0·032
Section B	0·025	0·015
Section C	0·043	0·038
Section D	0·036	0·031
Section E	0·013	0·011

Figure 19. Values of empirical parameters according to geometries tested by Bradbury et. al. 1988. Source: (Negro Valdecantos et al., 2013).

Similar to the method of (Jensen, 1984a), their formulation establishes a correlation between the significant wave height of a sea state, and the 0.1% of exceedance value of the wave force on the wall, for the different structure configurations. The distribution of the horizontal pressures is assumed to be uniform and rectangular. The vertical pressures triangular with a value of F_H/h_f at the front side and zero pressure at the landward side (CAMUS and FLORES, 2004a, Negro Valdecantos et al., 2013, Bradbury et al., 1988).

Bradbury et. al. (1988) proposed the following equation for the maximum horizontal force F_H:

$$\frac{F_{\mathrm{H}}}{(\rho g h_{\mathrm{f}} L_p)} = \frac{aH_{\mathrm{S}}}{A_{\mathrm{c}}} - b \quad (3.10)$$

Where:

- h_f is the height of wave wall in m.
- L_p is the peak period wavelength in m.
- a, b are empirical coefficients as shown in Figure 19.

The rest of the parameters are the same as used in the method by Jensen.

They provide substantially less data on the uplift force and the pressure distributions on the crown wall (Pedersen, 1996). They assume that the maximum vertical pressure coincides with the maximum horizontal pressure. The maximum vertical force is calculated by:

$$F_V = (\rho g B_c L_p / S)(a H_S / A_c - b) \qquad (3.11)$$

Where:

- S is a safety factor.
- B_c is the width of the crown wall in m.

The method proposes a coefficient of friction μ with a value of 0.50 for calculating the wave wall's stability. The formula does not include the armour layer's width, nor any reduction in the pressures because of its existence (Negro Valdecantos et al., 2013). Similar to the method by (Jensen, 1984a), this one is also derived from a limited range of parametric variations and should be used within their range, given in Table 4.

Table 4. Parameter ranges used in model tests by Bradbury et. al. 1988. Source: (CIRIA et al., 2007).

Cross-Section in Fig. 15	Parameter ranges in tests		
	A_c	H_s/A_c	H_s/L_{0p} (S_{0p})
A	5.6 – 10.6	0.76 – 2.50	0.016 – 0.036
B	1.5 – 3.0	0.82 – 2.40	0.005 – 0.011
C	0.10	0.90 – 2.10	0.023 – 0.070
D	0.14	1.43	0.040 – 0.050
E	0.18	1.11	0.040 – 0.050

British Standard -Maritime Structures (1991)

According to the (British Standards Institution, 1991), with the assumption that waves do not break upon the crest structure, the wave pressure P_w (in kN/m^2) is assumed to be proportional to the difference between the significant wave height and the crest height above still water, uniform over the whole height of the vertical face and is calculated from the following empirical formula which is similar to the ones from Jensen 1984 and Bradbury et. al. 1988:

$$P_w = KW_wL\left(\frac{H_s}{H_c} - 0.5\right) \qquad (3.12)$$

Where:

- H_s is the significant wave height at the structure site in metres.
- H_c is the crest height of rubble mound in m.

- L is the wavelength corresponding to the significant period in a water depth equal to that at the structure site, in metres.

- W_w is the unit weight of water (typical value for fresh water = 9,81 kN/m^3 and seawater = 10,05 kN/m^3).

- K is a dimensionless coefficient (limited model testing) and is varying from 0.025 to 0.19 for (from rounded stones to Tetrapods). A value of 0.25 is suggested for preliminary calculations.

In (British Standards Institution, 1991) a separate formula for the uplift pressures is not provided. It is assumed that in the case of no crawn wall key, a uniform uplift pressure equal to the horizontal pressure on the vertical face should be assumed to act beneath the base of the structure. This diminishes fairly uniformly towards the leeward edge of the superstructure but the value of the minimum pressure will depend upon the permeability of the layers immediately beneath it. “The pressure generated under the crest structure will depend on the level of its foundation relative to the height of the wave run-up. Decrease of uplift pressure from the seaward side to the land side will depend on wave uprush level, wave period and permeability of the founding layer” (British Standards Institution, 1991). Although the formula is provided in a widely used manual, the experiments that is based upon, the parameters that were tested or its validity range are not stated.

Pedersen (1996)

Pedersen (1996) developed a semi-empirical method based in a theoretical approach similar to (Günback and Göcke 1984), where the wave force on a crown wall is linked to the run-up height, combined with a parametric analysis of the results of small-scale physical model tests under the action of non-breaking irregular waves. He performed 373 different tests, with about 5000 waves each, to derive his formulation (Van Heemst, 2014, Pedersen, 1996). According to (Nørgaard et al., 2013), the tests were limited to deep and intermediate water conditions and as such are not validated for depth limited design conditions which are present at many sites. Double-layer randomly-placed rock and Dolos armours as well as double-layer (flat and randomly-placed) Cube armours were tested. According to (Pedersen, 1996) the type of armour did not significantly influence wave forces on crown walls (Molines et al., 2018). He concluded that the maximum forces were generated only by wave impact. The formulation allows for the estimation, for a sea state, of the horizontal force, tilting moment and uplift pressure with a 0.1% of exceedance probability (CAMUS and FLORES, 2004a, Pedersen, 1996).

Pedersen assumed that the impact pressure, p_m is determined by the stagnation pressure that corresponds to the up-rush velocity at the edge of the armour crest, based on a hypothetical run-up wedge. The wave collapses (stagnation) perpendicularly against the wall with a velocity equal to the up-rush velocity at the crest edge, which creates the impact pressure (CIRIA et al., 2007). The hypothetical run-up wedge that is used for calculation is depicted in Figure 20.

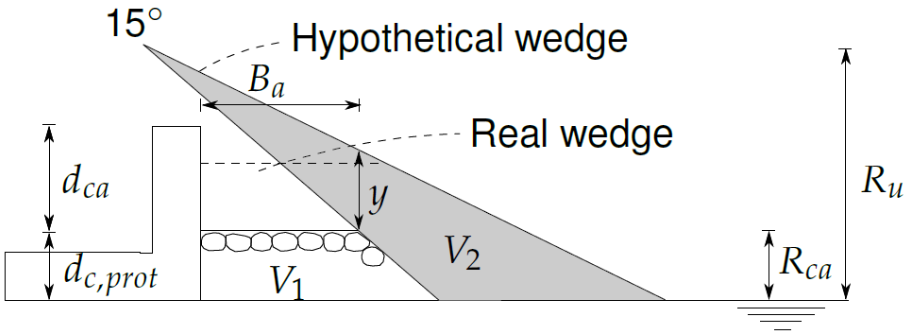

Figure 20. Run-up wedge assumption included in the method by Pedersen 1996. Source: (Pedersen, 1996).

Pedersen first calculates the impact pressure on the unprotected crown wall. Secondly, this value is reduced to obtain the pressure for the protected part of the crown wall. As such, the pressure model proposed has two rectangular distributions, one for the zone protected by the crest berm and the other for non-protected zone (see Figure 21). The horizontal impact pressure is calculated for the unprotected part of the crown wall. A reduction of 50% is applied to calculate the horizontal pressure at the protected part of the crown wall. This value is independent on the breakwater geometry, for example the number of stones used for protecting the crown wall. As such, it appears to be arbitrary parameter (Van Heemst, 2014).

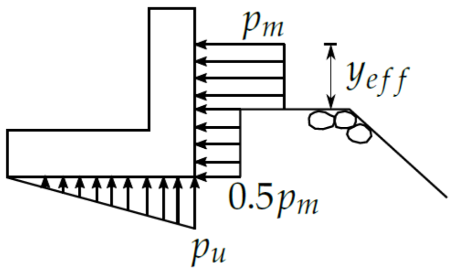

Figure 21. Pressure distribution according to Pedersen 1996. Source: (Pedersen, 1996).

The horizontal force is obtained from the pressure records by spatial integration of both pressures. The variables used in the calculations can be seen in Figure 22.

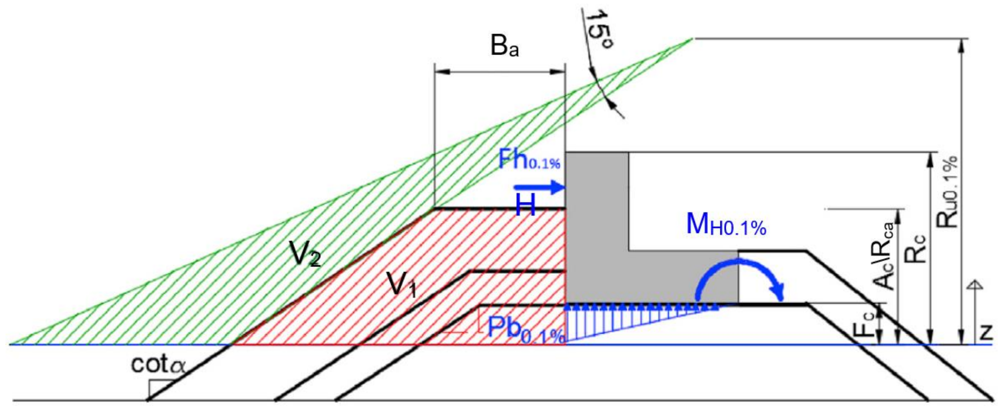

Figure 22.Variables used by Pedersen (1996). Source: (Molines et al., 2018)(modified)

Based on the above, the pressure due to the horizontal wave impact is defined as:

$$p_m = g\rho_w(R_{u0.1\%} - A_c) \tag{3.13}$$

Where:

- A_c is the vertical distance from SWL up to the armour crest in m.
- $R_{u,0.1\%}$ represents the run-up level exceeded by 0.1% of the waves according to (Van der Meer and Stam, 1992) in m.

The corresponding equations as formulated by (Van der Meer and Stam, 1992), which depend on the breaker parameter, ξ_m (Iribarren number that corresponds to mean period T_m) are given below in equations 3.14 to 3.17. The method is referring to an exceedance of 0.1%, meaning that the calculated run up height is surpassed by 0.1% of the waves of the wave field.

For $\xi_m \leq 1.5$

$$\frac{R_{u,0.1\%}}{H_s} = 1.12 \cdot \xi_m \tag{3.14}$$

And for $\xi_m > 1.5$

$$\frac{R_{u,0.1\%}}{H_s} = 1.34 \cdot \xi_m^{0.55} \tag{3.15}$$

With a maximum limit for the run-up (for permeable structures P > 0.4) of:

(3.16)

$$\frac{R_{U,0.1\%}}{H_s} = 2.58$$

Where:

$$\xi_m = tan\alpha / \sqrt{H_s / L_{0m}} \tag{3.17}$$

With the impact pressure known, the horizontal wave force can now be calculated. This is done in equations 3.18 to 3.20. The thickness of the run-up wedge y is calculated by:

$$y = \frac{R_{u,0.1\%} - R_{ca}}{sin\alpha} \frac{sin 15^\circ}{cos(\alpha - 15^\circ)} \tag{3.18}$$

And the effective height of the impact zone y_{eff} by:

$$y_{eff} = min[\frac{y}{2}; d_{ca}; 0] \tag{3.19}$$

Where d_{ca} is the unprotected height of the crown wall in m., it is equal to R_c-A_c and can be observed in Figure 20. If $R_{u0.1\%} < A_c$, then a value of $y_{eff} = 0$ should be used.

Using these, the total horizontal force which is exceeded by 0.1% of the waves can be calculated as:

$$F_{H,0.1\%} = 0.21\sqrt{\frac{L_{0m}}{B_a}}(1.6 p_m y_{eff} + V \frac{p_m}{2} d_{c,prot}) \tag{3.20}$$

Where:

- B_a is the berm width of the armour layer in front of the crown wall (see Figure 20, Figure 22).
- V is equal to $Min\left\{\frac{V_2}{V_1}, 1\right\}$ in m^2, where V_1 and V_2 correspond to Figure 20 or Figure 22.
- L_{0m} is the deep water wavelength corresponding to the mean wave period in m.
- $d_{c,prot}$ is the protected height of the crown wall in m (see Figure 20 and Figure 9).

Pedersen (1996) also provides formulae for the wave generated turning moment, $M_{H,0.1\%}$ (Nm) corresponding to 0.1% exceedance probability, which is linked to the maximum load by:

$$M_{H,0.1\%} = aF_{H,0.1\%} = 0.55(d_{c,prot} + y_{eff})F_{H,0.1\%} \tag{3.21}$$

The uplift pressure is addressed less in his method; however, he presents an indication on how to determine the uplift force. He proposes a triangular distribution that satisfies the pressure continuity law at the seaward side of the crown wall slab and linearly reduces to zero at the heel of the superstructure. The uplift force is then obtained by integrating the uplift pressure distribution over the horizontal part of the crown wall. The uplift pressure, $p_{U,0.1\%}$ (or $p_{b,0.1\%}$) at the seaward corner of the crown wall base exceeded by 0.1% of the waves is calculated as:

$$p_{U,0.1\%} = 1.0V p_m \tag{3.22}$$

The above design equations 3.20 to 3.22 correspond to the central estimates. The standard deviations are given in Table 5.

Table 5. Standard deviations for the equations in the method by Pedersen 1996. Source: (Pedersen, 1996)

Corresponding equation	Standard deviation parameter	Value
3.20	σ (0.21)	0.02
3.20	σ (1.6)	0.1
3.21	σ (0.55)	0.07
3.22	σ (1)	0.3

An overview of the parameters used in the method by Pedersen is given in the following Table 6.

Table 6. Overview of the parameters used in the method by Pedersen 1996.

Parameter	Description	Dimension
p_m	Horizontal wave impact pressure	$N/m^2/m$
$R_{u,0.1\%}$	Run-up level exceeded by 0.1% of the waves	m
R_{ca} (A_c)	Vertical distance from SWL up to the armour crest	m
y	Wedge thickness	m
y_{eff}	Effective height of the impact zone	m
d_{ca}	Unprotected height of the crown wall	m
$F_{H0.1\%}$	Horizontal force which is exceeded by 0.1% of the waves	N/m
B_a	Berm width of the armour layer in front of the crown wall	m
V	Empirical coefficient	m
V_1, V_2	Volumes corresponding to Figure 20, Figure 22.	m^2
$M_{H,0.1\%}$	Overturning moment which is exceeded by 0.1% of the waves	Nm/m
L_{0m}	Deep water wavelength corresponding to mean period	m
$d_{c,prot}$	Protected (by armour) height of the crown wall	m
$p_{U,0.1\%}$ ($p_{b,0.1\%}$)	Uplift pressure which is exceeded by 0.1% of the waves	$N/m^2/m$

The validity of the equations proposed by Pedersen is limited to the following parametric ranges shown in Table 7. According to (Pedersen, 1996), for very long waves that do not break on the slope (surging conditions), the predicted values of the formula are higher than the ones observed in test.

Table 7. Parameter ranges for the method proposed by Pedersen 1996. Source (Camus and Flores, 2004b, Molines et al., 2018, Pedersen, 1996, CIRIA et al., 2007):

Parameter	Symbol	Range
Breaker parameter using T_m	ξ_m	1.1 – 4.2
Relative wave height	H_s/A_c	0.5 – 1.5
Relative run-up level	R_e/A_c	1.0 – 2.6
Relative berm width	A_c/B	0.3 – 1.1
Front side slope	$\cot\alpha$	1.5 – 3.5

The result of the Pedersen formulation is a wave force which is exceeded by 0.1% of the waves. As mentioned, his tests were quite extensive in quantity and duration which make the method quite reliable within its validity range. This method was also tested by (Camus and Flores, 2004b) outside its validity boundaries, providing the most reliable results between all the methods that they tested outside their validity ranges. He followed the reasoning of (Günback and Göcke 1984) for reducing the horizontal pressure by a factor of 0.5 at the protected part of the crown wall, independently of the breakwater geometry, which again appears as arbitrary.

As mentioned in the previous chapter, the influence of a freeboard is not taken into account in the formulations of Pedersen to calculate the uplift force. Also, Pedersen mentions the appearance of a phase lag between the occurrence of the maximum horizontal and vertical forces, but it is not addressed further or quantified.

Martin et. al. (1995 & 1999)

Martin et al. 1999 with minor modifications to their first proposal in (Martin et al., 1995), describe a method to calculate wave forces on crown walls for the case of regular waves, which follows the same reasoning as the one from (Günback and Göcke 1984) with the wave pressure being correlated to the run up height. The authors tested a small scale model cross-section of the Príncipe de Asturias Breakwater at the Port of Gijón (Spain) with 120 tonne (for the armour layer) and 90 tonne (for the core) randomly-placed cubes, which is a relatively permeable structure compared to conventional mound breakwaters. The method was compared to results from laboratory tests carried out by (Burcharth et al., 1995) and (Jensen, 1984b) obtaining fairly good agreement. Making use of their results, they introduced the influence of the type of armour through coefficients calibrated using the virtual run-up estimations (Molines et al., 2018, Martin et al., 1999, Nørgaard et al., 2013, Martin et al., 1995).

Another similarity between the methods of (Günback and Göcke 1984) and (Martin et al., 1999) is assuming an impact pressure and a hydrostatic pressure. The different aspect that (Martin et al., 1999) introduce is the distinction between two load situations, separated for two pressure peaks in the pressure distribution. One for the maximum horizontal impact pressure that is generated during the sudden change of direction of the wave bore front due to the impact with the crown wall, and one for the maximum horizontal hydrostatic (pulsating) pressure that occurs when the water mass rush down the wall after reaching the maximum run up (CIRIA et al., 2007). The authors consider that the dynamic pressure and the pseudo-hydrostatic (pulsating) pressure occur at different instants in time during the evolution of the run-up process. For both kinds of pressures, the formulation defines the horizontal force and uplift pressure, for one individual wave. Following, in order to determine the stability of the crown wall against sliding and overturning, they assess each of the two load situations separately and design based on the highest load (CAMUS and FLORES, 2004a, Molines et al., 2018, Martin et al., 1995, Martin et al., 1999).

The wave run-up height used by in this method is based on the surf similarity parameter in deep water ξ_0 and two empirical coefficients A_u and B_u which depend on the type of armour unit and are given in Table 8. An incoherence is observed in these parameters for the values adopted for cubes and blocks. A lesser run-up is obtained with the values for the cube-type elements than with the block-type elements. However, the opposite should be the case, as "cubes break the sheet of water less and they also shore up, presenting a smoother surface and, therefore, increasing the run-up figure" (Negro Valdecantos et al., 2013).

$$\frac{R_u}{H} = A_u\left(1 - e^{B_u \cdot \xi_0}\right) \tag{3.23}$$

In which:

$$\xi_0 = \frac{\tan\alpha}{\sqrt{\frac{2\pi}{g} \cdot \frac{H}{T^2}}} \tag{3.24}$$

Table 8. Parameters A_u and B_u for calculating run-up in the method by Martin et al. 1999. Source: (Negro Valdecantos et al., 2013)

	Rip-rap	Rock fills	Blocks	Cubes	Tetrapods	Dolos
A_u	1.757	1.370	1.152	1.05	0.930	0.700
B_u	-0.435	-0.600	-0.667	-0.670	-0.750	-0.820

Thus, the proposed model is based on the appearance of two out-of-phase peaks in time. The dynamic pressure peak, which is usually the largest peak but with a short duration, and the reflective pressure peak which lasts longer. The pressure distribution proposed by (Martin et al., 1995) can be observed in Figure 23. Both pressure peaks are related to the berm width, B, and berm height, A_c. The authors relate them to the dimensionless coefficients α, μ and λ, which depend on the wave steepness H/L, the relative berm width B/L, the number of armour units on the berm and they are calibrated from their tests (Nørgaard et al., 2013, Martin et al., 1999).

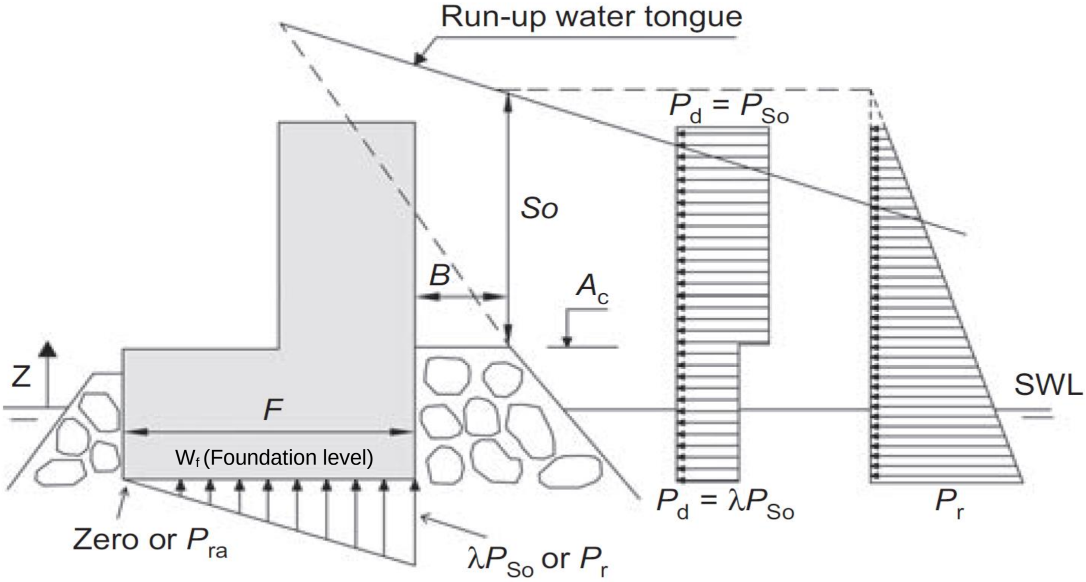

Figure 23. Pressure distribution according to Martin et al. 1999; SWL, low sea level. Source: (Martin et al., 1995)(modified)

The dynamic peak (impact) pressure P_{S0} in (N/m²) at the unprotected region of the crown wall face is calculated as:

$$P_{S0} = a \cdot \rho_w \cdot g \cdot S_0 \text{ for } A_c < z < A_c + s \tag{3.25}$$

In which:

$$S_0 = H\left(1 - \frac{A_c}{R_u}\right) \tag{3.26}$$

and

$$a = 2.9\left(\frac{R_u}{H}\cos\alpha\right)^2 \tag{3.27}$$

The dynamic pressure as function of z, which includes the protected crown wall face, is given by:

$$P_d(z) = \begin{cases} P_{S0} & \text{for } z > A_c \\ \lambda P_{S0} & \text{for } w_f < z < A_c \end{cases} \tag{3.28}$$

In which:

$$\lambda = 0.8 \cdot e^{-10.9 \cdot \frac{B}{L}} \tag{3.29}$$

The λ parameter reduces the pressure due to the presence of the armour layer. It is calculated by using the graph of Figure 24, which was obtained by means of reduced model tests or by eq.(3.29) which fits the experimental data.

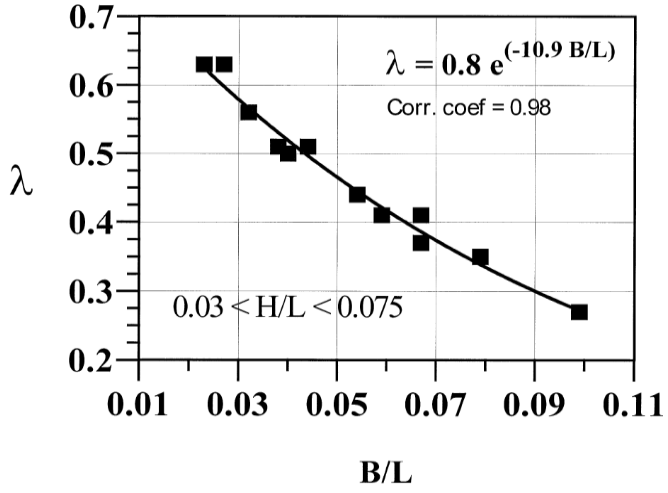

Figure 24. Experimental variation of λ vs. B/L (H and L measured at the toe of the breakwater). Source: (Martin et al., 1999).

P_r is the reflective peak pressure (pulsating pressure) which occurs immediately after the dynamic pressure peak and is described by:

$$P_r(z) = \mu \cdot \rho_w \cdot g(S_0 + A_c - z) \quad \text{for } w_f < z < A_c + S_0 \tag{3.30}$$

Where the dimensionless reduction parameter μ was evaluated experimentally from monochromatic wave tests and its value can be gained with the use of Figure 25. It depends on the wave steepness H/L and the non-dimensional berm width B/le. The parameter le is the equivalent size of the rubble units, and is calculated by:

$$\text{le} = \sqrt[3]{\frac{W}{\gamma_r}} \tag{3.31}$$

Where:

- W is the total weight of the armour unit.
- γ_r is the specific weight of the armour unit.

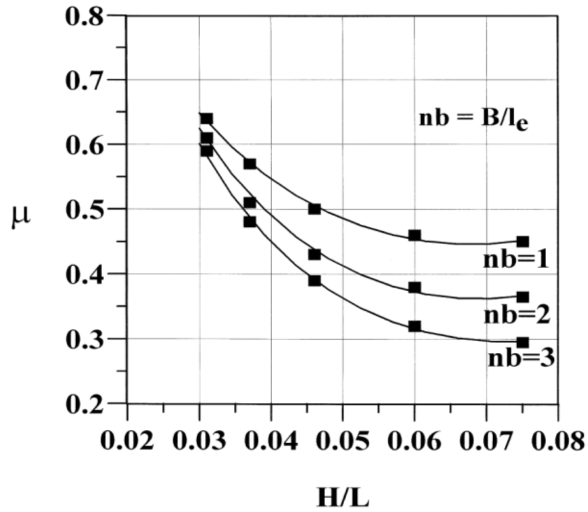

Figure 25. Experimental variation of μ vs. H/L and B/le as a parameter (H and L measured at the toe of the breakwater). Source: (Martin et al., 1999).

The trend of experimental values for μ form an exponential curve fitting to:

$$\mu = a \cdot e^{c(H/L-b)^2} \tag{3.32}$$

The best fit parameters a, b, and c in eq. (3.32) where derived by (Martin et al., 1999) for one to three armour units on the berm (for relatively large units and a porous core) and are given in Table 9.

Table 9. Best fit parameters for the calculation of μ in the method of Martin et al. 1999.

B/le	a	b	c
1	0.466	0.068	259.0
2	0.362	0.069	357.1
3	0.296	0.073	383.1

For the uplift pressures underneath the crown wall, a triangular distribution according to the continuity of pressures at the foot located on the attack side is assumed, which reduces linearly to zero. The reflecting pressure at the leeward side of the crown wall base is influenced by the porosity on which the crown wall is founded. If the foundations are below the sea level, (Martin et al., 1999) proposed a trapezoidal distribution including the hydrostatic pressure corresponding to the foundation level. There is no uplift pressure for the dynamic pressures if the foundation level is above high tide.

Thus, for the first peak, where dynamic pressures occur, the pressure underneath the seaward edge of the crown wall is approximately equal to λP_{S0}, while the dynamic pressures are negligible at the heel (landward edge). During the second peak, where reflecting (pulsating) pressures occur, if the base of the crown wall is low enough the uplift pressure at the seaward edge will be approximately equal to $P_r(z=W_f) = P_{re}$. At the heel they will be equal to P_{ra} as taken from Figure 26.

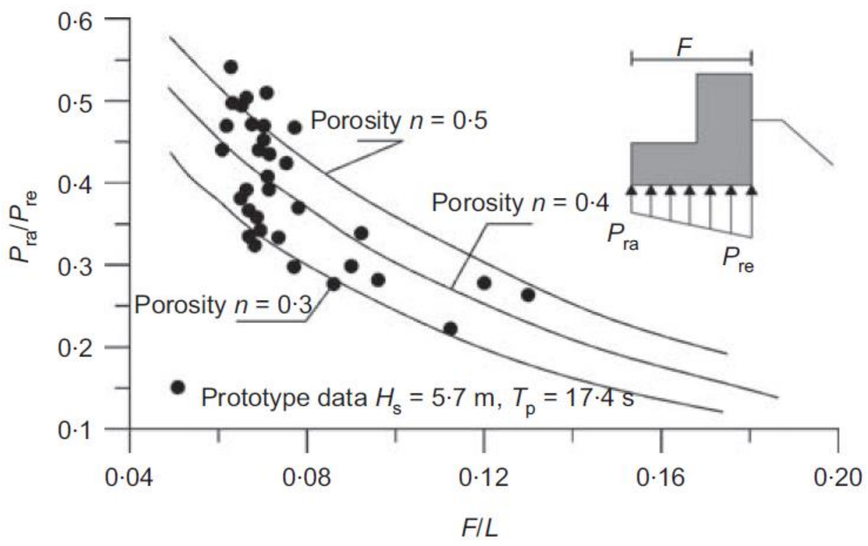

Figure 26. Reflecting (pulsating) pressure at the heel of the crown wall vs. F/L (L calculated at the toe of the breakwater) according to the method of Martin et al. 1999. Dots are experimental data from Gijon prototype (n≈0.4). Source: (Martin et al., 1999).

This method has been derived for individual waves and as such, the maximum forces and moments can be obtained using the maximum wave height of the sea state (CIRIA et al., 2007). In the following Table 10 the notation used in the method of Martin et al.1999 is defined.

Table 10. Overview of the parameters used in the method by Martin et al. 1999. Source: (Martin et al., 1999, Negro Valdecantos et al., 2013)

Parameter	Description	Dimension
α	Non-dimensional parameter containing information on the celerity of the mass of water s_0 wide at level A_c	–
S_0	The width of the sheet of water ascending on the slope at level A_c (maximum run-up level)	m
a	The angle formed by the main armour layer slope with the horizontal	deg.
A_c	Vertical distance from SWL up to the armour crest	m
λ	Nondimensional parameter introducing the berm's effect into the pressures on the wave wall's protected area	–
R_u	The maximum run-up, (maximum ascent of the sheet of water on the slope)	m
μ	Nondimensional parameter less than 1	m
ρ_w	Sea water density such that $\rho g=\gamma_w$ (kN/m^3)	kN.s^2/m^4
g	The acceleration due to gravity such that $\rho g=\gamma_w$ (kN/m^3)	m/s^2
B	Berm width of the armour layer in front of the crown wall	m
F	Length of the bottom part of the crown wall	m
W_f	The height of the base level relative to SWL	m
H	The design wave height (at breakwater toe)	m
L	The length of design wave (at breakwater toe)	m
le	The equivalent side of the main armour layer's units	m
z	The vertical coordinate with its origin at design sea level and positive in an ascending direction	m
P_{S0}	Dynamic peak (impact) pressure at the unprotected crown wall face	N/m^2
$P_d(z)$	Dynamic peak (impact) pressure as a function of z	N/m^2
$P_r(z)$	Reflective peak pressure (pulsating pressure)	N/m^2
P_{re}	Uplift pressure for reflective pressures on the seaward side of the crown wall slab	N/m^2
P_{ra}	Uplift pressure for reflective pressures on the heel of the slab	N/m^2

The authors present a thorough method that incorporates a lot of parameters and introduces factors not taken in to account in previous methods, such as the parts of the geometry of the structure (e.g. number of armour units in front of the crown wall) (Negro Valdecantos et al., 2013, Camus and Flores, 2004b). Their approach of separating the wave pressures into a dynamic and a pseudo-hydrostatic (pulsating) part, describes the physical process better than any of the other proposed formulas (Camus and Flores, 2004b). Moreover, they introduce the trapezoidal uplift pressure distribution in the case of the reflective pressures, affected by the porosity of the underlying structure. They don't however address the situation of an increasing freeboard of the base of the crown wall.

Furthermore, the method by (Martin et al., 1999) is based on tests with monochromatic waves and not irregular random waves. The authors suggest extending the method to random irregular waves by performing zero crossing analysis to obtain individual H and T from a synthetic surface elevation time series based on a spectrum with Hs and Tp. The breaking criterion by Miche is suggested to be applied to each individual wave in the time series (Nørgaard et al., 2013, Martin et al., 1999, Molines, 2016). However, the authors do not clearly specify the wave height, wavelength or period to be used in the calculations.

The method however is only applicable for waves that reach the crown wall as broken waves as it does not consider shock impact events. "Its range of validity is therefore limited to waves that reach the structure as broken waves and surging/collapsing waves on the breakwater slope (ξ> 3)" (CIRIA et al., 2007). In this way the designed crown wall is designed on the side of safety as it is assumed that the wave impact occurs at the same time both on the vertical wall and on the crown wall base (Molines, 2016). Additionally, the wave steepness range in the tests was 0.03 ≤ H/L ≤ 0.075 at the breakwater toe, which further reduces the applicability range (Nørgaard et al., 2013). Moreover, the angle of wave incidence may be up to ±20 sexagesimal degrees. The application region of the method is given in the following Figure 27.

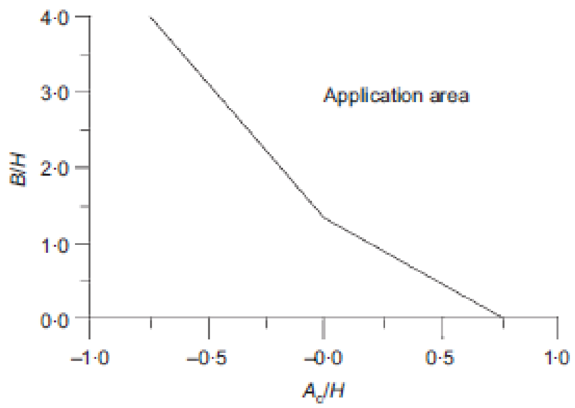

Figure 27. Range of validity of the method by Martin et al. 1992. Source: (Negro Valdecantos et al., 2013)

Another issue arises from the breakwater cross-section. As mentioned before, the method was proven for model tests of the Príncipe de Asturias breakwater in Gijón, Spain and that was the only cross-section geometry used (with varying berm width between tests). This breakwater has an unusual design where the core consists of heavy concrete blocks and the crown wall sits on them (Negro Valdecantos et al., 2013). Thus, leading to a very permeable material directly under the crown wall which can greatly affect the both the magnitude but also the relative timing between the uplift and horizontal forces.

Berenguer and Baonza (2006)

Berenguer and Baonza (2006) proposed a formula to determine the maximum forces on a crown wall exerted by non breaking waves. Their proposed formulations are the result of laboratory tests where some blocks of the armour layer were deliberately placed with a certain position to simulate the armour damage (Molines, 2016). Their formula considers the influence of the crown wall base level on the wave loads. The authors did not propose any distribution for the horizontal pressures and assumed a triangular distribution for the up-lift ones. Their experimental formulation was compared to 201 real Spanish breakwaters, where good agreement was found between the real crown wall weight and the calculated weight strictly for the condition of not sliding (Molines, 2016). The first step for determining the forces on a crown wall according to (Berenguer and Baonza, 2006), requires to calculate the run-up according to the formulation that is indicated in their proposed method:

$$R_{u2\%} = 0{\cdot}86\,\xi_p^{0{\cdot}54} H_S \gamma_\theta \tag{3.33}$$

Where:

- $R_{u2\%}$ is the wave run-up exceeded by 2% of the waves in m.
- H_s is the significant wave height (m).
- ξ_p is the Iribarren number referring to the length of wave associated with the peak period.
- γ_θ is the obliqueness factor according to De Waal's criterion (De Waal et al., 1996) where for short crested waves (Tp ≤ 7s):

  $$\gamma_\theta = 1 - 0{,}0022 \cdot \theta$$

  And for long crested waves (Tp > 7s):

  $$\gamma_\theta = 1 + 0{,}0004 \cdot \theta - 0{,}0001 \cdot \theta^2$$

- θ is the wave incidence angle, in sexagesimal degrees.

The horizontal force is given by:

$$F_X = \gamma_w h_h^{0{\cdot}5} L_p^{1{\cdot}5} \left(a \frac{R_{u2\%}}{A_c^{2/3} B^{1/3}} + b \right) \text{ if } (R_{u2\%} > R_c) \tag{3.34}$$

And

$$F_X = \gamma_w (R_{u2\%} - W_c)^{0{\cdot}5} \times L_p^{1{\cdot}5} \left(a \frac{R_{u2\%}}{A_c^{2/3} B^{1/3}} + b \right) \text{ if } (R_{u2\%} \le R_c) \tag{3.35}$$

The coefficients α and b depend on the force calculation, type of armour, Iribarren number and level of damage. They are obtained from Table 11.

Table 11. Coefficients for calculating the horizontal force in the method by Berenguer and Baonza. Source: (Negro Valdecantos et al., 2013)

Coefficient	Massive concrete blocks				Natural rock			
	No break		Break		No break		Break	
	$\xi_p \leq 3.25$	$\xi_p > 3.25$	$\xi_p \leq 3.25$	$\xi_p > 3.25$	$\xi_p \leq 3.25$	$\xi_p > 3.25$	$\xi_p \leq 3.25$	$\xi_p > 3.25$
α	0.0121	0.0118	0.0100	0.0093	0.0118	0.0103	0.0114	0.0044
b	-0.0094	-0.0119	-0.0067	-0.0084	-0.0115	-0.0129	-0.0103	-0.0024

If a crown wall with a base F is considered, then the total vertical (uplift) force is calculated by:

$$F_{YT} = F_Y + F_Y' = F_Y + \left(0{\cdot}017L_p - 0{\cdot}109F\right)\left(F - 0{\cdot}043L_p\right) \tag{3.36}$$

In which:

$$F_Y = \gamma_w h_h^{0{\cdot}5} L_p^{1{\cdot}5}\left(a\frac{R_{u2\%} - W_c}{A_c^{2/3}B^{1/3}} + b\right) \text{ if } \left(R_{u2\%} > R_c\right) \tag{3.37}$$

Or

$$F_Y = \gamma_w \left(R_{u2\%} - W_c\right)^{0{\cdot}5} \times L_p^{1{\cdot}5}\left(a\frac{R_{u2\%} - W_c}{A_c^{2/3}B^{1/3}} + b\right) \text{ if } \left(R_{u2\%} \leq R_c\right) \tag{3.38}$$

And

$$F_Y' = \frac{-0,217 \cdot F + 0,022 \cdot L_p + 0,012 \cdot L_p}{2} \cdot \left(F - 0,043 \cdot L_p\right) \tag{3.39}$$

The α and b coefficients of the foregoing equations are obtained from Table 12.

Table 12. Coefficients for calculating the vertical force in the method by Berenguer and Baonza. Source:(Negro Valdecantos et al., 2013)

Coefficient	Massive concrete blocks				Natural rock			
	No break		Break		No break		Break	
	$\xi_p \leq 3.25$	$\xi_p > 3.25$	$\xi_p \leq 3.25$	$\xi_p > 3.25$	$\xi_p \leq 3.25$	$\xi_p > 3.25$	$\xi_p \leq 3.25$	$\xi_p > 3.25$
α	0.0015	0.0004	0.0001	0.0014	0.0024	0.0014	0.0016	0.0001
b	0.0020	0.0028	0.0037	0.0017	0.0013	0.0012	0.0025	0.0034

Following, the moment due to the horizontal force:

$$M_X = \gamma_w h_f L_p^2 \left(a \frac{F_X}{\gamma_w h_f^{0.5} L_p^{1.5}} + b \right) \text{ if } (R_{u2\%} > R_c) \tag{3.40}$$

And

$$M_X = \gamma_w (R_{u2\%} - W_c) \times L_p^2 \left[a \frac{F_X}{\gamma_w (R_{u2\%} - W_c)^{0.5} L_p^{1.5}} + b \right] \text{if } (R_{u2\%} \leq R_c) \tag{3.41}$$

The α and b coefficients of the foregoing equations are obtained from Table 13.

Table 13. Coefficients for calculating the moment of the horizontal force in the method by Berenguer and Baonza. Source:(Negro Valdecantos et al., 2013)

Coefficient	Massive concrete blocks				Natural rock			
	No break		Break		No break		Break	
	$\xi_p \leq 3.25$	$\xi_p > 3.25$	$\xi_p \leq 3.25$	$\xi_p > 3.25$	$\xi_p \leq 3.25$	$\xi_p > 3.25$	$\xi_p \leq 3.25$	$\xi_p > 3.25$
α	0.113370	0.109490	0.119270	0.062150	0.123997	0.096651	0.121971	0.071884
b	190×10^{-6}	-80×10^{-6}	40×10^{-6}	60×10^{-6}	-2×10^{-6}	-67×10^{-6}	-72×10^{-6}	8×10^{-6}

And the moment due to the vertical force:

$$M_{YT} = F_Y (F - 0.018 L_p) + (F_{YT} - F_Y) \times \left(\frac{0.046 L_p - 0.217 F}{0.102 L_p - 0.651 F} \right) (F - 0.043 L_p) \tag{3.42}$$

An overview of the parameters used in the method by Berenguer and Baonza is given in the following Table 14.

Table 14. Overview of the parameters used in the method by Berenguer and Baonza 2006. Source: (Negro Valdecantos et al., 2013)

Parameter	Description	Dimension
F_X	Horizontal force exerted by waves on the wave wall	kN
F_{YT}	Vertical force (uplift pressure) exerted by waves on the wave wall	kN
M_X	Moment due to horizontal force	kNm
M_Y	Moment due to vertical force (uplift pressure)	kNm
γ_w	The specific weight of water	kN/m^3
W_c	The crown wall's base level relative to SWL	m
R_c	Vertical distance from SWL up to the crown wall crest	m
L_p	Local wavelength at the toe of breakwater connected to the peak period	m
A_c	Vertical distance between SWL and crest of armour	m
B	Berm width of the armour layer in front of the crown wall	m
F	Length of the base of the crown wall	m
h_f	Height of the crown wall	m

The validity of the equations proposed by (Berenguer and Baonza, 2006) is limited to the following ranges shown in Table 15.

Table 15. Validity range for the method by Berenguer and Baonza. Source: (Molines, 2016, Berenguer and Baonza, 2006).

Parameter	Symbol	Range
Breaker parameter using T_p	ξ_p	2.3 – 4.6
Relative wave height	H_s/A_c	0.7 – 1.7
Relative run-up level	R_e/A_c	1.0 – 3.1
Relative berm width	A_c/B	0.4 – 1.0
Front side slope	cotα	1.5 – 2.0
Berm width	B	3 armour elements
Length of the base of the crown wall	F	$0.027L_p$ – $0.1L_p$

Nørgaard et al. (2013)

The method proposed by (Pedersen, 1996) is based on scale tests in relatively deep to intermediate water. Tests with shallow water conditions and more accurate pressure sensors were carried out by (Nørgaard, et al., 2013), which showed that Pedersen overpredicted the loads for shallow water conditions. That led to them proposing an extension to the method of Pedersen adapting it to a new set of equations which gives more accurate results of wave loads for shallow water conditions but are also valid for intermediate and deep water.

Nørgaard et. al. (2013) tested double-layer rock armoured breakwaters and modified the term for run-up of (Van der Meer and Stam, 1992) in order to adapt the formula from (Pedersen, 1996) for shallow water conditions. The authors considered that if the incident irregular wave heights are Rayleigh-distributed then the wave run-up can also be assumed to be Rayleigh distributed. Thus, they proposed using $H_{0.1\%}$ both in shallow and deep water conditions to represent the virtual run-up exceeded by 0.1% of the waves ($R_{u0.1\%}$) in Pedersen's formula, by using $H_s/H_{0.1\%} = 0.538$ given by the Rayleigh distribution of (Battjes and Groenendijk, 2000), rather than the measured H_s (Molines et al., 2018, Molines, 2016, Nørgaard et al., 2013).

Furthermore, the authors noticed that the pressure gauges used by (Pedersen, 1996) could have been affected by dynamic amplifications, which led to the proposal of corrected fitted empirical coefficients (Molines, 2016, Nørgaard et al., 2013). The formulation for calculating wave forces on crown walls by (Nørgaard, et al., 2013) begins with the calculation of the maximum wave run-up as:

For $\xi_m \leq 1.5$

$$R_{u,0.1\%} = 0.603 \cdot H_{0.1\%}\xi_m \tag{3.43}$$

And for $\xi_m > 1.5$

$$R_{u,0.1\%} = 0.722 \cdot H_{0.1\%}\xi_m^{0.55} \tag{3.44}$$

Following with the total horizontal force:

$$F_{H,0.1\%,mod} = 0.21 \cdot \sqrt{\frac{L_{m0}}{B_a}} \cdot \left(p_m \cdot y_{eff} + \frac{p_m}{2} \cdot V \cdot d_{c,prot}\right) \tag{3.45}$$

They also suggested the overturning moment calculation as:

$$M_{H,0.1\%,mod} = (h_{prot} + \frac{1}{2} \cdot y_{eff} \cdot e_2) \cdot F_{Hu,0.1\%} + \frac{1}{2} \cdot h_{prot} \cdot F_{Hl,0.1\%} \cdot e_1 \tag{3.46}$$

In which:

$$F_{Hu,0.1\%} = 0.21 \cdot \sqrt{\frac{L_{m0}}{Ba}} \cdot p_m \cdot y_{eff} \tag{3.47}$$

$$F_{Hl,0.1\%} = \frac{1}{2} \cdot 0.21\sqrt{\frac{L_{m0}}{Ba}} \cdot p_m \cdot V \cdot d_{c,prot} \tag{3.48}$$

Where the coefficients e1 = 0.95 and e2 = 0.40 are introduced to bring the attack points of the loads into account for varying protection height of the structure (Nørgaard et al., 2013, Bekker, 2017) and the various variables in the equations are defined as the ones in the fore mentioned method by (Pedersen, 1996).

Nørgaard et al (2013) performed 162 new scale model tests, with different geometries from the ones tested by (Pedersen, 1996). As a result, the range of application of the Pedersen method, as well as its reliability, were extended. The authors divide the range into the case of a fully protected crown wall where d_{ca} = 0 and a partly exposed crown wall with d_{ca} > 0, which is listed in Table 16.

Table 16. Parameter ranges for the extended method proposed by(Nørgaard et al., 2013). Source: (Nørgaard et al., 2013, Molines, 2016)

Parameter	Symbol	Range	
		d_{ca} (R_c-A_c) =0 Protected Crown Wall	d_{ca} (R_c-A_c) >0 Exposed Crown Wall
Breaker parameter using T_m	ξ_{0m}	2.30 – 4.90	3.31 – 4.64
Relative wave height	H_s/A_c	0.50 – 1.63	0.52 – 1.14
Relative run-up level	R_e/A_c	0.78 – 1.00	1.00 – 1.70
Relative berm width	A_c/B_a	0.58 –1.21	0.58 – 1.21
Relative water depth	H_{m0}/h	0.19 – 0.55	0.19 – 0.55
Wave Steepness	H_{m0}/L_{0m}	0.018 – 0.073	0.02 – 0.041

Bekker (2018)

Bekker et al. 2018 conducted a series of scaled tests in order to investigate the effect of increasing crown wall base freeboard to its loading and stability. They concluded that when the freeboard increases from zero the previous methods greatly overestimate the forces and especially the uplift ones. During the experiments, (Bekker, 2017) observed that as the base level was increased, only a part of the base slab was becoming wet due to wave action. Thus, the distribution of the uplift force was not as previously assumed a triangle with a zero point at the landward end of the crown wall base slab, but in some cases the zero point was observed in shorter lengths.

They related the covered (wet or saturated) length x_c to the base freeboard for swell waves S_{0p} = 0.01 as:

$$X_c = B_c \quad \text{if } H_s/R_{ca} \geq 1.05$$
$$X_c = 0 \quad \text{if } H_s/R_{ca} \leq 0.64 \qquad (3.49)$$
$$X_c = B_c \times \left(2.41 \times \frac{H_s}{R_{ca}} - 1.54\right) \quad \text{if } 0.64 < H_s/R_{ca} < 1.05$$

And for storm waves S_{0p} = 0.04:

$$x_c = B_c \quad \text{if } H_s/R_{ca} \geq 1.35$$
$$x_c = 0 \quad \text{if } H_s/R_{ca} \leq 0.77 \qquad (3.50)$$
$$X_c = B_c \times \left(1.77 \times \frac{H_s}{R_{ca}} - 1.32\right) \quad \text{if } 0.77 < H_s/R_{ca} < 1.35$$

These values though come from visual observations and include a certain uncertainty.

From their measurements they concluded that also the shape of the upward pressure varies with varying wave height and freeboard. They propose two distributions as show in Figure 28, an S-shaped profile for small or zero base freeboard, where the base slab is wet in all its length, and a polynomial shaped profile for an increasing freeboard.

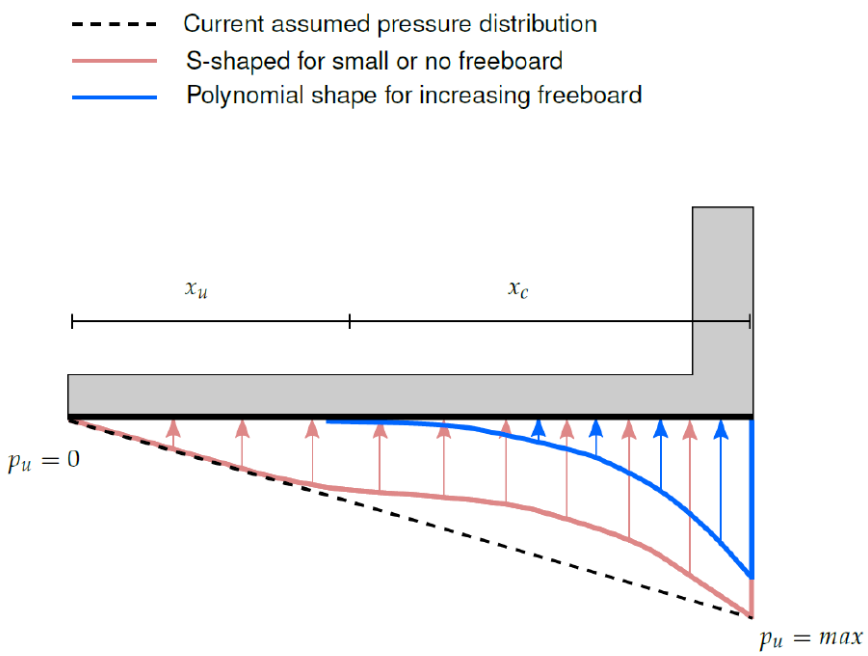

Figure 28. Uplift pressure distribution under base slab according to Bekker et al. 2018. Where x_c is the wet part of the base slab and x_u the dry part. Source: (Bekker et al., 2018).

Following, the authors proposed a reduction coefficient for the uplift pressures ($P_{U0.1\%}$ as calculated by the method of (Nørgaard, et al., 2013) which takes into account how much length of the base slab gets wet and correlate it to a dimensionless wave height $\frac{H_s}{R_b+d_a}$ (where R_b is the base freeboard and d_a is the protected crown wall height). The reduction coefficient by:

$$\gamma_v = 0 \qquad \text{for:} \qquad \frac{H_s}{R_b+d_a} < 0.62$$

$$\gamma_v = 1.2 \frac{H_s}{R_b+d_a} s_{op}^{-0.14} - 1.44 \qquad \text{for:} \qquad 0.62 \geq \frac{H_s}{R_b+d_a} \leq 1.30 \tag{3.51}$$

$$\gamma_v = 1 \qquad \text{for:} \qquad \frac{H_s}{R_b+d_a} > 1.30$$

Although it does not constitute a standalone method by itself, the proposal of Beker et. al can be regarded as an extension to (Nørgaard, et al., 2013). They are the first to investigate the uplift pressures in such detail and provide new insights in the pressure distribution, as well as the effect of the base freeboard. However, the results were validated only against one real world case, a breakwater extension in the port of Constanta in Romania. Thus, further validation of the results is needed. The validity of these relations is given in Table 17.

A drawback in their proposal is that their tests were conducted only for one specific cross-section and geometry, where only the wave conditions were varied. Thus, the influence of geometric variations, such as different armour elements, porosity or thickness, crown wall and breakwater geometry, are not included. Additionally, the base freeboard was varied by means of changes in the still water level, which induces changes on the incident waves. As such it is not clear which of the effects are results of the changed freeboard and which of the wave – structure interaction (such as waves breaking earlier on the breakwater slope).

Table 17. Range of application of formulas proposed by Bekker 2017 and Bekker et al. 2018. Source: (Bekker et al., 2018)

Parameter	Range
$H_s/(R_b+d_a)$	0.71 – 1.48
H_s/ L_{0p}	0.01 ; 0.04
R_b/R_{ca}	0.00 – 0.53
B_a /d_a	1.88
d_c / d_a	1.88
$d_{n50,c} / d_{n50,a}$	0.40
$(d_{n85} / d_{n15})_{,c}$	1.39
$(d_{n85} / d_{n15})_{,a}$	1.45
cota	2

3.2. Critical analysis of current methods

The preceding section presented the methods currently available for assessing the wave loads on crown wall structures. The interaction between waves and the structures is a complex process and the loads depend on the wave properties, as well as the geometrical properties of the breakwater and the crown wall. It can be concluded that none of the semi-empirical methods can be generally applied for accurately determining the pressures and their distributions, as they all come with their drawbacks.

Each method has a limited range of application, can be only used either for broken or non-broken waves and none of the methods succeed in including all of the factors that influence the loadings, although some include more parameters than others. For example, the influence of the type of armour on wave loads attacking the crown walls is negligible for authors such as (Pedersen, 1996) or introduced through fitted empirical coefficients in the methods by (Martin et al., 1999) where it affects the run-up or in the method by (Berenguer and Baonza, 2006) where it affects the forces. According to (Negro Valdecantos et al., 2013) who did a comparative analysis of some of the currently available methods, the methods were based on tests covering a broad series of sea states, although the slopes considered are of only two types: 1:1.5 or 1:2. Also, the range of the number of armour layer units used is limited, with the exception of (Martin et al., 1999). "This leads to the application of a method to slopes that largely diverge from those used in the tests on which those methods are based, possibly giving rise to erroneous results" (Negro Valdecantos et al., 2013). Some of the methods were based on tests based on limited breakwater cross-sections or peculiar designs (e.g. Martin et al. 1999), making their applicability uncertain to different geometries. Moreover, in most cases an arbitrary reduction of the horizontal force by 50% for the crown wall part protected by the armour layer was observed.

According to (Guanche et al., 2015), methods where waves are considered arriving non broken upon the crown wall (e.g. Pedersen 1966, Berenguer and Baonza 2006) tent to overestimate the forces, while (Martin et al., 1999) suggests that in most real-life cases the waves arrive broken at the crown wall. One cannot however draw the conclusion that methods considering broken waves necessarily provide better results. In some of the methods a lack of definition of the used parameters for the calculations, such as the wave height, was observed. Additionally, not all of the methods provide their range of validity and as such one needs to know the conditions under which the considered formulations were obtained before applying them. As the results from different formulations provide a high dispersion, (Negro Valdecantos et al., 2013) recommends using more than one method, as well as physical model tests, during the design stage before confirming the final design.

Furthermore, in order to review the available methods and give an idea of the divergences obtained when the formulations are applied outside their ranges of application, (CAMUS and FLORES, 2004a) compared measured values from their physical experiments to calculated values from the design methods of (Günback and Göcke 1984), (Jensen, 1984a), (Bradbury et al., 1988), (Pedersen, 1996) and (Martin et al., 1999) including also data out of the valid range of the formulations. Their evaluation showed that a better insight of the physical process can be achieved by means of the formulation by (Martin et al., 1999), due to the distinction between impact and pseudo-hydrostatic (pulsating) forces, and to the possibility of obtaining the probability distribution of the wave forces given that of the individual wave heights. Nevertheless, the method by (Pedersen, 1996) is the most reliable for the estimation of maximum horizontal forces, uplift forces and tilting moments of a sea state. This method showed also good results for F_H and M_H when used outside of the range of application of the method (CAMUS and FLORES, 2004a, CIRIA et al., 2007). For that reason, in addition to it being the most broadly used formula for practical applications, the method of (Pedersen, 1996) and its extension according to (Nørgaard et al., 2013) will be used for comparisons in this study.

Uplift pressures and forces

It can be concluded that the horizontal pressures and their distribution has been addressed quite more than the vertical ones. One of the reasons that the uplift pressure is less addressed, is that a different scale law must be applied to represent the water motion inside the breakwater core in a physical model (Pedersen, 1996). However, as seen in the previous chapter, to make a stability analysis for sliding or overturning of a crown element, both the horizontal and vertical forces must be determined.

In most of the proposed methods a linear, triangular distribution of the uplift pressures was assumed, with pressure continuity between the horizontal pressure at the lowest point of the frontal vertical wall and the vertical pressure at the seaward corner of the crown wall base. However, (Bekker et al., 2018) proposed different distributions of the uplift pressures and connected them with the crown wall base freeboard. All of the methods estimated the maximum up-lift forces using the maximum horizontal pressure at the lowest point of the vertical wall assuming they occur simultaneously, however according to (Bekker et al., 2018, Pedersen, 1996, Nørgaard et al., 2013) there is a phase lag between the appearance of the two maxima, especially in the case of steep waves, or for an increasing base slab freeboard.

Molines (2016) noticed that overestimations up to three times are possible when comparing the calculated up-lift force assuming pressure continuity with the measured up-lift force from small-scale 2D tests. The investigations by (Bekker et al., 2018, Jacobsen et al., 2018, Molines et al., 2018, Van Heemst, 2014) proved that the current design methods are greatly overestimating uplift pressures if the base of the crest wall is above SWL and that as the base freeboard increases, the forces decrease. Bekker et al. 2018, by investigating the effect of the base freeboard to uplift forces and connecting it to the wet part of the base slab, proposed a reduction coefficient for the uplift pressures of (Nørgaard et al., 2013). This however requires further validation as it is based on one experimental setup.

As fore mentioned, the uplift pressures have not been investigated as thoroughly as the horizontal ones. Parametric investigations regarding the influence of various parameters such as wave parameters, freeboard, breakwater slope angle, armour berm width, layer porosity and thickness that have been conducted for the horizontal pressures are yet to be implemented for the uplift ones.

4 Findings from literature and Study Approach

As explained in the previous chapter, the existing empirical formulations are predicting the uplift forces with large inaccuracies. Especially in the case of increasing freeboard of the base of the crown wall, where the pressures measured from physical and numerical experiments are significantly lower than the ones predicted from the empirical methods (Van Heemst, 2014, Bekker et al., 2018, Jacobsen et al., 2018). Both (Jacobsen et al., 2018) and (Bekker et al., 2018) observed an overprediction of up to 500% from the method of Pedersen. This probably is due to the fact that his experiments were with a crest wall element that had its base at the still water level, while the investigations of (Jacobsen et al., 2018) and (Bekker et al., 2018) were based on tests with an increasing distance between the base of the crown wall and the still water level (base freeboard).

Two other parameters that significantly impact the uplift forces are the pressure distribution shape and the wet part of the crown wall base. These two parameters determine the area over which the pressures are integrated to calculate the force. For example, even with the same pressure magnitude (at the seaward part of the crown wall base), if the distribution shape is changed or the wet area reduced, then the resulting uplift force could be a number of times smaller. Not taking into account these parameters can lead to overestimation of the vertical forces.

Furthermore, the phase lag between the maximum horizontal and vertical forces that appears during one wave, has been observed by different researchers as discussed in the previous chapter, but has not yet been quantified. All current design methods assume that these maxima occur at the same time. This becomes important, as if the two maxima do not appear simultaneously then the parameters used in equation 2.1 that decide the critical design condition will not be the maximum forces but reduced ones. For example, the critical condition could be at the moment of maximum horizontal force with an accompanying vertical force smaller than the maximum, or at a moment where both forces are lower than their maximum values. That would result in a notable reduction of the critical weight of the superstructure. In the present report, as critical weight (W_c) is used the weight that results from equation 2.1 (shown in the equation as F_G) while critical condition refers to the time were this critical weight gets its maximum value.

4.1. Knowledge gaps

The conducted literature study shows that there are a few knowledge gaps that need to be addressed. Firstly, the influence of the crown wall base freeboard needs to be investigated in more detail, as the existing literature is preliminary and based in only two and very similar setups, which also used a different approach for the varying freeboard. More precisely, (Bekker et al., 2018) chose to increase the base freeboard by decreasing the still water level (Figure 29, A). This method will hereby be referred as Method I. This method will also have an impact on the wave propagation, as the waves will start interacting with the bottom and the structure sooner. That will have an effect on wave run-up on the breakwater which is the main parameter affecting the wave loads. Thus, when comparing the different scenarios, differences could result from the different waves and wave-structure interaction rather than the changed freeboard.

On the other hand, (Jacobsen et al., 2018) chose to keep the same water level and raise the crown wall structure by adding more core material underneath it (Figure 29, B and Figure 30). This method will hereby be referred as Method II. The second approach corresponds better to the procedure of designing a breakwater, as the water level will be known and the height of the breakwater is to be decided. However, in that way the whole structure geometry is changed for each setup (e.g. larger volume of less permeable material underneath the crown wall, increased vertical wall unprotected height etc), which could again provide different results, which don't showcase only the effect of changing freeboard. It is thus interesting to acquire a better understanding of the effect and the differences between the two methods of increasing the freeboard.

Additionally, through numerical modelling small increments in freeboard can be implemented, which are difficult to implement in a laboratory setting, which can provide a better insight on the effect of increasing freeboard to the magnitude of the pressures, their distribution and the wet base length.

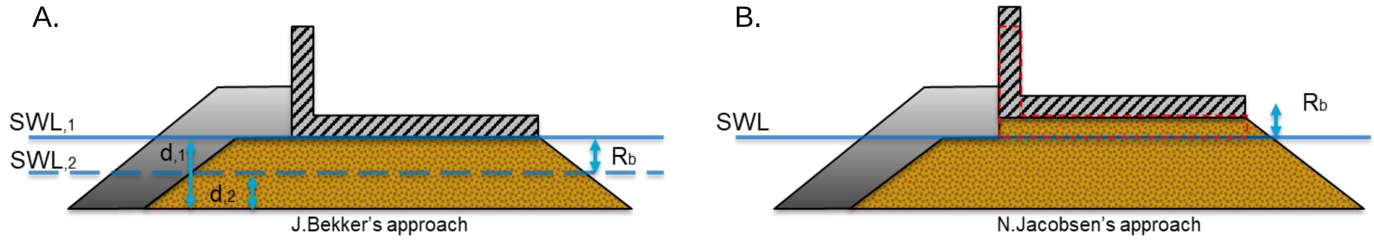

Figure 29. The different methods of increasing freeboard implemented by A) Bekker et.al 2018 and B) Jacobsen et al. 2018. SWL is the still water level, d is the depth and R_b the base freeboard.

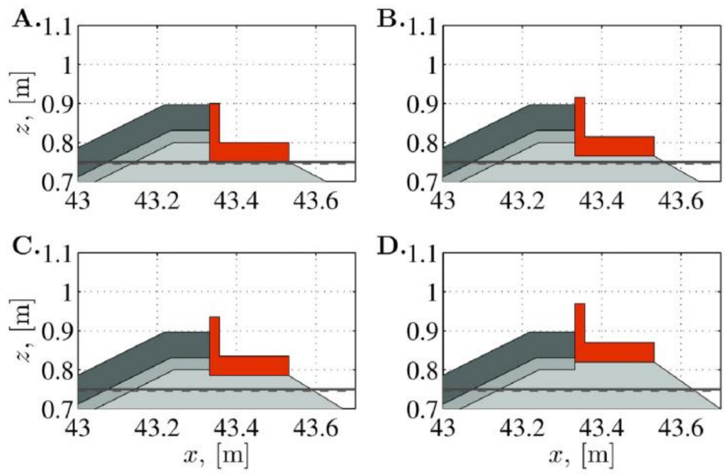

Figure 30. Examples of the layout from increasing the freeboard through increase in vertical displacement of the crest wall element from the numerical test of Jacobsen et al. 2018. A: R_b = 0.000 m. B: R_b = 0.015 m. C: R_b = 0.035 m. D: R_b = 0.070 m. Source: (Jacobsen et al., 2018)

Secondly, Bekker et. al 2018 presented three interesting findings that need to be further investigated and validated as they are only based on his dataset. These proposals are the shapes of uplift pressures distributions, the correlation between base freeboard and wet base length, followed by the relation between the wet base length and the uplift force as discussed in section 3.1. Through the last two, he proposed the reduction coefficient for the uplift pressures as calculated by the method of (Nørgaard et al., 2013) which was also discussed in section 3.1. All three proposals provide significant differences from the existing predictions from empirical methods and could help in a more accurate design process in the future. However, the author mentions issues with the pressure measurements and that his results are rather qualitative than quantitative. Moreover, the wet base length in his experiments was only observed visually and as such contains some uncertainty. As such his proposals remain to be further validated, refined and quantified through more tests.

Furthermore, the phase lag between the maximum forces is of great interest, however most conducted investigations relating to it were inconclusive. A reason for that could be that in physical experiments unrealistic peak pressures were observed due to air entrapment underneath the crown wall element and other similar 2D-effects as suggested by (Pedersen, 1996) and (Bekker, 2017). To resolve this, during post processing the pressures in previous investigations were heavily filtered, removing measurements appearing in specific frequency ranges, resulting in many peaks with large magnitude that appear within a short timespan to be removed, while the basic shape of the pressure distribution over time was preserved. This peaks that were removed due to filtering however are important when investigating the phase lag. Making use of a numerical model such as OpenFOAM and removing the entrapped air with the ventilated boundary condition that it incorporates, is expected to give a better insight to the phase lag between the maximum forces, both in the condition of zero freeboard, but also for increased one.

In addition, it becomes evident that there are large knowledge gaps when it comes to the effect of various parameters such as breakwater slope, layer porosity, protective berm width, height and other geometric parameters to the uplift forces. Parametric investigations have taken place in the past, studying the effect only to the horizontal forces (as the ones that resulted in the empirical methods discussed in section 3.1), but such investigations remain to be implemented for the uplift forces as well.

It is known that porosity affects the flow through the porous medium, but as such has an effect to the uplift forces. Changes to the layer porosity of the armour layer, filter layers and core have not been quantitively addressed. This can be divided to a number of investigations, one for instance is the effect various porosity values to the uplift forces. Another is the effect of changing the relative porosity between two adjacent breakwater layers. That could result in part of the flow to be diverted due to the change in resistance, which in return would affect the loading. Similarly, using different grading of the breakwater layers or varying the number of filter layers will play a role on the permeability of the structure and as such to the uplift forces.

Also, no literature was found which studies the effects of a changing breakwater slope to the uplift pressures. As the changing slope affects the wave-structure interaction and the portion of the wave energy that is reflected and dissipated within the breakwater it can by hypothesised that it will also affect the uplift pressures.

4.2. Methodology

This thesis addresses the stability of a crown wall element on top of a rubble mound breakwater. Based on the conducted literature study, the knowledge gaps were identified and it was concluded that the present state of knowledge is very limited when it comes to the prediction of the uplift forces and as such of the stability of crown wall elements. It is difficult to obtain an expression describing the physics of waves progressing and breaking on a breakwater slope, the flow through the porous medium and the impact between the water jet and the solid superstructure as it is affected by numerous parameters. A better insight can be gained by studying the effects of changing each parameter separately. The previous physical experiments have provided new knowledge, however there are several gaps remaining to be filled.

In order to acquire new information about the subject, a series of numerical tests were conducted where the variation of different geometrical parameters influencing the uplift forces was investigated. The choice of the numerical approach allows for easier parametric variations in smaller steps. The study goals were accomplished by a series of parametric numeric model simulations where each parameter is examined keeping all other influencing parameters constant. In this way a profound understanding of the importance of each parameter on the wave load exerted on the crown wall can be established.

The dataset of (Bekker, 2017) was also used for the analysis and to draw comparisons. The simulations are based on his physical scaled model and the process is thoroughly explained in the following chapter. In brief, the model was setup according to the dimensions and boundary conditions of the experiments of (Bekker, 2017), followed by a sensitivity analysis to some parameters in order to finalize the setup. Using that setup an effort to validate the model with the experimental results was made, however in order to reach forces within an acceptable error margin from the experimental values, the parameters (ventilated boundary layer) that had to be used in the model were not representing the physical values anymore. Thus, the validation is deemed not representative of the physics occurring. Following, a setup with values similar to the ones used and validated by (Jacobsen et al., 2018) was used as a reference case, to which the changes in freeboard were compared and analysed.

In order to reach the study steps that follow, pressures were measured along the vertical and bottom faces of the crown wall, along with the water surface at the toe of the breakwater and at points along the base of the crown wall. From these, timeseries of the base wet length, the horizontal and vertical (uplift) forces, the critical weight for sliding condition, the vertical (uplift) pressure distributions, as well as the phase lag between the maxima were determined.

Based on the identified knowledge gaps, the numerical model was applied in order to answer the following research questions:

1. What are the effects of different methods of increasing base freeboard on the crown wall loading and the base wet length?

In order to answer the first question, the following sub-goals are defined:

- Determining the maximum wet base length for varying freeboards with different methods of freeboard increasement.
- Determining the vertical and horizontal forces for varying freeboards with different methods of freeboard increasement.
- Determining the critical weight (sliding criterion) and critical condition for varying freeboards with different methods of freeboard increasement.
- Comparing the resulting forces to the ones calculated by empirical methods.
- Comparing the resulting maximum vertical forces to the ones calculated by the use of Bekker's reduction coefficient.

Used graphs: The dimensionless wet base length (X_c/L_p) against the dimensionless base freeboard (R_b/H_s) at the time of maximum F_V, the relative difference in maximum vertical force $F_{V,max}$ against the dimensionless base freeboard (R_b/H_s), the relative difference in maximum horizontal force $F_{H,max}$ against the dimensionless base freeboard (R_b/H_s), horizontal pressure distributions for varying freeboards, the maximum vertical $F_{V,max}$ and horizontal $F_{H,max}$ for freeboard increase methods against the dimensionless base freeboard (R_b/H_s) and the relative difference in maximum critical weight $W_{c,max}$ against the dimensionless base freeboard (R_b/H_s).

2. What is the shape of the uplift pressure distribution during critical condition for varying freeboards and how is it compared to recent proposed distributions shapes?

To answer this question, additional to the sub-goals followed in Study goal 1:

- Compare the resulting uplift pressure distributions, during critical condition, to the distributions proposed by Bekker et al.

- Compare the resulting uplift pressure distributions, during critical condition, for different methods of increasing the base freeboard.

Used graphs: The position on the crown wall against the measured pressures for varying freeboards R_b and both methods of freeboard increasement (uplift pressure distributions).

3. What is the time difference between the occurrence of maximum horizontal and vertical forces during the interaction with the maximum wave?

In order to answer this question, the following sub-goals are identified:

- Determining the lag between the occurrence of both force maxima by cross correlating the force time signals.

- Determining the vertical force at the moment the horizontal force is maximum and vice versa.

- Determining the time of maximum critical weight (sliding criterion) and the forces during that moment.

Used graphs: The dimensionless time lag (Time lag/T_p) against the dimensionless base freeboard (R_b/H_s) between maximum horizontal and vertical forces is analysed. The horizontal and vertical forces in different time moments against the dimensionless base freeboard (R_b/H_s). The dimensionless time lag (Time lag/T_p) between maximum horizontal and vertical forces against the breakwater slope.

4. What are the effects of breakwater slope variations on the horizontal and vertical forces, critical weight and uplift pressure distribution shape?

In order to answer this question, the following sub-goals are identified:

- Determining the wet base length for varying breakwater slopes.

- Determining the vertical and horizontal forces for varying breakwater slopes.

- Determining the critical weight (sliding criterion) and critical condition for varying breakwater slopes.

- Comparing the resulting forces to the ones calculated by empirical methods.

- Determining the uplift pressure distribution during critical condition for varying breakwater slopes.

Used graphs: The relative difference in maximum vertical force F_V, horizontal force F_H and critical weight W_c against the breakwater slope, the mean water surface elevation against the location along the flume (set-up).

5 Numerical Analysis

As briefly discussed in the previous chapter, it was decided to use numerical modelling with OpenFOAM for the investigations required to achieve the set study goals. The only literature found studying the effect of freeboard to vertical forces on crown wall elements are the ones from (Jacobsen et al., 2018) and (Bekker et al., 2018, Bekker, 2017). The dataset from the later was made available and is used in the current study. Thus, the pressure measurements from the physical experiments of (Bekker, 2017) where post processed and used as reference, while his physical setup was used as basis for the numerical model. In that way the numerical model could be calibrated and validated with the physical experiments and its resulting in higher certainty of the results.

The OpenFOAM numerical model and the waves2foam toolbox have however already been used successfully by (Jacobsen et al., 2018) for a similar case of studying the horizontal and vertical forces exerted on a crown wall element on top of a rubble mound breakwater and a good match was found with the physical experiments that the authors conducted to validate the model.

In the first section of this chapter firstly the used dataset of (Bekker, 2017) is presented following with a description of how the numerical model was set up. The second section focuses on the sensitivity analysis implemented on the setup of the first section in order to reach the final computational mesh and boundary conditions to be used. The fourth section details an effort that was made to validate the numerical model with the physical experiments and the results drawn from that. Finally, the last section gives an overview of the test cases uses for the investigation.

5.1. Numerical model setup

The numerical model was setup to represent the physical setup of J. Bekker. In this section the procedure details of setting up the numerical simulation are discussed.

Dataset of J. Bekker

J. Bekker conducted a series of scaled physical tests in the water laboratory of TU Delft. He determined the global stability of the crown wall by scaling its weight. Further, he used pressure gauges on the vertical and bottom faces of his crown wall element to measure the pressures induced from varying wave conditions and freeboards. The freeboard was changed by means of lowering the still water level in the wave flume. However, the author mentions issues with the pressure gauges, as well as with entrapped air underneath the crown wall influencing the measurements. Thus, they should be used in a qualitative mean rather than for quantitative comparisons.

Additionally, he ran a series of tests with varying the weight of the crown wall element under steady wave conditions in order to deduce the critical weight. In these tests the weight was progressively reduced until failure. Then it was increased again in smaller increments to acquire a more accurate critical weight. As such these measurements can be referred as quite accurate and used for quantitative comparisons.

The geometrical scale of the experiments was 1:30, the flume had an effective length of 42 m, width of 0.80 m and height of 1 m. The structure was located 28 m from the wave generator. The scaled structure was made up of the core and an armour layer with a slope of 1:2, a notional permeability of the breakwater P= 0.5

and made use of rock with density ρ_s = 2600kg/m^3. The crown wall element was an L-shaped wooden structure with length of 0.30 m, height of 0.15 m and width of 0.26 m. Through a series of tests the author measured that the friction factor μ_s was in the range of 0.73 to 0.75 for wet conditions of the crown wall base and 0.68 to 0.71 for dry conditions (These numbers refer to the crown wall section that is used in the current study, as J. Bekker had three different sections). Sketches of the setup and the main dimensions can be observed in Figure 31 (A and B) while the main parameters are presented in Table 18.

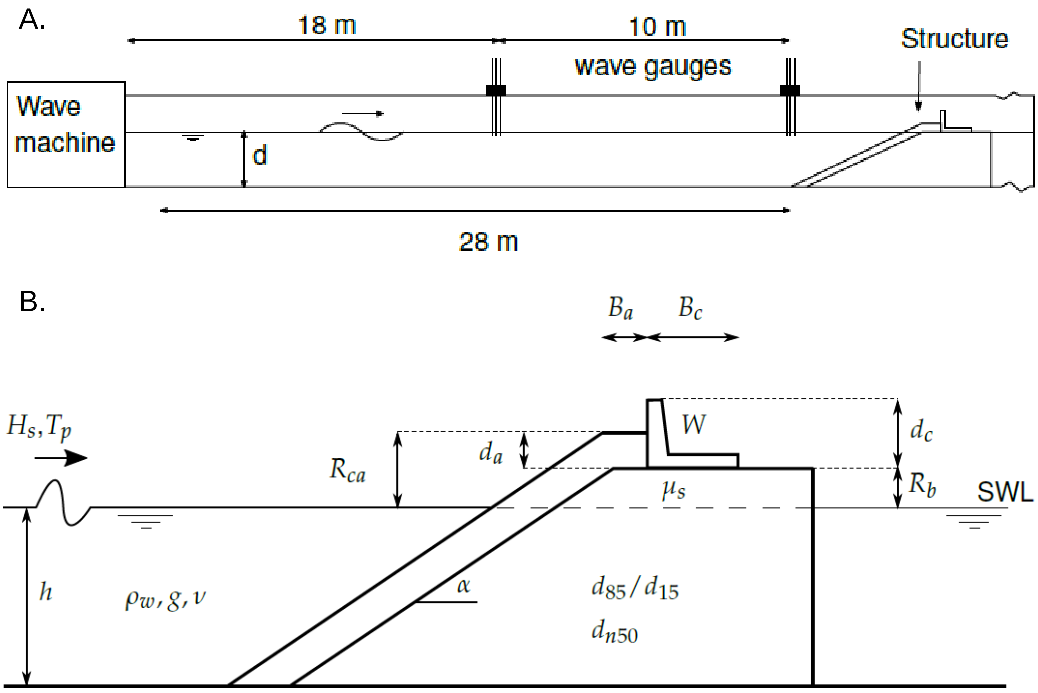

Figure 31. Setup of the physical experiment of J. Bekker. Source: (Bekker, 2017, Bekker et al., 2018).

Table 18. Parameters used in the physical experiments of J. Bekker. Source: (Bekker, 2017).

Parameter	Symbol	Range / Value	Unit
Significant wave height	H_s	0.09 – 0.16	m
Peak period	T_p	1.22 – 3.18	s
Water depth	h	0.56 – 0.65	m
Base (foundation) freeboard	R_b	0.00 –0.09	m
Armour crest freeboard	R_{ca}	0.08 – 0.17	m
Angle of structure slope	a	26.7	°
Armour berm width	B_a	0.15	m
Structure width	B_c	0.3	m
Crown wall height	d_c	0.15	m
Armour layer thickness	d_a	0.08	m
Core nominal grain diameter	$d_{n50,co}$	0.0145	m
Armour nominal grain diameter	$d_{n50,ar}$	0.0365	m
Core grading type	$d_{85}/d_{15,co}$	1.39	–
Armour grading type	$d_{85}/d_{15,ar}$	1.45	–
Weight of crown wall	W	30–700	N/m
Static friction coefficient	μ_s	0.72–0.77	–
Water density	ρ_w	1000	kg/m^3
Gravitation acceleration	g	9.81	m/s^2
Kinematic viscosity	v	10^{-6}	m^2/s

The locations in which the pressure gauges were located can be observed in Figure 32.

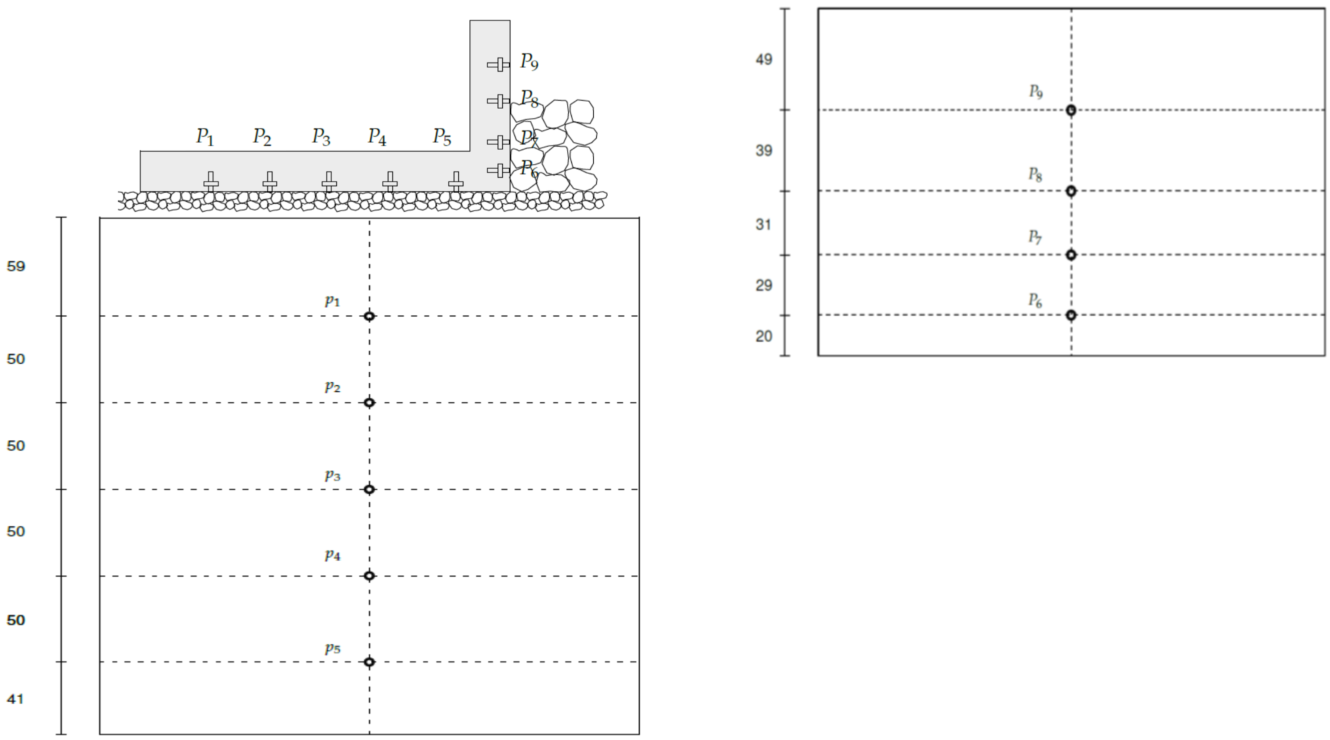

Figure 32. Locations of pressure probes along the crown wall in the physical setup of J. Bekker. Distances in mm. Source: (Bekker, 2017) (modified)

J. Bekker tested different wave conditions falling under two wave types, swell waves with s_{0p}= 0.01 (surging breaker type) and storm waves with s_{0p}= 0.04 (plunging/collapsing breaker type). He observed that in the first case waves surge up and down the slope of the breakwater with minor air entrainment, leading to less energy dissipation before hitting the structure in comparison to plunging/collapsing breakers. That resulted in higher exerted load on the crown wall from swell waves when compared to storm waves for same wave height and freeboard (Bekker, 2017). The author tested freeboards of 0 m, 0.03 m, 0.06 m and 0.09 m, that due to the scaling corresponds to 0.9 m,1.8 m and 2.7 m in reality. For each input wave condition the pressure time signal was recorded for all pressure gauges with an interval of 0.01 sec, as well as the resulting wave height and peak period at the toe of the structure.

In the present study the measured pressure gauges time signals were post processed accounting for all calibration and instrument effects and as there only a few pressure gauges along the faces of the crown wall they were interpolated and extrapolated along the length of the faces to create steps of 0.001m. For each timestep the part of the base that was wet was assumed to be where the measured pressures were positive. By integrating the pressures along the wet length, the horizontal and vertical force signals were computed.

Following, by making use of equation 2.1 a time signal of critical weights for failure against sliding was computed. These computed time signals and their maxima were then used in the analysis. The post-processing procedure is outlined in Figure 33.

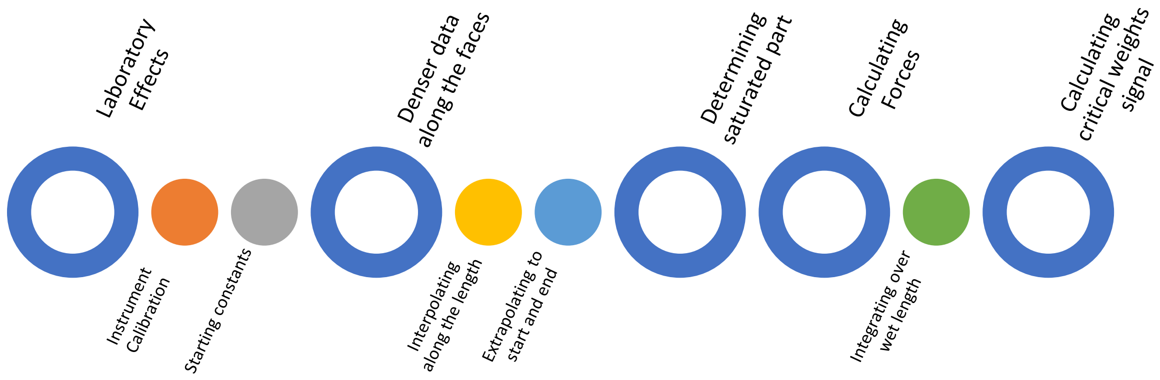

Figure 33. Procedure of post-processing the experimental data for the present study.

Due to restriction of time, one test case from the physical experiment was chosen to be used for validating the numerical model and followingly to be used as a reference base case for comparison with cases with parametric variations. The test case chosen is a swell wave condition with zero base freeboard (0.65m SWL), wave height 0.10295 m and peak period 2.55 sec. Under these wave conditions the crown wall was stable for 11.931 kg but failed for 11.427 kg which result in a critical weight of around 115 N. The reasons for choosing this specific condition are the higher loads exerted under swell waves mentioned above, a zero freeboard so that comparison with existing empirical methods is possible (they only account for zero freeboard) and finally as the critical weight was available (not available for all test cases).

Numerical setup

The simulation procedure in OpenFOAM involves many input parameters and different types of boundary conditions and flow parameters are possible to apply on the flow domain. If the combinations of input parameters and boundary conditions is not correct, then either the simulation will give error, or the results will not be accurate. Thus, for developing the model an iterative procedure of changing parameters and trial and error is required in order to develop a stable and accurate model. The case is developed using waves2Foam library and explained in this paragraph, by following the step by step simulation procedure of OpenFOAM. The procedure follows three steps, pre-processing, simulation and post-processing. The computational domain setup, meshing and introduction of boundary conditions are the main features of pre-processing. The post-processing includes the visualization and plotting of desired variables and results. These two steps are under user control, while the simulation is handled by OpenFOAM. The steps followed can be observed in Figure 34.

Figure 34. Procedure followed for the numerical simulations.

Computational Domain

One of the first tasks to be faced in Computational Fluid Dynamics (CFD) is the generation of a suitable computational mesh. The size and grading of the computational domain are very important factors which influence directly the time required for simulation, the accuracy of the results and the stability of the simulation. The computational domain for wave generation has three regions i.e. wave generation region, CFD simulation region and wave absorption region. The size of every region is defined based on different factors. If sizes of the regions are small, the fluid does not have enough space to develop the flow properly which affects the results. If the computational domain is large compared to what is required, it results in extra computational cost and complexity in handling mesh and results. Thus, choosing the size and how fine or coarse (number of computational cells) of the domain is a balance between accuracy and efficiency in means of computational expense and time.

As the geometry of the computational domain is rather simple, it was more convenient and efficient to develop the mesh of the computational domain using the blockMesh utility native to OpenFOAM. The computational domain can be built up from one or more blocks with various lengths, expansion ratios and grading in each of the three directions. An example can be observed in Figure 35 where the left image represents a simple grading on a single block where the numbers of cells in x and y directions are defined to create rectangles of the user's request. The image in the middle depicts vertical expansion on a simple block where the grid becomes vertically denser around the middle with an expansion ratio defined by the user. The right image depicts three blocks where the top and bottom blocks have vertical expansion becoming denser towards their lower and upper boundaries respectively (red lines), while the block in the middle is simple graded. The last approach is better fitted for use with waves2Foam as it is easier to keep an aspect ratio between the x and y directions closer to one, something important for stability issues. The procedure of using the meshing options is well documented in (Greenshields, 2018). After trial and error and due to stability issues of the model, a simple grading scheme was chosen for the computational domain were additional refinement was added on a later stage to areas of interest.

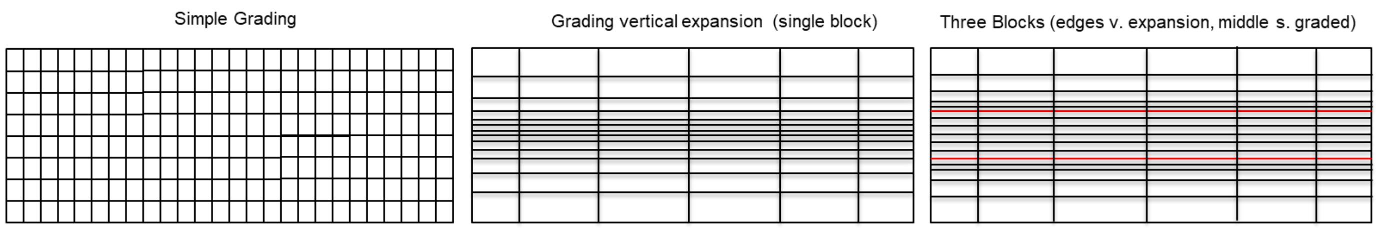

Figure 35. Example of some of the grading options for the Mesh available in OpenFOAM.

OpenFOAM cannot simulate totally 2D flow instead a 3D domain is required with a very small, one cell thickness as compared to other dimensions with empty boundary condition on the side walls. This prevents the fluid flow along the thickness hence flow behaves like a 2D flow. The height of the of the domain was chosen to be 1 m, the same as that of the flume used for the physical experiments. The length of the numerical flume however was chosen as quite shorter than the actual length of 42 m as that would make the model very demanding computationally. Thus, a length of 15 m was chosen for the numerical flume with the toe of the breakwater placed at 12 m from its start. That way the length was shortened as compared to the physical flume from the start and end of the flume, as can be observed in Figure 36. Hence, there is a length larger than 1.5 times the wavelength available in front of the breakwater.

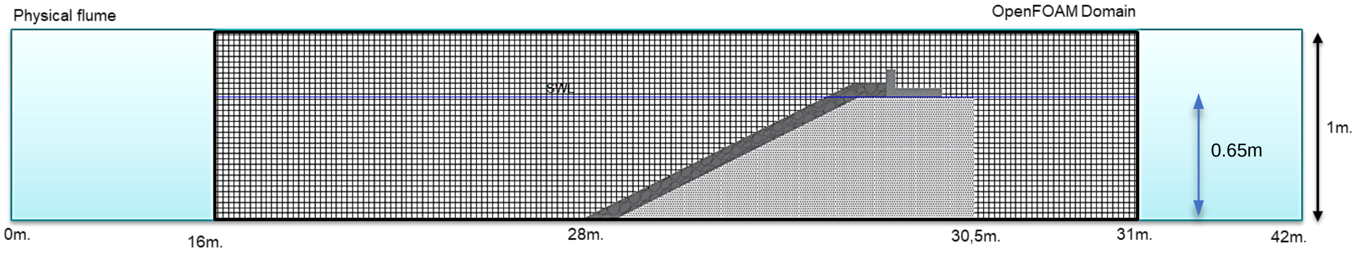

Figure 36.Sketch of computational domain in relevance to the physical flume. Dimensions not to scale.

The size and grading chosen for the domain can be observed in Table 19. For stability reasons the ratio d_x/d_y was kept close to one. The requirements of the grid proposed in literature are for the vertical direction 5 to 10 cells over a wave height in the area around the water surface and for the horizontal direction 100 to 150 cells over L_{0p}. Although under these requirements the chosen domain might seem too coarse (3.5 cells over wave height and 323 over L_{0p}), an approach of refining locally at areas of interest was chosen, which can provide a computationally cheaper solution. This is further explained in the following paragraph. The final selection of the computational domain was based on the performed sensitivity analysis which is discussed in the following section of this chapter.

Table 19. Size and grading of the computational domain (without local grid refinements).

Direction	Length [m]	Cells	d_i [m]
x-axis	15	485	0.0289
y-axis	1	34	0.0294

Apart from the domain definition, the types of surfaces comprising the boundaries of the computational domain are also defined in this stage. Each boundary is assigned a specific type depending upon its role in the flow domain as can be observed in Figure 37.

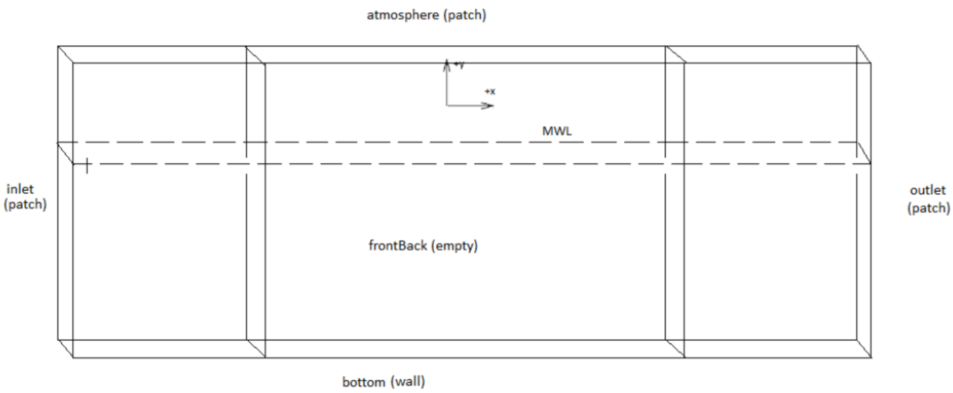

Figure 37. Computational Domain Boundaries and their assigned types.

Mesh Structures

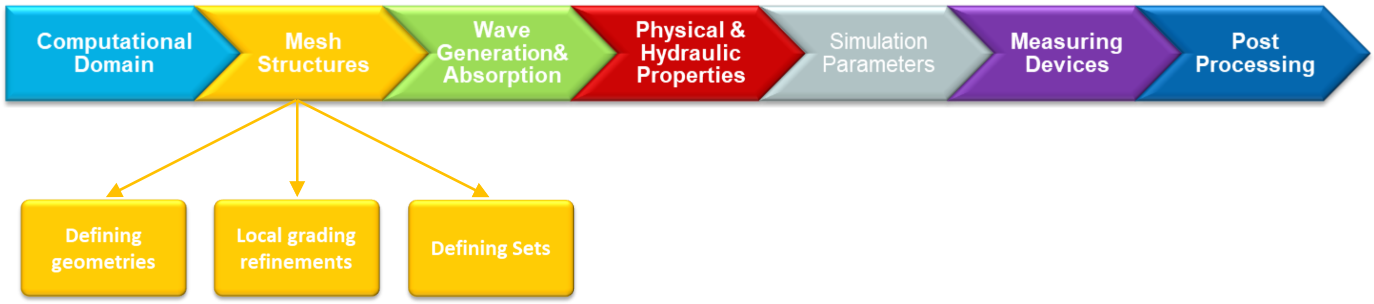

There is a variety of mesh generation techniques. As the geometries get more complex, and consist of multiple elements, the process becomes a complicated and tedious task. “Effort is required to ensure the generated mesh is of sufficient to both accurately represent the geometry and provide a high quality solution.” (Ingram et al., 2004).The most common approaches are using a structured body-fitted mesh utilizing a multi-block structure where blocks may overlap, or using a completely unstructured body-fitted mesh.

In the present study the generated static mesh comprises of the core, armour and crown wall with the dimensions of the physical experiment of J. Bekker. For the generation of the mesh an alternative approach followed with using Cartesian cut cells. “This conceptually simple approach “cuts” solid bodies out of a background Cartesian mesh, resulting in the formation of fluid, solid and cut grid cells.” (Ingram et al., 2004). In order to generate the cut cells the body surfaces are represented using polylines, whose knots are defined in an anti-clockwise direction and their coordinates are defined according to a CAD drawing.

After the geometries have been added in the domain specific surfaces are set with unique names and are divided into their own “sets” such that the waves2Foam tools can save calculation results along these surfaces instead of the whole domain, can allocate special grading refinement etc. Such surfaces for example are the bottom and vertical faces of the crown wall as can be observed in Figure 38.

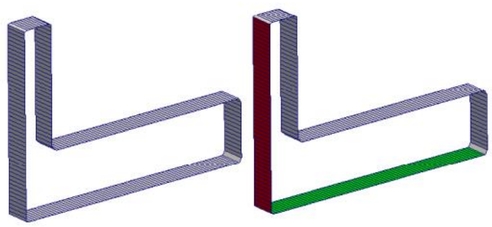

Figure 38. Division of the vertical and bottom surfaces of the crown wall block into separate sets.

As previously discussed, an approach of local grading refinement of the computational mesh was used. In order to do that the tool snappyHexMesh available in waves2Foam toolbox was used. This allows for a local refinement either within specific geometries or around them. Different levels of refinement can be added for user specified distances, where for each level of refinement the computational cells defined in the computational domain are divided into four cells. This way, one level of refinement will result in four cells instead of one, two levels of refinement in sixteen cells, three levels of refinement in sixty-four cells etc. An example can be observed in Figure 39. Considering the axis-wise grading the d_x and d_y are reduced by half for each refinement level. Thus, for the first refinement level d_x is 0.0144 m and d_y 0.0147m, for the second refinement level 0.0072 m and 0.0074 m respectively and for the third 0.0036 m and 0.0037 m respectively. This can provide a very fine grid in specified areas of interest keeping the rest of the computational domain grid coarse and the computational cost less.

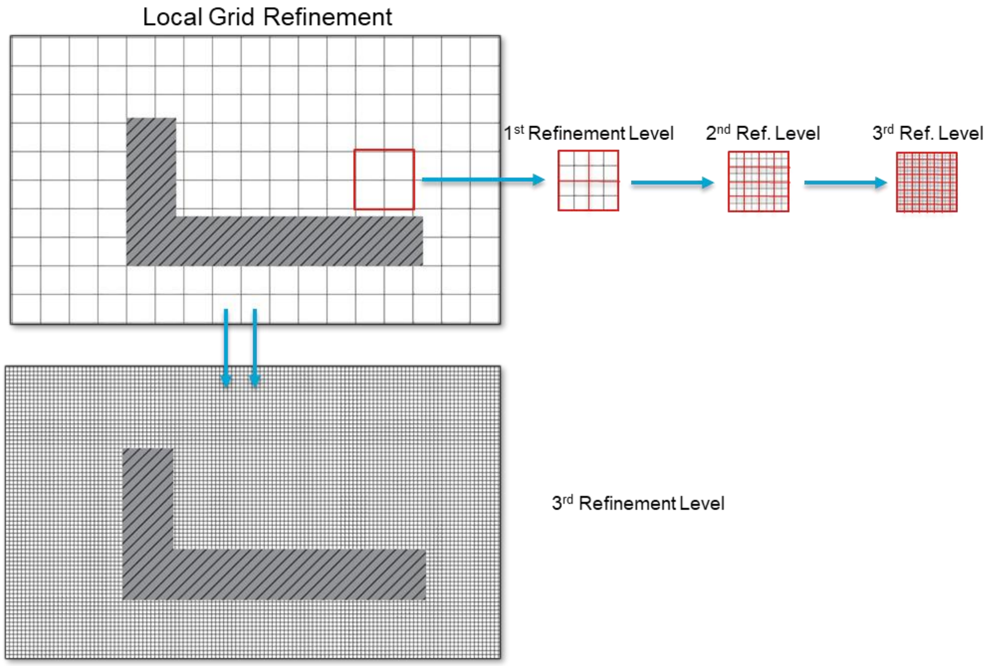

Figure 39. Local Grid Refinement example.

Through the sensitivity analysis process two local refinements were selected. The first was a refinement of one level in a zone around the water surface which will allow for a more detailed modelling of the free surface and more robust simulation. This was implemented by the addition of a rectangle geometry with length 13.55 m starting at the start of the numerical flume and vertically from 0.45 m to 0.8 m (highest point of the crown wall). Within that geometry the computational cells were refined once, as can be observed in Figure 40. In the following simulations for investigating the effects of freeboard, were the SWL was reduced, the rectangle was also widened so the water motion occurs within its boundaries. This way there are around 646 cells over L_{0p} and 7 cells over one wave height, which is deemed sufficient.

The second local refinement implemented was around the crown wall element as the interactions between waves and the element are the focus of these study and the measured pressures need detail. Three refinement levels where chosen. The refinement is happening gradually so there are no instabilities created due to the steep change from coarse to fine grading. The first refinement is in an area 18 cm around the crown wall, the second refinement in an area 6 cm around the crown wall and the third refinement 3cm around the crown wall. This way the cells close to the faces of the crown wall where the pressures are measured are approximately 3.65 x 3.6 mm. Choosing between two and three levels of refinement, as well as the distance around the crown wall to be refined was a balance between detail and computational expense as the local refinement greatly increases the number of computational cells in the domain. Both local grid refinements can be observed in Figure 40.

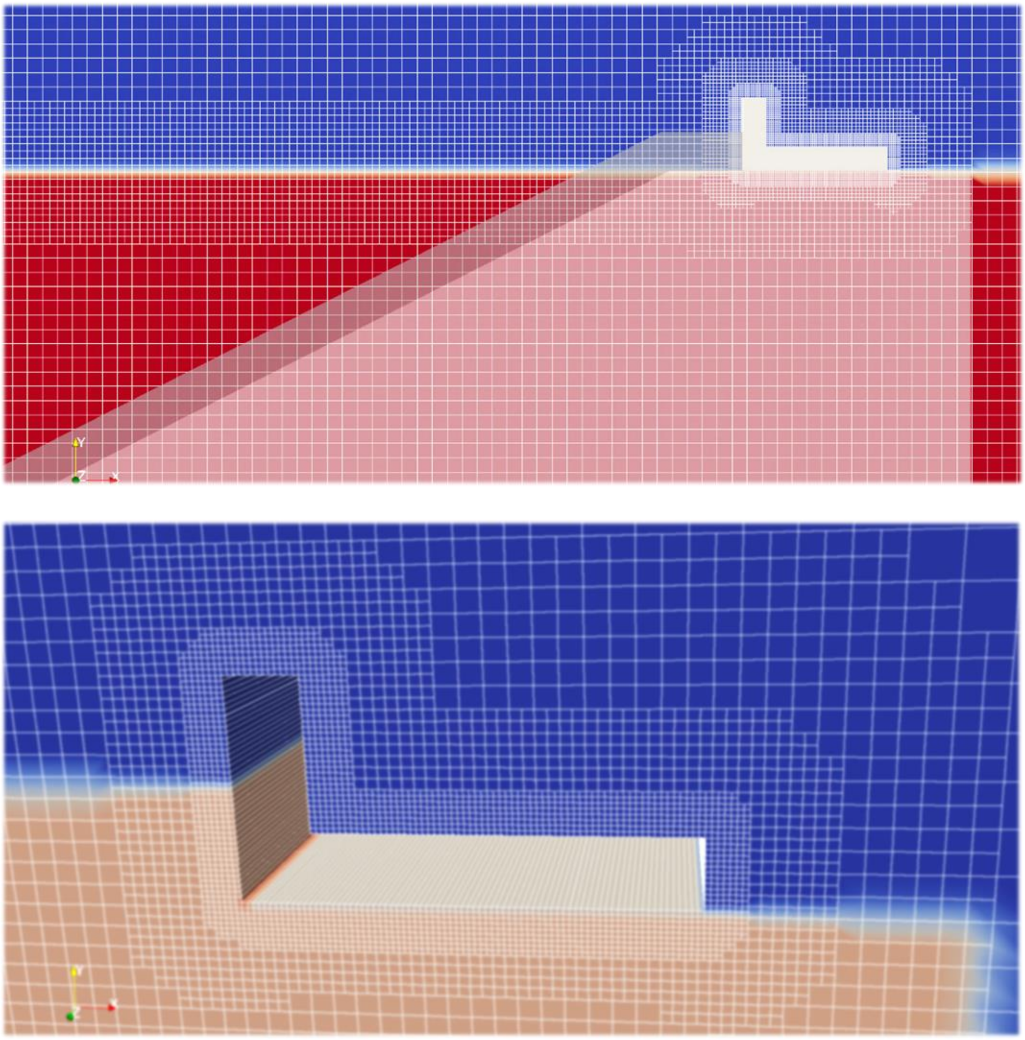

Figure 40. Local grid refinement around the free surface and the crown wall element. Image from post processing with Paraview.

Wave Generation and Absorption

Waves2Foam is not a complete model for free surface wave generation and impact calculations over structures, instead it is an OpenFOAM library for generating waves in the OpenFOAM domain and all the other involved operations are performed by OpenFOAM. Currently the method applies the relaxation zone technique (active sponge layer) and a large range of wave theories are supported and integrated in waves2Foam toolbox. Additionally, the user has the option to input other wave theories with desired relationships and input parameters. Moreover, the use of an external source for wave generation is possible by coupling OceanWave3D as a boundary condition (Paulsen et al., 2014, Engsig-Karup et al., 2009).

The first approach for wave generation was to use the available wave paddle signals from the physical experiment as an input to OceanWave3D. However, wave gauge measurements from the physical experiment were not available, an input which was considered necessary for validating the generated waves from the wave paddle. Thus, it was chosen to use a JONSWAP wave spectrum with inputs similar to the ones used by J. Bekker for generating waves instead. Thus, a JONSWAP wave spectrum was generated with inputs of H_s = 0.10295 m, T_p = 2.55 sec, γ = 3.3. For defining the spectrum in waves2Foam the water level and number of wave components is also required. The water level for the reference case was 0.65 m (0 base freeboard), which in the following cases for changing freeboard was reduced. The number of wave components choses was N= 100, which resulted from the calibration and validation of the model. As a wave spectrum is based on a statistical approach where completely different wave timeseries can lead to the same wave spectrum, a seeding random phase option is implemented where the first generation of the spectrum phases is random but for the following simulations the exact same waves are generated (same wave at a specific time moment). That allows for analysis and comparisons between different simulations in the time domain.

Following, the rectangular relaxation zones at the inlet (wave generation) and outlet (wave absorption) of the computational domain were defined. Relaxation zones keep the flow smooth by restricting the wave reflection and secondary wave components generation adjacent to the vertical boundaries. The VOF method allows the inlet relaxation zone to smoothly transform the analytical solution at its start, to a fully non-linear CFD solution at its end. Similarly, the outlet relaxation zone transforms the fully non-linear CFD solution to a no-wave (constant) condition at the outlet boundary through outlet relaxation zone. A weighing parameter is introduced that increases exponentially from 0, at the inlet, to 1 at the end of inlet relaxation zone as can be observed in Figure 41. Similarly, value of this weighing parameter decreases exponentially from 1 at the start of outlet relaxation zone to 0 at outlet (Figure 41).

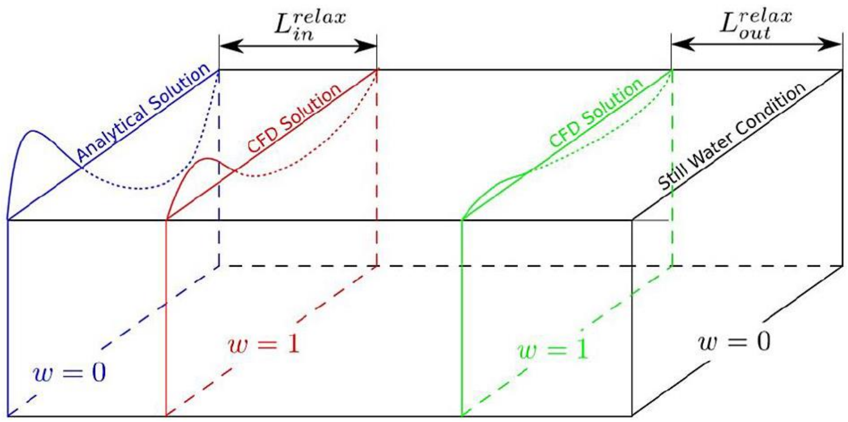

Figure 41. Illustration of Relaxation Zones. Source: (Wu et al., 2015).

Figure 42 shows the relaxation zones in the computational domain, where the gradual change of weighting can be observed. The inlet relaxation zone has a length of 2.48 m, while the outlet relaxation zone (type potential current) has a length of 1.36 m.

Figure 42. Relaxation zones in the model's computational domain (due to length middle part is cropped out). Post processing with Paraview.

Physical and Hydraulic properties

The major parameters defined are shown in Table 20. The values kept as default are not discussed. The layer porosity used in the physical experiment was not specified, however it was a rather porous construction where the notional permeability coefficient was found to be P= 0.5. By visual observation of the structure, use of prominent manuals such as (CIRIA et al., 2007) and the available material grading curves, as well as changes during the calibration and validation, the value for the layer porosity of n= 0.4 was chosen for both the armour and the core.

In Table 20, KC is the Keulegan–Carpenter number for the stones in eq.2.9. According to (Jacobsen et al., 2015), the KC number a parameter difficult to estimate, because of the rapid damping of the wave energy through the permeable structure. "..ideally the KC number should be used with a temporal and spatial distribution; the temporal variation to account for the changing hydrodynamics during an irregular time series." (Jacobsen et al., 2015). In this paper, an estimating approach was introduced based on the incident wave field and shallow water wave theory, which is also used to calculate the KC number for each case in the current study. A similar approach has been used in (Higuera et al., 2014a) and (Jensen et al., 2014a). The values given in Table 20 are for the reference case, while as the water level is varied, so are the KC values. The estimation of the KC values is given by:

$$KC = \frac{H_{m0}}{2}\sqrt{\frac{g}{h}}\frac{T_p}{D_{n50}} \tag{5.1}$$

Where:

- H_{m0} is the spectral or significant wave height.
- g is the magnitude of the acceleration due to gravity.
- h is the water depth at the toe of the structure.
- T_p is the peak wave period.

It must be mentioned that this approach neglects the gradual increase in the nonlinear resistance coefficient b with the decrease in the orbital velocities, as the waves are dampened inside the structure. According to (Jacobsen et al., 2015) however, the damping of the quadratic velocity goes faster to zero than the linear increase in the KC-number, thus the nonlinear resistance becomes less important.

The standard values of α = 1,000 and β = 1.1 that are chosen to be used in the current study have given good results in a comparison with a range of experimental data sets by (Jacobsen et al., 2015). However, (Losada et al., 2016), their Table 2, have shown that a wide range of coefficients applied by different researchers, produced the same results for interchanged values of α and β. In the current study, fixed coefficients are used both for the armour and core. The resistance terms of eq.2.8 and eq.2.9 are parameterised by the layer porosity, the nominal grain dimeter and the varied KC number.

It was chosen not to apply turbulence in the current model setup (Laminar flow). Following the reasoning of (Jacobsen et al., 2015), that the dissipative and reflective properties of a permeable structure are the main interest of this investigation and that there is hardly any production of turbulence outside of the permeable structure which needs modelling. Turbulence is produced inside the permeable structure, but as pointed out in (Jensen et al., 2014b, Jacobsen et al., 2015), the resistance coefficients that are used to describe the bulk resistance over the permeable structure, include all dissipative effects including turbulence. If a turbulence model was added to the numerical framework, it would mean that these dissipative effects would be implemented twice, resulting in lower energy within the structure than reality. The system of equations inside and outside of the structure is the same (Jacobsen et al., 2018), which would mean that if turbulence is added for the water outside of the permeable structure then the dissipation would have to be implemented twice inside the structure.

With regards to the ventilated boundary layer introduced in section 2.4, a great number of values were tested for the geometrical openness e and the loss coefficient ξ during the attempt to validate the model. However, as the final values were unrealistic, an openness of 3% with a ξ coefficient of 1.5 was chosen for both the vertical and the bottom surfaces (boundaries) of the crown wall. These values were chosen as they have already been used and validated by (Jacobsen et al., 2018), showing good results.

Table 20. Properties defined in the numerical model.

Parameter Name	Value
Armour porosity	0.4
Core porosity	0.4
Armour KC	13.971
Core KC	35.168
α closure coef. (armour & core)	1000
β closure coef. (armour & core)	1.1
Water density	1000 kg/m^3
Viscosity of water	1x10^{-6} m^2/s
Type of fluid (air)	Newtonian
Viscosity of air	1.48 x 10^{-5} m^2/s
Density of air	1 kg/m^3
Type of flow	Laminar
Geometric openness e (front and bottom)	3%
loss coefficient ξ (front and bottom)	1.5

Simulation Parameters

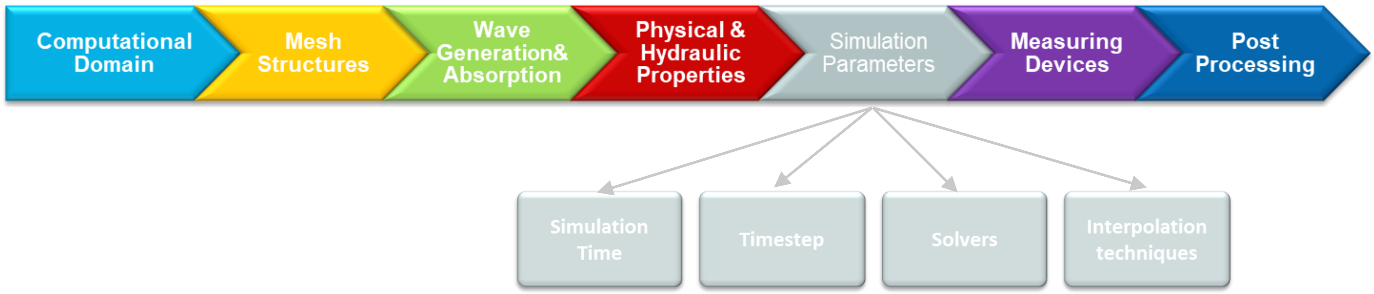

The next step was to define several simulation parameters as the solving utilities, duration of the simulation, the time step between each iteration, time step between storing values and the tolerances. The solvers and interpolation techniques used are Preconditioned conjugate gradient (PCG), Geometric agglomerated Algebraic MultiGrid preconditioner, Preconditioned bi-conjugate gradient (PBiCG) and Simplified Diagonal-based Incomplete Cholesky preconditioner, details on which can be found in the OpenFOAM user guide. All the tolerances are pre-defined as in tutorial files hence there was no need to change them.

The simulation time was chosen based on Tm= 2.04 sec for 300 waves to be 612 sec. That corresponded to 304 simulated waves (zero down crossing analysis) for the reference case (with the same simulation time the number of simulated waves changes as the simulation parameters change, however the number was kept around 300 waves). This simulation time was chosen as it provided a good balance of accuracy and required computation time through the sensitivity analysis. The timestep dt of the simulation was chosen to be 0.001 sec as the pressures under investigation show variations in a timescale of fraction of a second, with significant peaks appearing rapidly. However, the time control was set to adjustableTimeRun, which means that the value of time step is not fixed, but it can be changed, while solving, by OpenFOAM upon need. The decisive factor for the change of the timestep is the courant number which was set to not gain a value larger than 0.2. The smaller the courant number, the greater the accuracy. Literature suggests that it should not take a value larger than 1. Thus, when the courant number value is calculated and exceeds 0.2, OpenFOAM automatically makes the timestep even shorter than the defined 0.001 sec. Simulation results were generated in around 98 hours for the reference case, which greatly varied for each of the following simulations (~60-140 hrs) as the mesh also had to change.

Measuring devices

Finally, the required measuring devices were defined. The wave elevation is not stored by OpenFOAM itself, instead wave elevation measuring gauges are installed at desired points in the computational domain to have the free surface plots at desired time instants. Wave gauges were defined along the length of the flow domain, with a spacing of 0.1 m, for measuring the free surface elevation. Additional wave gauges were defined at the toe of the structure. Following, pressure gauges were defined along the vertical and bottom faces of the crown wall element measuring the dynamic pressure. A set of gauges at the exact locations of the pressure gauges used in the physical experiment of (Bekker, 2017) where defined in order to compare with the measurements from the experiment, calibrate and validate the model. Moreover, more dense sets of gauges (every 0.01 m) were defined along the vertical and bottom faces of the crown wall for the investigations of this study. Finally, another line of wave gauges was defined along the bottom face of the crown wall, at the same locations as the dense pressure gauges, so the wet surface of the crown wall base can be measured. An illustration of the defined wave gauges can be observed in Figure 43. The bulk of the wave gauges, as well as the ones at the toe of the breakwater, were set to save their output every 0.1 sec. (0.1/ Tp ≈0.04), while the ones at the bottom of the crown wall on every timestep (0.001 sec, 0.001/Tp ≈4×10^{-4}). The pressure gauges were set to return output every timestep as well.

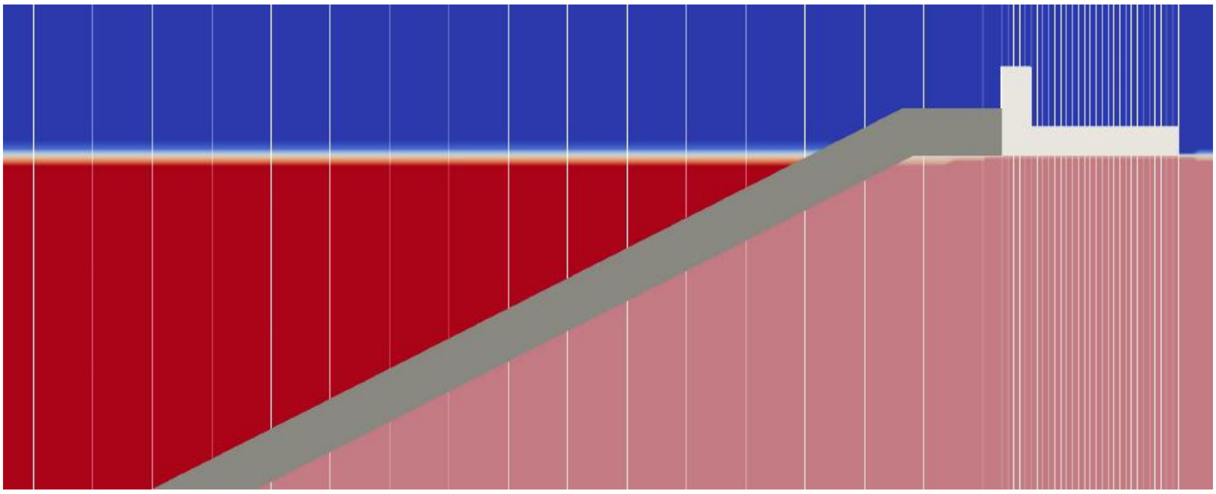

Figure 43. Illustration of defined bulk wave gauges and of wave gauges at the locations of the pressure probes. Post processing with Paraview.

Post processing

ParaView is the open software used for the visual post-processing. Other commercial post-processing software are also available with different options of post-processing. An illustration of the generated wave for the reference case, developed in paraView, is shown in Figure 44, where the water surface elevation of only a portion of the computational domain is shown for better view, as computational domain is very large as compared to its height. The wave elevation for time steps ranging from 52.6-53.8 seconds where largest wave of the simulation propagates from the most left in the top image, towards the structure is shown to display the wave propagation.

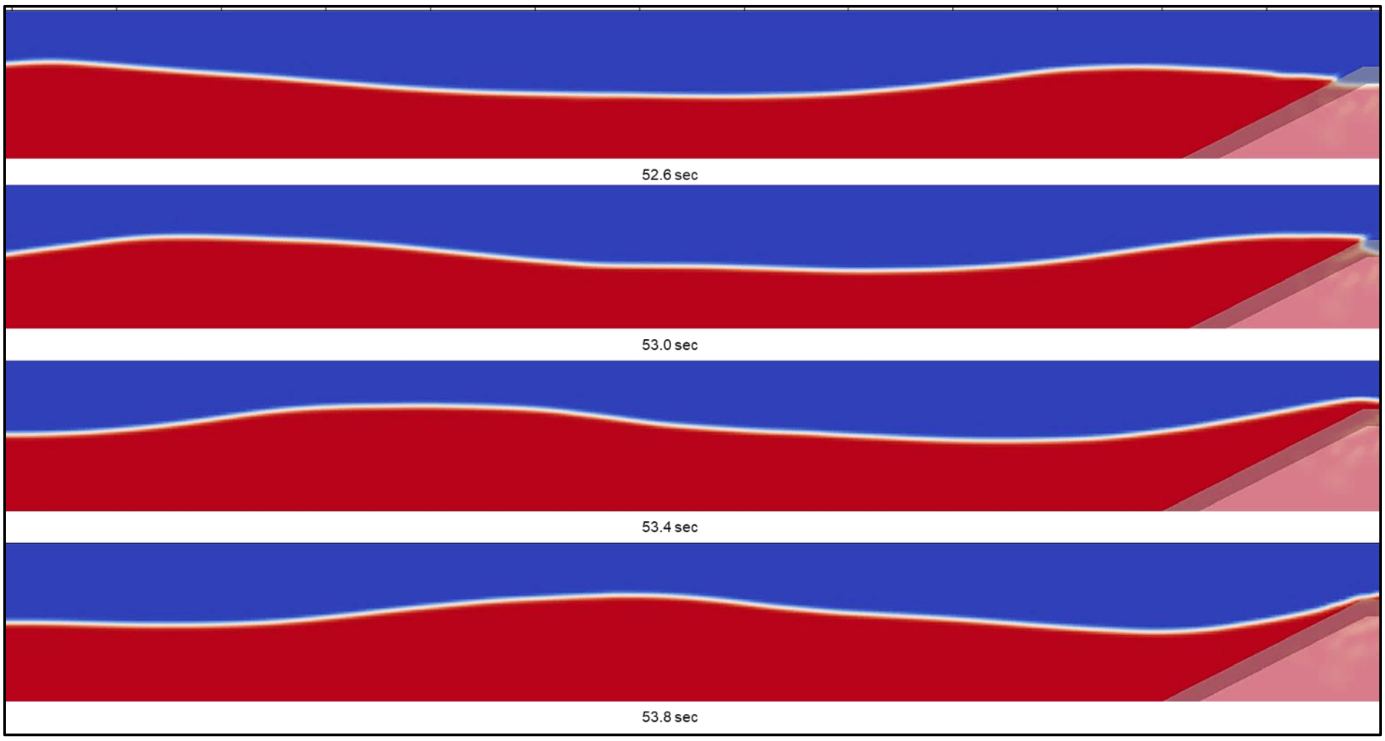

Figure 44. Wave propagation between timesteps 52.6 -53.8 sec. Part of the flume in view. Post processing with ParaView.

The surface elevation reading at time instant of 56.5 seconds, after the maximum wave of the simulation is past the structure and into the relaxation zone, is shown in Figure 45, where the surface elevation of complete computational domain is displayed. At the outlet relaxation zone, the wave fully dissipates approximately within one third of the length of the zone. It means the length of relaxation zone chosen for the test case is sufficient for dissipating the waves.

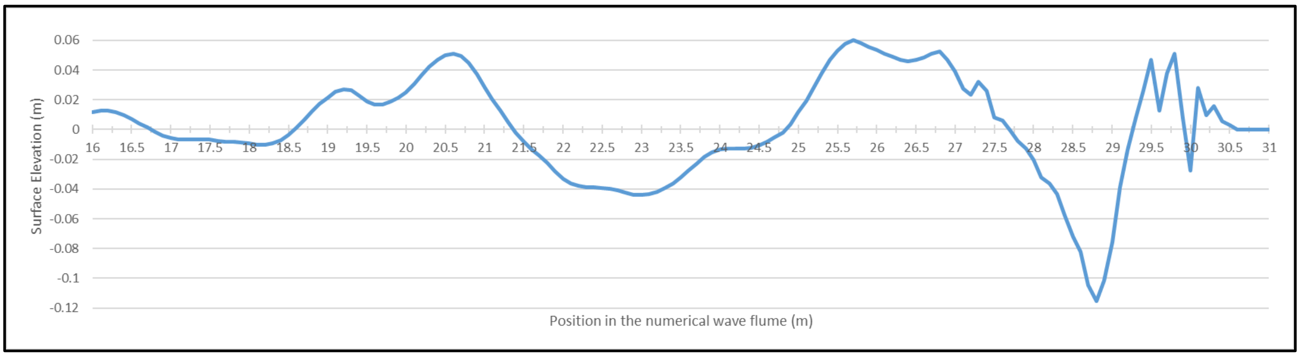

Figure 45. Surface Elevation along the length of the numerical wave flume at time instant 56.5 sec.

An illustration of the interaction between the maximum simulated wave and the crown wall element is shown in Figure 46. Details such as the entrapped air, the overtopping volume of water and change in the wet length of the base of the crown wall can be observed.

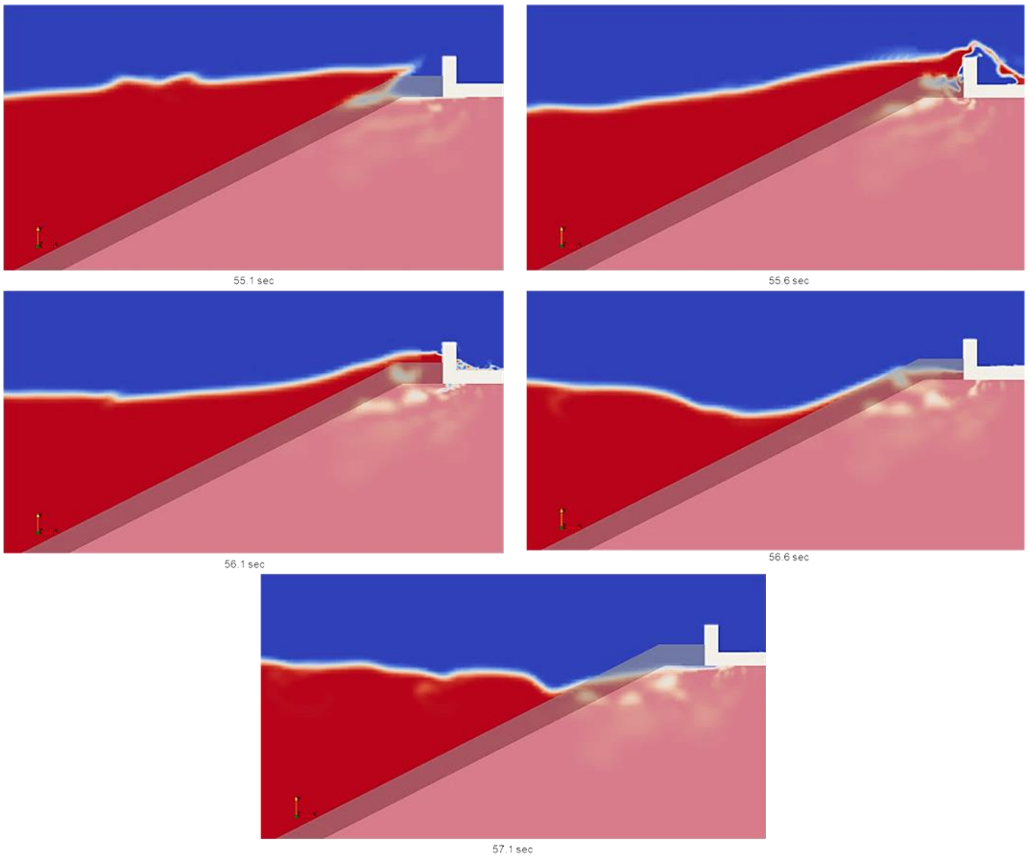

Figure 46. Interaction between the maximum simulated wave and the crown wall structure in timesteps ranging from 55.1 to 57.1 sec. Post processing with ParaView.

The wave gauge signals were decomposed into incoming and reflected waves with the method of (Zelt and Skjelbreia, 1992). This method assumes fully linear waves and as the simulated waves are non-linear it results in some inaccuracies in the capturing of the wave energy. The incoming wave surface elevation resulting from this processing is then used to define the significant and spectral wave heights, as well as the wave period.

The measured pressures were post processed as follows:

1. The timestep was interpolated with a constant timestep of 0.001 sec, as the resulting measurements from OpenFOAM are not equidistant.

2. For the vertical surface of the crown wall, for each timestep, it was assumed that it was wet when the measured pressures were positive. For each timestep the pressures were integrated along the wet surface to calculate the horizontal force time signal. By using equation 2.1. a time signal of critical weights for failure against sliding was computed.

3. For the bottom surface of the crown wall, for each timestep, it was assumed that it was wet when the wave gauges that corresponded to each pressure gauge had non-negative measurement. Then similarly to the horizontal, the vertical forces and critical weight time signals were computed.

4. The maxima of each time signal were identified.

5. The pressures along each surface (pressure distribution) at the moment of maximum critical weight were plotted.

5.2. Sensitivity analysis

Many of the model parameters needed to be calibrated in order to reach a balance between accuracy and computational requirements. For that purpose, a sensitivity analysis was performed, under which the wave properties, as well as the rest of the simulation parameters in each test were kept constant, while changes were made to the following:

1. Computational domain grading

2. Local refinement levels

3. Total simulation time (number of simulated waves)

4. Relaxation zone length

During the sensitivity analysis three parameters were examined, the changes at the surface elevation at the toe of the structure, the changes in vertical pressures and the changes in horizontal pressures. The method followed was starting from what is expected to provide a less accurate solution (e.g. coarser grid mesh, fewer waves etc), but with a less computational expense, and then using values that are more computational demanding but result in more accurate results. Each case was compared with the previous tested case to investigate the difference.

The outcome that would provide the most accuracy would be such that there is no change observed because of the change in the tested value. Which would mean that the tested parameter is fine enough to not influence the results anymore. However, that would require a computational grid so fine, along with a very large number of simulated waves, that would result in a very long computation time for the scope of this study. One downside of the VOF-model is that it has a long run time and produces a large amount of data. As such, tasks such as sensitivity analysis and the validation that follows in the next section that require a large number of simulation and results to be compared, become difficult and tedious tasks. Minding the above, it was decided to repeat the procedure until the difference was equal or smaller to 15%. The procedure is schematized in Figure 47. A similar procedure was undertaken for determining the parameters of the coupled OceanWaves3D model, as though it was not used in the investigation it is not further discussed.

The relaxation zone length was examined to deduce the required length to fully dissipate the incoming wave.

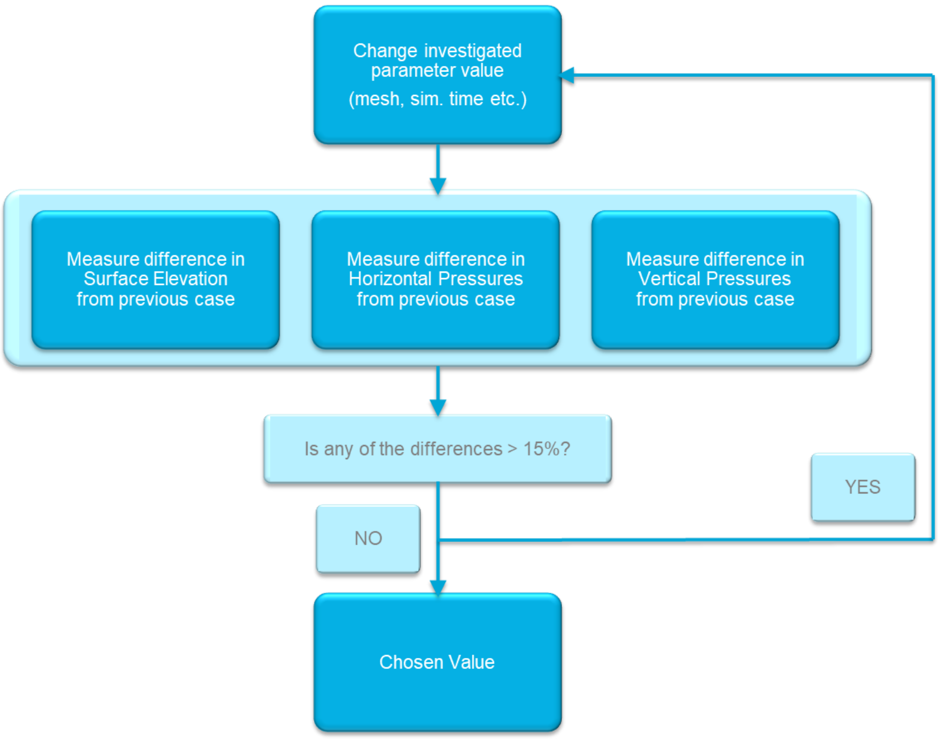

Figure 47. Sensitivity Analysis procedure in the current study.

As the procedure required a large number of simulations (approximately 25) they are not listed in detail. The final values used were described in the previous section of numerical setup. Some observations from the procedure of the sensitivity analysis were:

- The size of the mesh grid greatly influences the measured surface elevation and the computed pressures on the crown wall. Moreover, as we step from coarser to finer mesh, results show big differences, but for further refining the mesh, the difference becomes smaller.

- The local refinement, as expected, had a similar effect as a denser grid. With one level of refinement around the free surface and around the crown wall, the defined computational domain grid mesh was reduced by half, providing similar values. That greatly reduced the required computation time. Another two refinement levels were added around the crown wall element in order to achieve sufficient accuracy of the measured pressures. A fourth refinement level showed small differences (< 10%), while greatly increased the computational time, thus it was not implemented.

- The larger the number of simulated waves the closer the simulated wave height at the toe to the experimental values, as in the experiment a number ≥1000 waves were used. Moreover, with a larger number of simulated waves the statistical parameters are better captured (e.g. H_s, $F_{0.1\%}$ etc). Additionally, similarly with the mesh with more waves the difference decreases. However, the computational time for such a large number of waves is too long. Various numbers of simulated waves were tested in the range 250 to 600. As this parameter most directly impacts the required computation time, with more simulation time producing more simulated waves, it was chosen to simulate a minimum of 300 waves in order to achieve the pre mentioned balance of accuracy and required computation time.

Furthermore, regarding the courant number, initially a maximum value of 0.35 was chosen which was the value used in waves2Foam tutorial cases and also by (Jacobsen et al., 2018). However, during the simulations with varying water levels there were stability issues with the model. These were resolved by lowering the maximum courant number to 0.2. By a quick investigation it was found that this change in maximum courant number significantly affected the measured forces on the crown wall, thus for any comparisons to be valid, all of the simulations were run with the value of 0.2.

5.3. Numerical model calibration and validation

In order to measure the accuracy of a numerical model in predicting the physics that occur in the real world, determining how credible and trustworthy they are, it is a common approach to validate it. The validity of numerical models is usually established by quantitatively measuring the agreement between predictions provided by the model and observations in experiments, representing the real world. Having a validated model implies the model is adequate for the intended purpose in terms of accuracy, uncertainty and applicability.

OpenFOAM and waves2Foam toolbox have been successfully used and validated in numerous studies modelling regular and irregular waves, floating structures and the interaction between waves and porous structures. Some examples are the works of (Chen et al., 2014, Jacobsen et al., 2015, Jacobsen et al., 2017, Jacobsen et al., 2018, Hu et al., 2016, Elsafti and Oumeraci, 2017, Ransley et al., 2019, Hayatdavoodi et al., 2014). The model has been used to model the case of (Jacobsen et al., 2018), which uses quite similar parameters and sizes to the physical experiment of (Bekker, 2017), showing a good match with their conducted physical experiments. As such, it can be considered to provide accurate predictions for the interactions between waves and the permeable structure, as well as the resulting pressures.

Although the model was validated for the case of (Jacobsen et al., 2018), it was decided to also validate it for physical experiment that was used as the basis for the model. The case chosen from the physical experiment was described in the previous case. In order validate the model the agreement between the modelled and experimentally measured waves and crown wall loading needed to be quantified. To achieve the validation also a degree of calibration is necessary. The parameters to be calibrated, -for the waves- are the computational mesh and the number of wave components in the input JONSWAP wave spectrum, -for the loading- the layer porosity (limited changes) and the ventilated boundary openness and ξ coefficient (main calibration parameters). The approach followed was to first reach an acceptable agreement between the model and the physical experiment for the waves and using the parameters that led to that, attempt the same for the loading.

Wave validation

For validating the waves, the first approach was a time domain comparison, where the time signals of the water elevation resulting from wave gauges defined in the numerical model would be compared with the wave gauges measurements of the physical experiment (at the same location). At this stage the wave paddle signal of the physical experiment was used as an input to the numerical model. This approach would thus result in a very accurate comparison, which would have demonstrated if the exact waves are accurately replicated in the model.

However, the wave gauge measurements from the physical experiment were not available, which led to a new approach. As fore mentioned, the JONSWAP wave spectrum discussed in section 5.1. was used as an input to the model. Then it was chosen to have a comparison in the frequency domain, using the post processed surface elevation measurements (decomposed incoming wave) of the model, at the location of the toe of the breakwater. It was determined that with the available data, that was the most suitable way to validate the proper propagation of waves in the numerical flume. In order to achieve that, a theoretical JONSWAP amplitude spectrum was composed, using as input the measured values from the physical experiment at the toe of the breakwater that were available. Following, by post processing the wave gauge measurements (bulk surface elevation) at the toe of the breakwater from the numerical simulations, the resulting amplitude spectrum was composed (from hereby referred to as simulation spectrum). Consequently, the theoretical and simulation spectra were compared to quantify the degree of agreement.

In order to reach an acceptable agreement between the two spectrums, first the number of wave components comprising the JONSWAP wave spectrum used as an input to the model were varied. A typical value found in literature, as well as in tutorial cases is 100 wave components. The number of wave components tested was 50, 100, 150, 300 and 600. A value between 100 to 150 wave components resulted in a spectrum (and loading) closer to the values of the physical experiment and as such the typical value of 100 was chosen. The simulation spectrum was already in close agreement with the theoretical one, and a small refinement to the mesh led to the comparison shown in Figure 48 where the theoretical and simulation spectra are plotted together. In Figure 48 illustrated with black line is the theoretical spectrum and the red lines display its 90% confidence intervals, while the blue line represents the simulation spectrum and the green lines its 90% confidence intervals. It can be observed that the peaks of the spectra (maximum amplitude) are matching both in the frequency they appear at and their magnitude, while their curves are following a similar shape. The relative difference of the mean of the two spectra is 3.84%, while the relative difference of their standard deviations 0.34%. According to the above it can be concluded that there is a good agreement between the model prediction and the physical experiment.

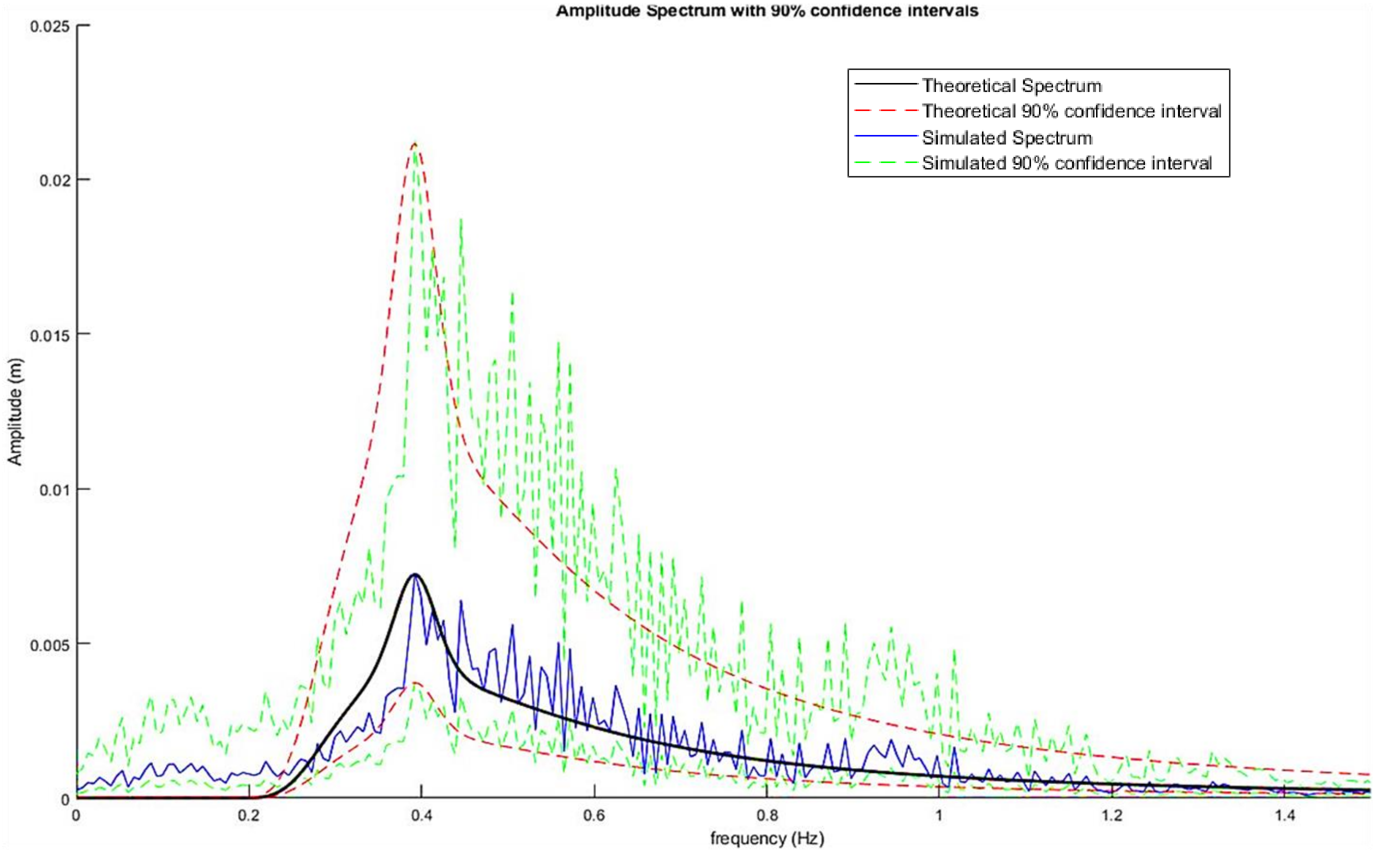

Figure 48. Amplitude spectrum at the toe of the structure.

Validation of wave loads

The next step was to validate the loading on the crown wall. There are several parameters, interconnected with each other, that directly correlate to the loading. These are the vertical and horizontal pressures, the vertical and horizontal forces and the critical weight resulting from equation 2.1. In order to validate the loads several steps were followed.

First, it was observed that the maximum pressures measured for specific pressure gauges and the moment in time they appear (both from the physical experiment and simulations), do not correspond to the maximum forcing. That is a result of two observations, which both affect the pressure distribution. Firstly, a large pressure measurement in one gauge can be combined with lower (or zero) pressure measurements in other gauges, thus when intergraded over the surface area it provides a lower force than in a case with lower point pressure but higher overall pressure in all the gauges of that crown wall face.

The second observation regards the vertical pressures and force and relates to the wet base length X_c. With a smaller wet length, the area of integration greatly reduces, thus the vertical force is greatly reduced, even if the point pressure is high. An example can be observed in Figure 49. Considering this fact, the individual pressures are not used for the validation or the analysis that follows. The maximum horizontal and vertical pressures are however monitored for every simulation to ensure they are in the same order of magnitude with experimental values and values predicted from the empirical methods.

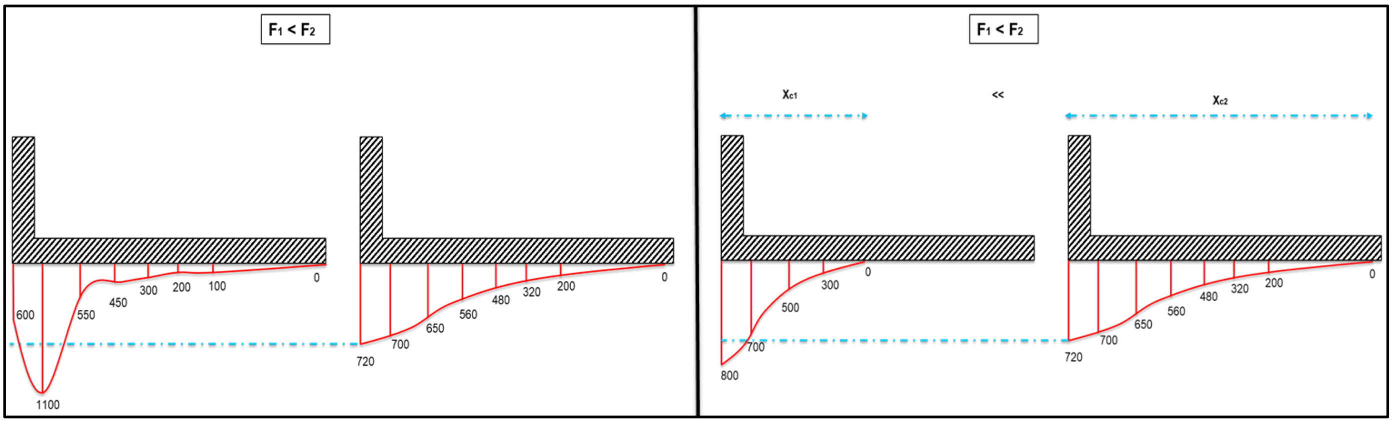

Figure 49. Example of relation between point pressure and total force.

Secondly, using the methods of (Pedersen, 1996) and (Nørgaard et al., 2013) as detailed in section 3.1., along with post processing of the data from the physical experiment for the chosen case, resulted in the data presented in Table 21. In Table 21, the pressures and forces from the empirical methods are the mean value that fall within a range of plus or minus 30% from that mean as detailed in section 3.1. Also, X_c is given as the percentage of the base that was wet at the moment in time where the critical weight gets its maximum value. The other two methods assume that the whole base is wet. The method including the reduction factor of (Bekker et al., 2018) is not included as for the case of zero base freeboard in produces results identical to (Nørgaard et al., 2013).

Table 21.Parameters resulting from empirical methods and J Bekker's physical experiment (test case TO21004) post processing.

Method	Parameter					
	$P_{H,max}$ [Pa]	$P_{V,max}$ [Pa]	$F_{H,max}$ [N]	$F_{V,max}$ [N]	$W_{c,max}$ [N]	X_c [%]
Pedersen 1996	1820.84	1820.84	228.82	273.13	578.21	100
Nørgaard et al., 2013	2109.33	2109.33	193.54	316.40	574.45	100
Physical exp. (TO21004)	1208.00	863.37	108.64	84.15	229.01/ 160.96/ 115.89*	38.67

*In Table 21 the maximum critical weight for the physical experiment gets two values. The reason for that is that by analysing the experimental data and the data from all the conducted simulations for the sensitivity, calibration and validation led to an important preliminary result. The maximum critical weight (as calculated by equation 2.1) does not occur for a combination of the maximum horizontal and vertical forces. This is explained in detail at the start of the following chapter (analysis). Additionally, as previously discussed, during the physical experiment the actual weight of the crown wall that leads to failure was measured, which is the most accurate measurement. For the investigated case that corresponds to a critical weight value of around 115 N. Thus, three cases can be distinguished:

- The maximum critical weight assuming that the maximum horizontal and vertical forces happen at the same moment in time, $W_{c,max}$ = 229.01 N. This is the assumption used by all the empirical methods.
- For each time step, using the time signals of horizontal and vertical forces in equation 2.1, results in a time signal of critical weights (Wc). The maximum critical weight is the maximum value of this time signal. For the chosen case that results in $W_{c,max}$ = 160.96 N.

- The critical weight resulting from failure tests with varied weights, $W_{c,max}$ = 115 N.

Following, targets were set for the calibration and validation. It can be observed that the value that results from post processing of the measured pressures of J. Bekker (160.96 N) is quite larger the more trustworthy value from the failure (stability) tests (115 N). The target maximum critical weight for calibration and validation is the 115N, but this can be achieved with a different combination of horizontal and vertical forces in equation 2.1. Thus, the approach followed, to be closer to the physical proportions between horizontal and vertical forces, was to use the forces that correspond from the measurements at the moment in time with the maximum critical weight. The combination of these forces in equation 2.1 results in $W_{c,max}$ = 160.96 N, so it was calculated that if these forces are reduced by 28%, equation 2.1 will result in $W_{c,max}$ = 115.89 N. That way the proportion of the forces remain the same while the target critical weight is achieved. These reduced values were used as a target horizontal and vertical force, as seen in Table 22. Another target set was comparing the resulting vertical force amplitude spectrum of the simulation and the physical experiment and achieving a good agreement between the two.

Table 22. Computation of target forces.

	$F_{H,max}$ [N]	$F_{V,max}$ [N]	$W_{c,max}$ [N]
Value from pressures	76.55	58.91	160.96
Value from failure tests	-	-	~115
Target	55.11	42.41	115.89

A series of simulations were carried out, firstly as the loading on the crown wall is sensitive to the porosity and the exact value was not specified, different values of layer porosity for the armour and core were tested. On one hand to determine which ones would lead to better agreement with the targets and on the other to achieve a better insight of the effect of porosity on the loading. A total of 21 simulations with different layer porosities were performed (some of them combined changes in the ventilated boundary layer). The physical experiment is considered to have layer porosity in the range between 0.3 and 0.45. Nonetheless, also unrealistic large values (0.5 to 0.8) and core having a larger porosity the armour were also tested to examine their effect.

There was another reason for testing this large range of porosities. According to (Bekker, 2017, Bekker et al., 2018) and as can be calculated by equation 3.49 and 3.50 for his inputs, for the case of zero base freeboard, the base should be completely wet with no effect of X_c on the vertical forces. However, the post processed data for the case chosen for the investigation (zero base freeboard), as shown in Table 21, resulted in X_c= 38.67% at the moment of maximum critical weight, meaning most of the base was not wet. In contrast, all the simulations with zero base freeboard, for all porosities, resulted in a completely wet base the moment of maximum critical weight. That made the calibration and validation exceptionally difficult, as the vertical forces resulting from the numerical model were quite larger than the ones measured in the physical experiment. Thus, many values of layer porosity were used in an attempt to decrease the length of the base that is wet (without success). Finally, as mentioned in section 5.1, a layer porosity n=0.4 was chosen for both the armour and the core.

Some preliminary general findings from these tests were:

1. Changes in layer porosity do not result in a linear trend on the loading (horizontal & vertical forces and critical weight) as for example both n=0.4 and n=0.75 resulted in lower loading than n= 0.5. No clear connection was established.

2. Changes in layer porosity have an effect both on horizontal and vertical forces.

3. Changes in layer porosity have an effect on where the wave breaks (on the breakwater slope or on the crown wall vertical face)

4. Large changes in porosity change the wave (moment in time) at which each of the maximum forces are found. For example, in some cases it was not at the highest wave of the timeseries. The maximum vertical and horizontal forces can appear in different waves due to this effect.

5. Although not quantified, it was visually observed that having a large difference between the porosity values of the armour and core changed the flow within the porous structure and the way the wave interacts with the crown wall. An example can be observed in Figure 50.

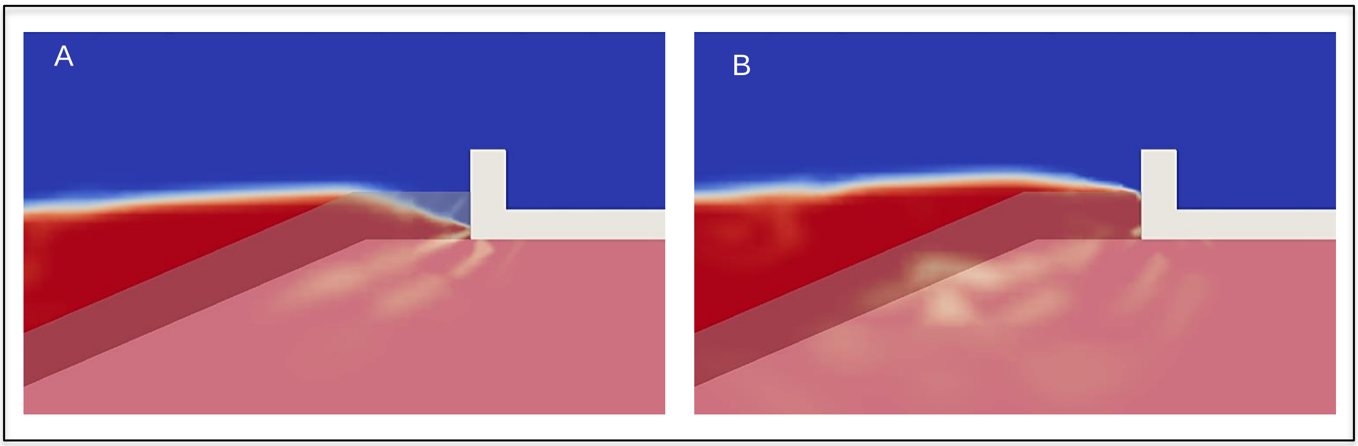

Figure 50. Visual difference in wave-structure interaction (same moment in time) for different layer porosities. In A: armour porosity 0.4, core porosity 0.7. In B: armour and core porosity 0.4. Post processing with Paraview.

A parametric investigation on the effects of porosity is out of the scope of this study, however it was established that it significantly influences the wave-structure interactions and the magnitude of pressures and forces. There is a large number of interesting investigations focused on the relation between vertical forces, horizontal forces and layer porosity that could be carried out in future studies.

The next step was to vary the degree of openness (e) and the loss coefficient ξ of the ventilated boundary layer trying to attain a better agreement between the forces resulting from the simulation and the set targets. This was a complex process as there are four parameters to vary, e and ξ for both the vertical and bottom faces of the crown wall, while it was found that changes in any of them result in changes to both the horizontal and vertical forces, without a linear trend. A total of 77 simulations were undertaken. Again, for all simulations the base was fully wet under critical conditions. In Figure 51 and Figure 53 the effect of changes of e and ξ on the loading are shown. In Figure 51 one can see that the increase of the degree of openness for both the bottom and vertical face of the crown wall simultaneously leads to a decrease in the horizontal maximum pressures and forces and the opposite for the vertical. However, changing the degree of openness on one face only leads to reduce of the loading on that face, as illustrated in Figure 52. That showcases the complexity of calibrating these parameters as separate values on the two faces interact with the exerted loading on each face. Adding the calibration of the loss coefficient ξ separately for each face increases that difficulty. In Figure 53, a clear trend is observed where an increase in the loss coefficient ξ (for both faces simultaneously), the corresponds to an increase in the loading.

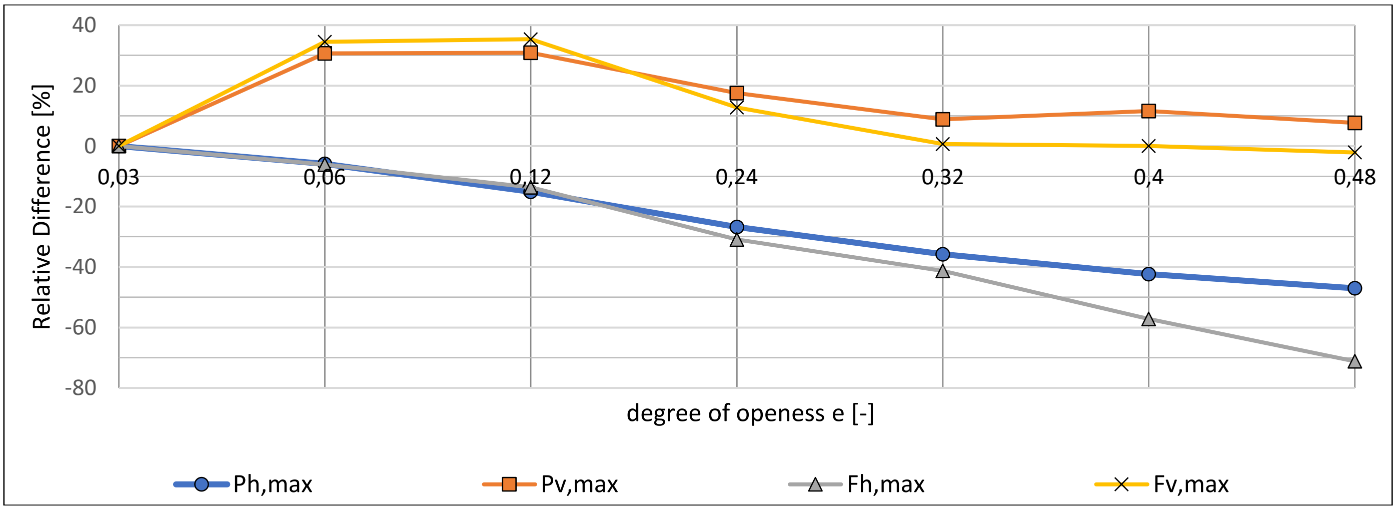

Figure 51. Relative difference to loading for varying ventilated boundary openness e, on both crown wall faces simultaneously, compared to the reference case of e=0.03.

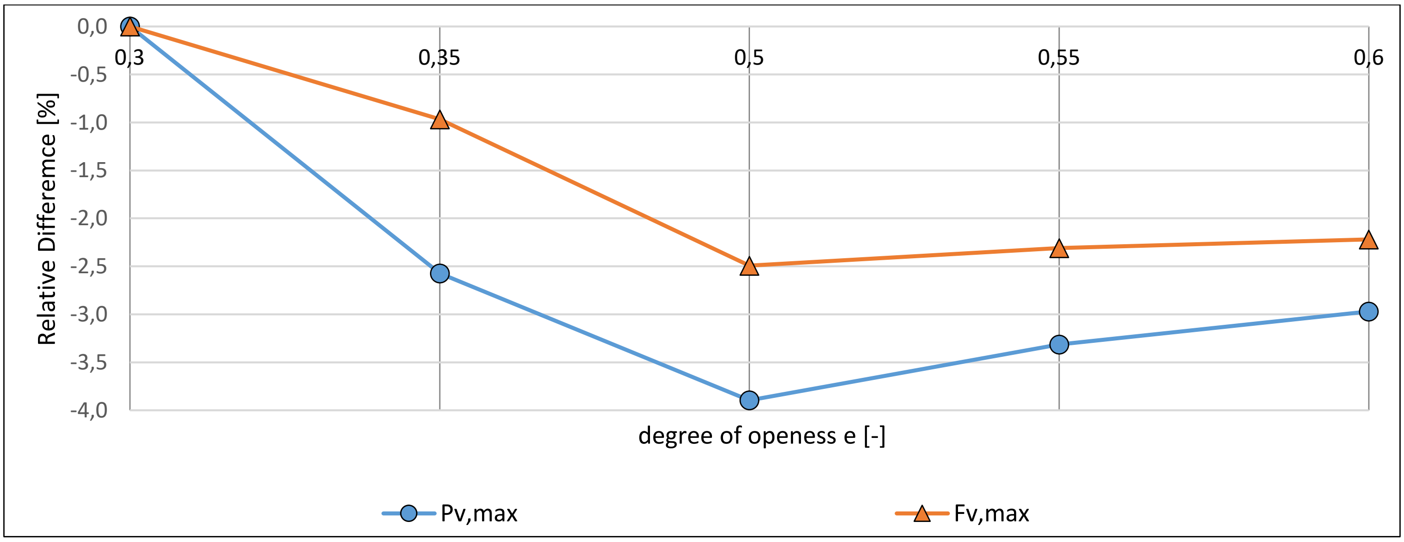

Figure 52. Relative difference to loading for changing degree of ventilated boundary openness e, for only the bottom crown wall face, compared to the reference case of e=0.03.

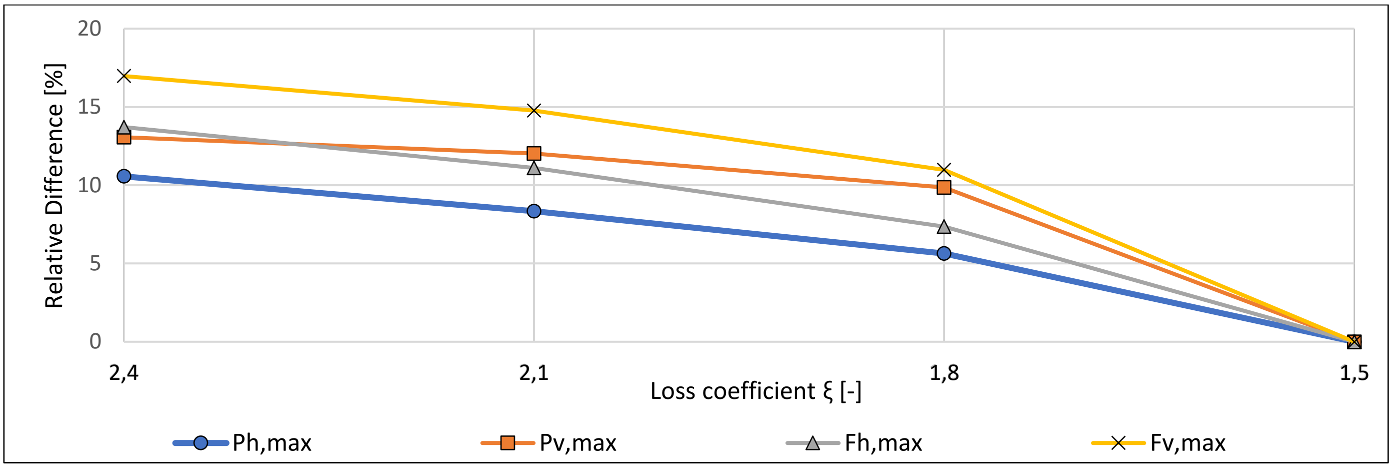

Figure 53. Relative difference to loading for varying ventilated boundary loss coefficient ξ, on both crown wall faces simultaneously, compared to the reference case of ξ =1.5.

The calibration and validation effort started with a maximum critical weight around five times larger than that of the target. After the calibrations the closest achieved value was 33.45% larger than the target maximum critical weight, with the horizontal force at the moment in time of critical condition being 27.35% lower than the target and the vertical force at that moment 138.78% higher than the target. In Figure 54 where the black line illustrates the uplift (vertical) force amplitude spectrum resulting from the physical experiment with the respective confidence intervals shown in red and with a blue line the spectrum resulting from the calibrated model with the respective confidence intervals in green colour. Although the values do not show a very good agreement, one can observe that the curves follow a similar shape.

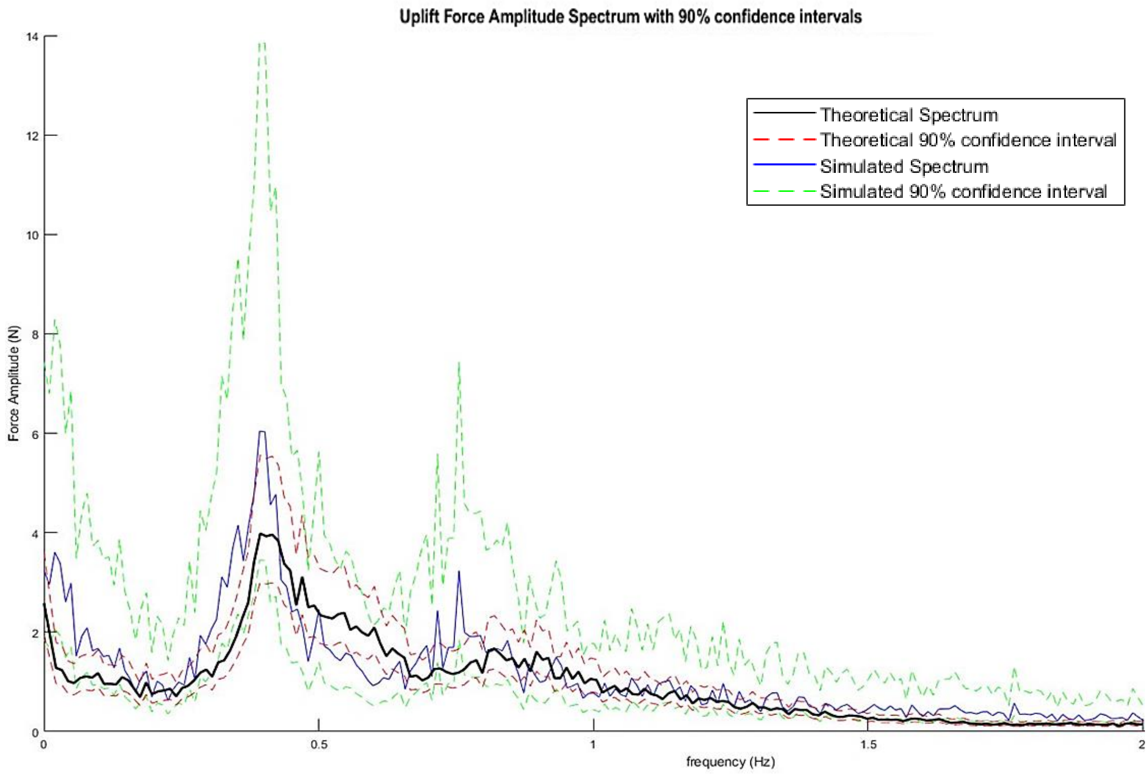

Figure 54.Uplift Force Amplitude spectra from physical experiment and numerical simulation.

As mentioned, the largest problem was the degree of saturation. The completely wet base in the simulations led to significantly larger vertical forces than the target. To achieve the fore mentioned calibration, the parameters used for the ventilated boundary condition were e= 0.7, ξ= 0.6 for the vertical face of the crown wall and e= 0.45 and ξ= 1.5 for the bottom face. Such values of openness are unrealistically large (correspond to an opening of 45% and 70% of the respective surfaces) and result in large volumes of water flowing out of the computational domain. As such they do not represent the interactions taking place in the real world. Thus, even though they result in a loading closer to the target, they cannot be used to provide accurate results. For the investigations that follow a degree of openness e= 0.03 and a loss coefficient ξ= 1.5 were used, values that were used and validated by (Jacobsen et al., 2018). Thus, for the base reference case chosen which was used for comparisons in the following investigations, the inputs are detailed in Table 20, while the results in Table 23.

Table 23. Results for reference case. $F_{H,crit}$ and $F_{V,crit}$ are the forces that correspond to the moment of critical condition.

$P_{H,max}$ [Pa]	$P_{V,max}$ [Pa]	$F_{H,max}$ [N]	$F_{V,max}$ [N]	$W_{c,max}$ [N]	$F_{H,crit}$ [N]	$F_{V,crit}$ [N]	X_c [%]
2844.90	2874.50	235.84	546.30	744.16	148.40	546.30	100

In
Table 21, one can observe large discrepancies between the values calculated by the empirical methods and the results of the physical experiment. The physical experiment measurements result in forces and a critical condition a few times smaller than the empirical methods. According to (Bekker, 2017), for zero base freeboard the empirical methods and the physical experiments should show good agreement, which is not the case for the post processed data of the selected case. It can be observed that the results of the chosen reference case shown in Table 23 show a better agreement to the ones calculated with the empirical methods with only the maximum vertical force and the corresponding critical weight being larger. The reasons for this difference between the post processed experimental data and the empirical methods could be a different method of post processing of the pressure measurements, the case and corresponding data chosen could be an outlier of the physical experiment or there is a possibility of undetected errors either in the physical experiment or the numerical model setup.

An interesting finding through the tests of degree of openness values, was observing a substantial influence of the openness for the case of zero freeboard which contradicts the observations of (Jacobsen et al., 2018). In their paper, the authors showcase a quantitative analysis of the degree of openness, where they conclude that for zero base freeboard the openness hardly affects the magnitude of the uplift force. In contrast, when they increased the elevation of the crest wall above still-water level they observed a significant influence of the openness, since the free surface displacements below the crest wall were large enough to create a cavity between the crest wall and the free surface. “The presence of this cavity lends importance to the ventilation. Higher elevations of the crest wall above the still-water level will ultimately prevent the formation of cavities, making the degree of openness irrelevant because the air is easily ventilated below the crest wall.” (Jacobsen et al., 2018).

5.4. Further investigations

In this section a brief description of the simulations undertaken for the investigation is given. The base reference case was described in detail in the previous sections of this chapter. By implementing changes on that case, the following cases were investigated:

Five cases where all the other parameters were kept constant but the base freeboard R_b was increased by means of lowering the water level in the numerical flume. The simulated freeboards were 0.015 m, 0.03 m, 0.045 m, 0.06 m and 0.075 m which accounting for the experimental scale of 1:30 correspond to 0.45 m, 0.9 m, 1.35 m, 1.8m and 2.25 m. In the physical experiment of (Bekker, 2017) the three freeboards of 0.03, 0.06 and 0.09 m were used. Smaller increments were possible to be implemented in the numerical model which provide a better insight to the effects of an increasing freeboard. In the study of (Jacobsen et al., 2018) the tested freeboards were 0.005, 0.01, 0.015, 0.025, 0.035, 0.05 and 0.07 m, which with their scale of 1:36 correspond to 0.18, 0.36, 0.54, 0.9, 1.26, 1.8 and 2.52 m in reality.

An analysis was undertaken to identify the maximum freeboard where significant loadings on the crown wall can be observed and where the base still becomes wet. As can be observed in Figure 55 and Figure 56, for a base freeboard of 0.12 m the bottom face of the crown wall is completely dry during critical condition, while of a freeboard of 0.09 m around 5% is wet. Similarly, the vertical force for these two freeboards are observed to zero and very low and as such the maximum freeboard chosen to be investigated is the one of 0.075 m.

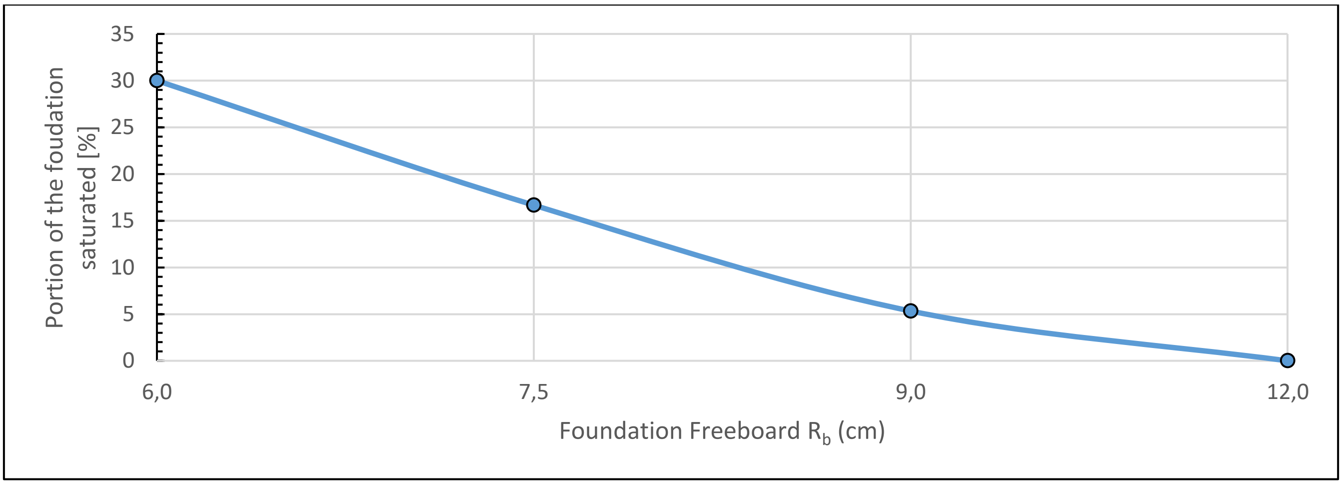

Figure 55. Wet portion of the base for varying freeboard.

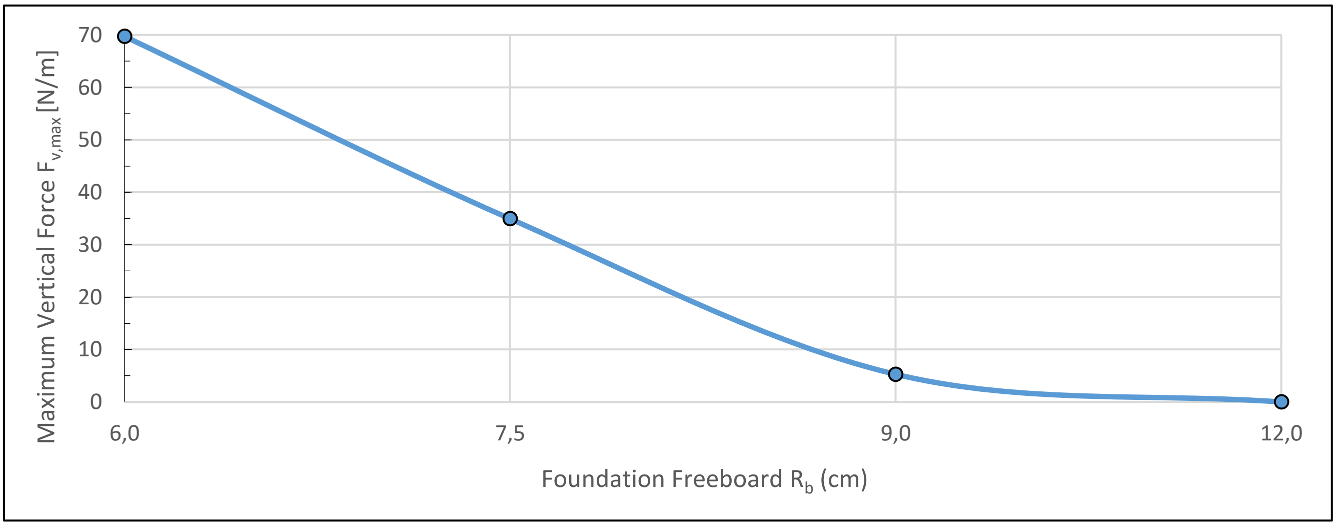

Figure 56. Maximum vertical force for varying freeboard.

Following, four cases with base freeboard of 0.03, 0.045, 0.06 and 0.075 m were simulated, where the freeboard increase was achieved by means of elevating the crown wall structure similarly with the method used by (Jacobsen et al., 2018) as shown in Figure 29 (B) and Figure 30. The rest of the parameters of the simulation were kept constant. These will allow for a comparison between the two methods of increasing the freeboard.

Finally, three cases of varied breakwater slope were implemented, with slopes of 1:15, 1:2.5 and 1:3 (plus the reference case with 1:2), in order to investigate the effect to the loading. The rest of the parameters were kept constant. There are two different ways of varying the breakwater slope. First starting at the same position of the toe, and changing the slope angle upwards, which will lead the whole superstructure to be moved within the numerical. The second is keeping the structure and the top of the breakwater as they were and changing the slope from the top point and downwards, which however changes the point where the toe is located in the numerical flume, as show in Figure 57. Both will have an effect to the wave propagation and interaction with the structure, but the second one was chosen as less parameters relating to the geometry of the crown wall and the loading are varied. This way the crown wall is located in the same position in the flume and the waves will have the same length to propagate before reaching the structure.

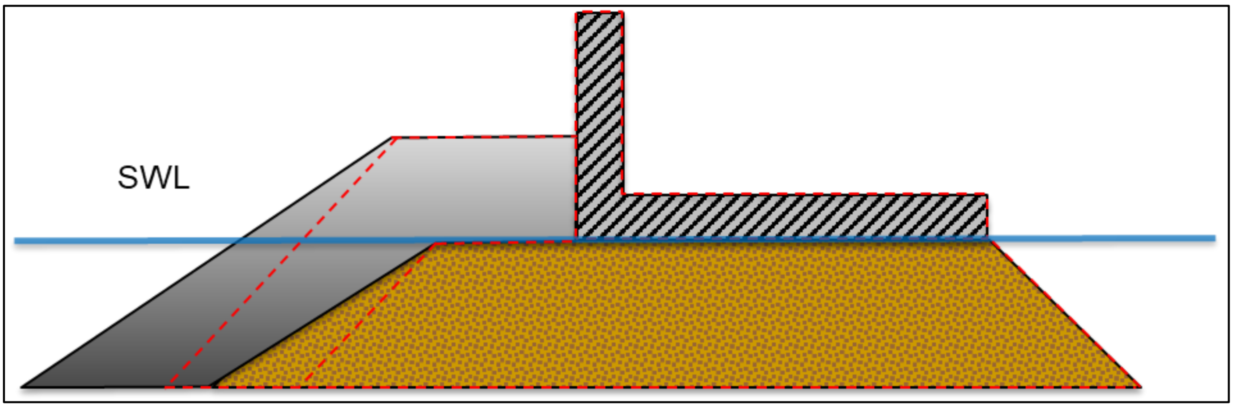

Figure 57. Followed approach to changing the breakwater slope. The red dashed line illustrates the starting structure, while the coloured sketch the structure resulting after changing the slope.

6 Results and Analysis

This chapter focuses on interpreting the results of the investigations. In the first section, some observations from the calibration and validation effort along with general findings concerning the timing of the maximum forcing and critical weight, as well as the effects of an increasing freeboard are discussed. The following sections focus on the analysis of the simulation results as defined in the study steps and sub-goals in section 4.2. More specifically, the second section concentrates on comparing the effects of increasing the base freeboard with different methods to the wet base length, on the maximum forces and critical weight. The third section focuses on the shape of the uplift pressure distribution for varying base freeboards. The fourth section is related to the time lag between the maximum horizontal and vertical forces. Finally, the fifth section presents the results of the investigation for varying breakwater slopes.

In the following Table 24 the simulated cases ID along with the basic inputs are presented for the investigation of varying freeboard with different methods. Method I of increasing the base freeboard refers to the one where this is done by lowering the still water level, while Method II to raising the elevation of the crown wall element. This was explained in section 4.1. All relative values in the graphs that follow are relative compared to their value for the reference base case FB0 (zero freeboard, 1:2 breakwater slope).

Table 24. Inputs for simulated cases for varying freeboard with methods I and II.

Case ID	SWL [m]	Base freeboard R_b [m]	Crown wall base elevation [m]	H_s [m]	T_p [sec]
FB0	0.65	0	0.650	0.10295	2.55
M1FB015	0.635	0.015	0.650	0.10295	2.55
M1FB030	0.620	0.030	0.650	0.10295	2.55
M1FB045	0.605	0.045	0.650	0.10295	2.55
M1FB060	0.590	0.060	0.650	0.10295	2.55
M1FB075	0.575	0.075	0.650	0.10295	2.55
M2FB030	0.650	0.030	0.680	0.10295	2.55
M2FB045	0.650	0.045	0.695	0.10295	2.55
M2FB060	0.650	0.060	0.710	0.10295	2.55
M2FB075	0.650	0.075	0.725	0.10295	2.55

6.1. General Observations

By analysing the results from the simulations conducted during the setup, calibration and validation, as well as the experimental data some preliminary findings arose.

<u>Time of occurrence of maximum critical weight and forces</u>

A first observation was that the two moments in time when the maximum vertical and horizontal forces appear are different from the time that a maximum point pressures occurs on a pressure gauge. That relates both to the point pressures measured by the rest of the wave gauges on that surface and to the wet base length, as they both form the pressure distribution. This was explained in more detail in section 5.3.

Secondly, the maximum critical weight for the sliding criterion (as calculated by equation 2.1) was found to always occur for the largest wave of the timeseries (maximum wave height).

Another crucial finding, that was also briefly mentioned in section 5.3, was that the maximum vertical (F_V) and horizontal forces (F_H), as well as the maximum critical weight (W_c) do not appear at the same moment in time. As also observed by (Bekker, 2017, Van Heemst, 2014, Pedersen, 1996), for each wave there is a time lag between the appearance of the maximum horizontal and vertical force. This is investigated in a separate section (6.4) following in this chapter. Thus, the maximum critical weight (critical condition) is found during the interaction of the structure with the largest wave, and within the time frame that the maximum horizontal and maximum vertical forces, for that wave, occur. The time of the critical weight can take the boundary values of this time frame (the specific time moments that either the maximum horizontal or maximum vertical force for that wave occur), but it also frequently appears in moments between the two. That is illustrated in Figure 58.

As such, to identify the maximum critical weight (critical condition) for each simulation the following process was followed. For each timestep in the physical or numerical experiment a time signal of the horizontal and vertical forces (F_H, F_V) was calculated by integration of the measured pressures in that timestep over the wet length of the corresponding crown wall face in that timestep. For each time step, using the time signals of horizontal and vertical forces in equation 2.1, resulted in a time signal of critical weights (W_c). The maximum critical weight is the maximum value of this time signal.

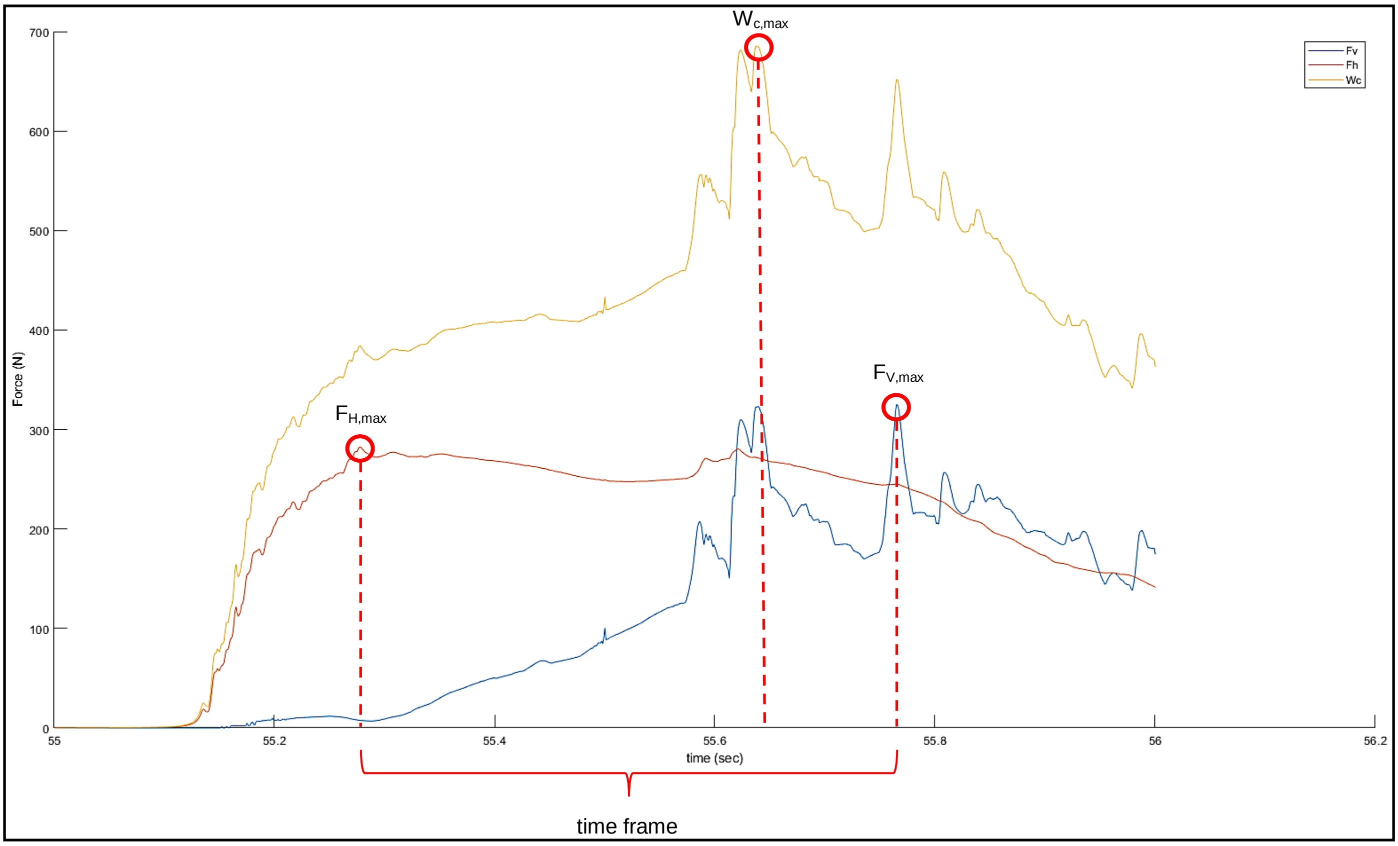

Figure 58.Time frame where critical conditions appear. Timeseries of horizontal and vertical forces and critical weight, focused near the time of maxima. Simulated case M2FB030, with base freeboard of 0.03 m, Method II.

This finding could have a significant consequence to the design and cost of crown wall elements. The empirical methods currently used are assuming that the maximum vertical and horizontal forces occur simultaneously, resulting in a critical weight from the two maxima used in equation 2.1. The difference between the critical condition calculated with that assumption, and the one found through numerical simulations and the physical experiment is considerable.

In Figure 59 the relative difference in critical weight calculated with the previous stated assumption to the ones resulting from the numerical simulations conducted for the investigation (as described in section 5.4) are illustrated as a histogram. It can be observed that the relative difference between the two can be over 20%, with the critical condition calculated assuming simultaneous maxima of the forces being the one overpredicting. The most frequent relative difference is between 10 and 15%. This finding although should be used with caution as this reduction is a result for the specific geometry used and only one wave condition.

This could lead to future designs with less required weight, and as such less concrete and cost. However, using this reduced critical weight for design should be done with caution, as it was also observed (as for example in Figure 58) that the mentioned time difference for some cases is quite short. Hence, even though this time lag does occur, it is uncertain to what degree the superstructure can "feel" these time lags as this relates to the natural frequency of the superstructure. Future studies could focus on the relation between natural frequency and time lag of the loading and its effect on the response of the crown wall.

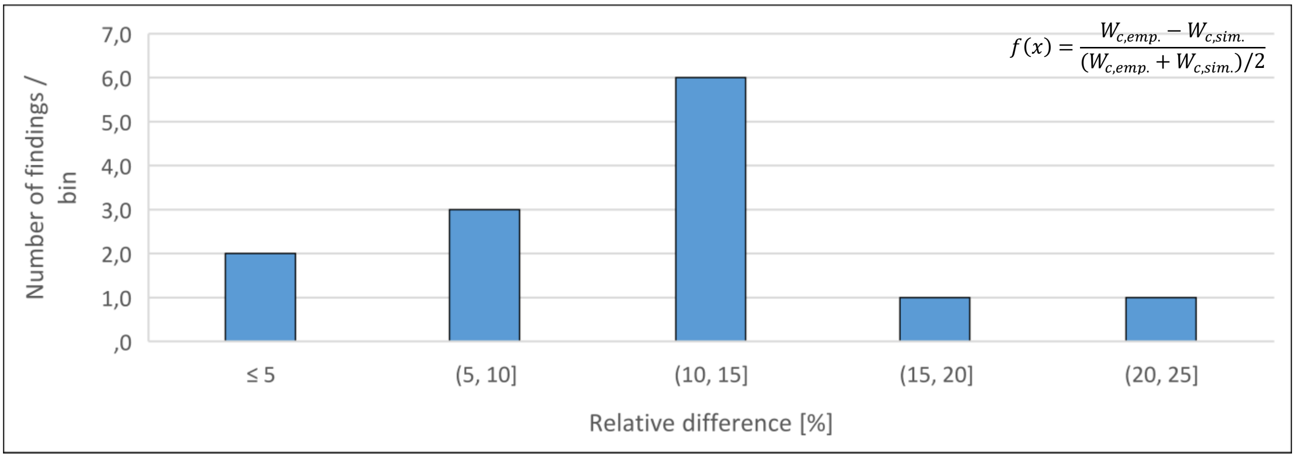

Figure 59. Histogram of the relative difference between critical weight from simulations and the one calculated assuming simultaneous maximum horizontal and vertical forcing.

Effect of increasing the base freeboard

Furthermore, it was observed that as the base freeboard (R_b) is increased, it leads to a reduction of the wet part of the crown wall element (X_c) during critical condition, similar to the findings of (Bekker, 2017, Bekker et al., 2018). This is showcased in Figure 60 where the decreasing trend of X_c for an increase of R_b is clear.

Additionally, with the increase of R_b the maximum vertical force $F_{V,max}$ also reduces, verifying that larger X_c results in higher vertical forces F_V, as the integration area is increased. Similarly, smaller X_c results in lower F_V. This can be observed in Figure 61 where the maximum vertical force can be reduced up to around 90%. At the same time, the maximum critical weight $W_{c,max}$ is also reduced with increased R_b, which is expected as it is connected to the vertical force F_V through equation 2.1. The maximum critical weight is only reduced by around half compared to the maximum vertical force, that is because of the influence of the horizontal force in the way it is calculated.

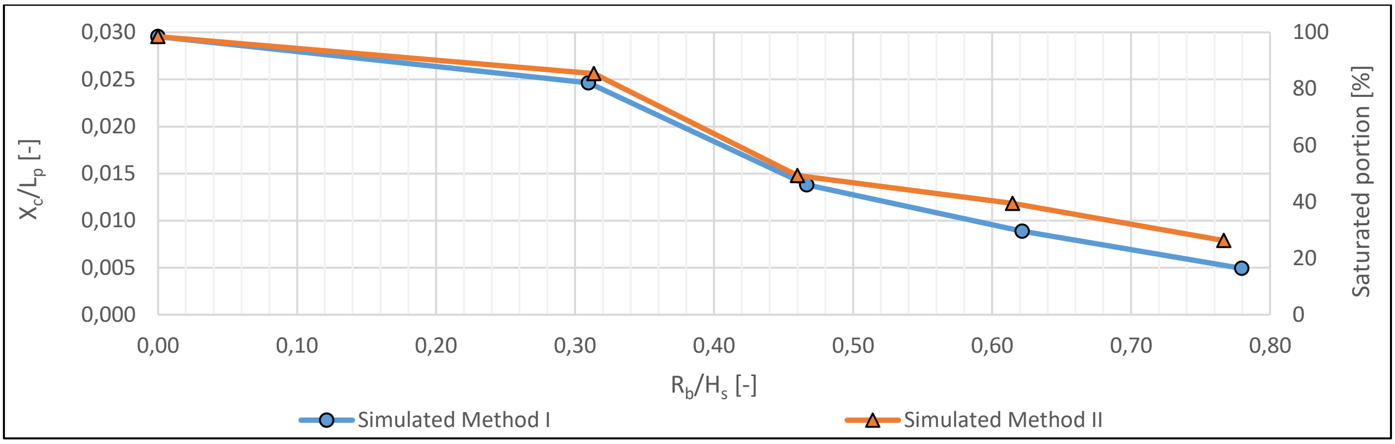

Figure 60. Dimensionless wet base length X_c/L_p against the dimensionless base freeboard R_b/H_s at the moment when the vertical force is maximum, for both methods. The secondary vertical axis shows the percentage of the crown wall bottom that is wet.

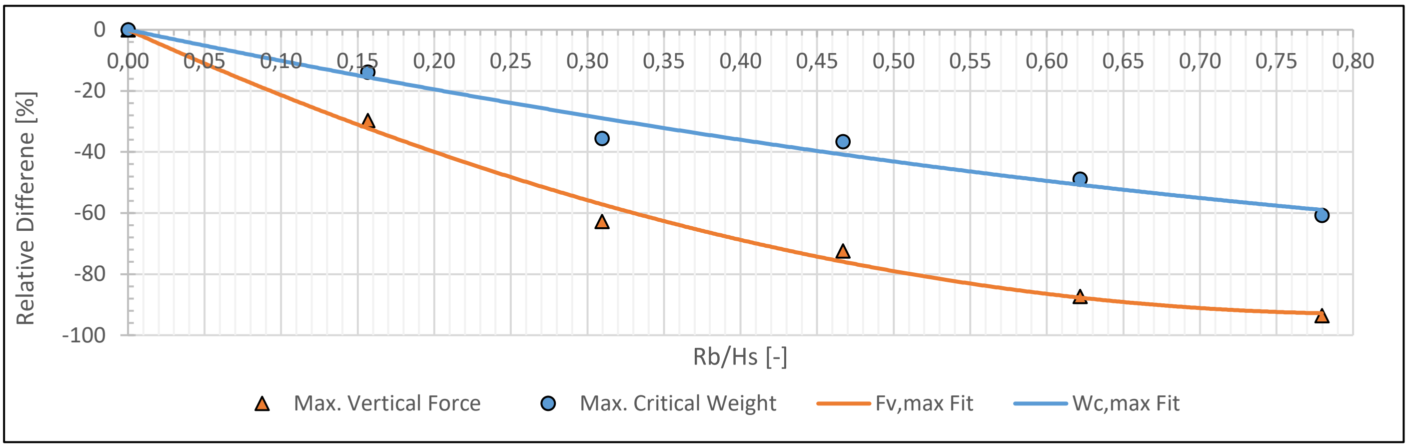

Figure 61. Relative difference of maximum vertical force $F_{V,max}$ and maximum critical weight $W_{c,max}$ to the reference case FB0 (R_b=0), data from Method I against the dimensionless base freeboard R_b/H_s.

6.2. Effect of different methods of increasing the base freeboard

In this section the effects of increasing the base freeboard R_b with methods I and II are investigated by comparing the results from the corresponding simulations to the reference case of zero freeboard (FB0). All the graphs presenting a relative difference, are referring to the difference between the value of each case to the reference base case. An overview of the results from the simulations is given in Appendix Table 1 of Appendix A. It is important to note that for all cases the incoming wave height and period was found to show insignificant changes (up to 1.24% with no specific trend).

<u>Wet base length</u>

Firstly, the investigation is focused on the wet base length X_c. In Figure 60 the clear trend of decreasing wet base length for increasing base freeboard was shown. In the same figure, comparing the two methods, it is observed that even though they show very similar trends, method I results in shorter X_c than Method II for the same R_b. Especially for larger values of R_b, the difference in X_c between the two methods grows larger.

The wet base length X_c resulting from the simulations was also compared with the proposed formulation for its calculation by (Bekker, 2017) given as equation 3.49 (for swell waves) in section 3.1. For method II the equation completely fails to predict X_c, resulting in a fully wet bottom surface. This is to be expected as the formulation is based on changes of the water level which in method II do not occur. For method I it was observed that the equation slightly underpredicts the wet length compared to the simulated results.

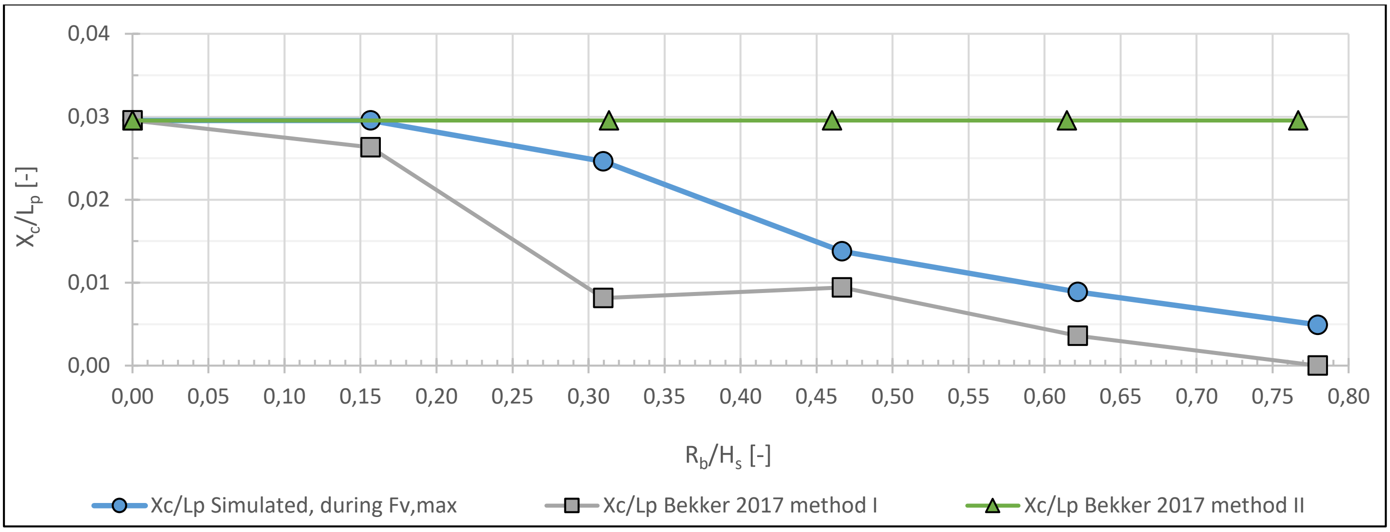

Figure 62. Dimensionless wet base length X_c/L_p during maximum vertical force (method I) and as calculated by the method of (Bekker, 2017) for method I and method II, against the dimensionless base freeboard R_b/H_s.

Effect on maximum forces

In this paragraph the investigation is focused on the forces exerted on the crown wall element. Figures 63, 68 and 71 illustrate the relative difference to the reference case of the maximum horizontal force F_H, maximum vertical force F_V and maximum critical weight W_c respectively. For each plotted value, the relative difference is taken to its starting value at the reference case (FB0). This is plotted against the increasing base freeboard with methods I and II.

For each case the loading has also been calculated and compared with the empirical methods of (Pedersen, 1996), (Nørgaard et al., 2013) and the reduction factor of (Bekker et al., 2018). As for every case the water level, wave height and period at the toe of the structure and some geometrical parameters change (e.g. empirical volume coefficient, protected crown wall height etc), the calculation result with the empirical methods is different for every case.

As discussed in the validation of wave loads paragraph of section 5.3, for zero base freeboard the empirical methods provide results significantly higher than the physical experiment case chosen (of J.Bekker) , but on the other hand the base reference case (FB0) on which all the comparisons are based provides a higher vertical force. That results in the critical weight to also be higher than that of the empirical methods. For that reason, the empirical methods are used to observe qualitatively if their relative differences from their starting values follow the changes in base freeboard and the curve shapes that result from the simulations and not as absolute values.

Horizontal Forces

Regarding the horizontal forces, in Figure 63 is observed that the simulations with both methods result in an increase of maximum horizontal force F_H as the base freeboard R_b increases. It would be expected that the horizontal forces decrease, especially for method I where with lower water level a larger run-up is required to reach the crown wall. For method II, previous research from (Jacobsen et al., 2018) found that the horizontal forces initially decrease when increasing R_b, followed by stagnation or increase for large values of R_b due to the increase of the unprotected crown wall height with this method. The simulated results of the current study show an opposite trend, which suggests issues with their reliability. Following, these horizontal force trends are explained based on the simulated results.

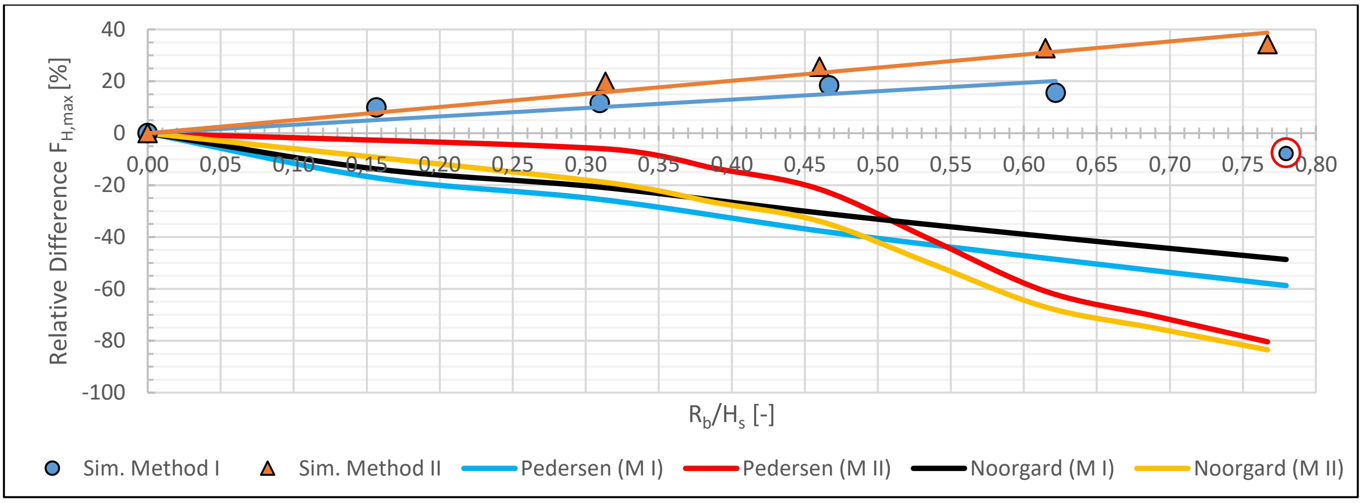

Figure 63. Relative difference of maximum horizontal force $F_{H,max}$ to the reference case (FB0) for varying dimensionless base freeboard R_b/H_s with both methods. Includes simulation results and calculations with empirical methods. Circled data point considered as an outlier.

When comparing the two methods, Method I shows lower maximum horizontal forces than Method II for all values of R_b. This is expected as for Method II a larger portion of the crown wall vertical face is not protected by the armour layer than in Method I, which increases the pressures on that part of the wall.

The increasing maximum horizontal force for Method I can be better understood by observing the horizontal pressure distribution Figure 64. The magnitude of the pressure slightly increases with increasing freeboard. However, it is the area that shows greater change. As the base freeboard increases, it is observed that the pressures at the lower part of the crown wall face (protected by the armour layer) increase significantly.

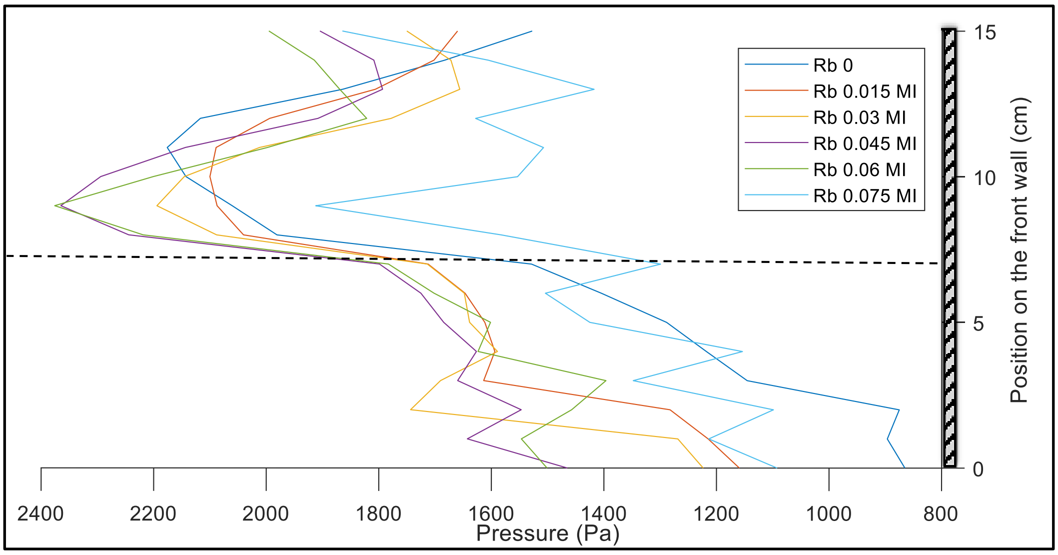

Figure 64. Horizontal pressure distribution at the moment of maximum horizontal force F_H for varying base freeboards R_b with method I. The dashed line shows the height of the armour layer protecting the crown wall.

The increasing pressure at the lower part of the vertical face can be related to change in the wave structure interaction as R_b increases, which can be observed in the following Figure 65. For larger R_b it is observed that less air is entrapped between the wave crest and the crown wall as there is space underneath the crown wall for it to escape. Thus, all the space is filled with water resulting in higher pressures. Additionally, as the water level is lower, the wave finds a higher wall, resulting in less overtopping. Thus, a larger volume of water is down rushing on the vertical face of the crown wall.

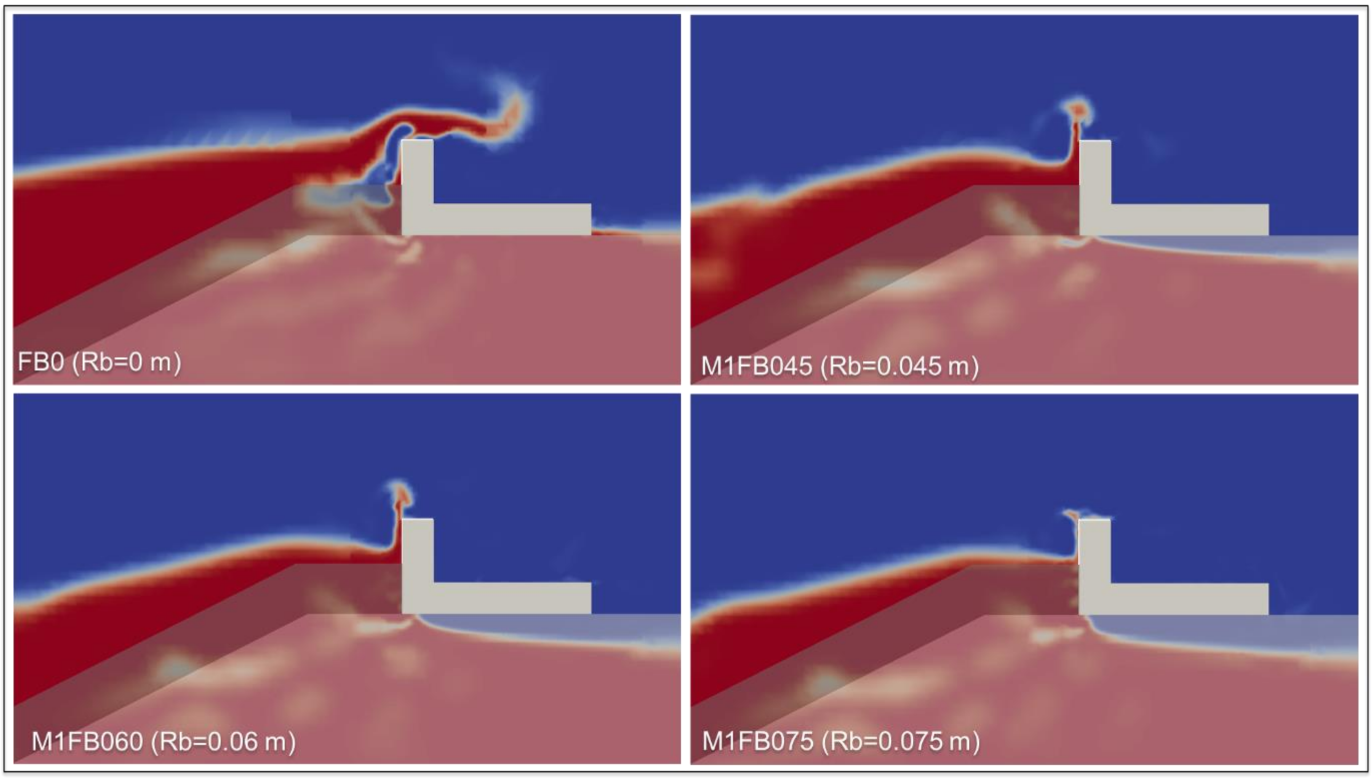

Figure 65. Wave-structure interaction at the moment of maximum horizontal force F_H for varying base freeboard R_b with method I.

The lowest horizontal force resulting for case M1FB075 with the largest freeboard (R_b=0.075 m) of method I (circled data point in Figure 63) is decided not to be trusted, as the pressure distribution observed in Figure 64 demonstrates a very spiky, non-smooth curve with significantly lower pressures compared to all the other simulation results. On the bottom right of Figure 65 which corresponds to that case, some air entrapment along the vertical face is observed that is probably the cause of this bizarre pressure distribution. This result does not match the rest of the observations and as such is considered an outlier.

Better insight in the increase of the maximum horizontal force for Method II can be obtained from Figure 66Figure 64. When analysing the horizontal pressure distribution, similar to method I, the magnitude of the pressure slightly increases with increasing R_b, while more significant differences are found for the area of the pressure. For small R_b high pressures are accumulated around the upper-middle part of the crown wall face, with lower pressure at the top and bottom of the vertical crown wall face. As R_b increases, it is observed that the pressures at the edges of the crown wall face increase significantly.

The same reasoning for the increasing pressure at the lower part of the vertical face mentioned for method I holds true also in this case. Additionally, there is an effect related to the protected height of the crown wall. For method II, as the crown wall is elevated, less of its vertical face is protected by the armour layer, resulting in increasing pressure which is shown in Figure 66.

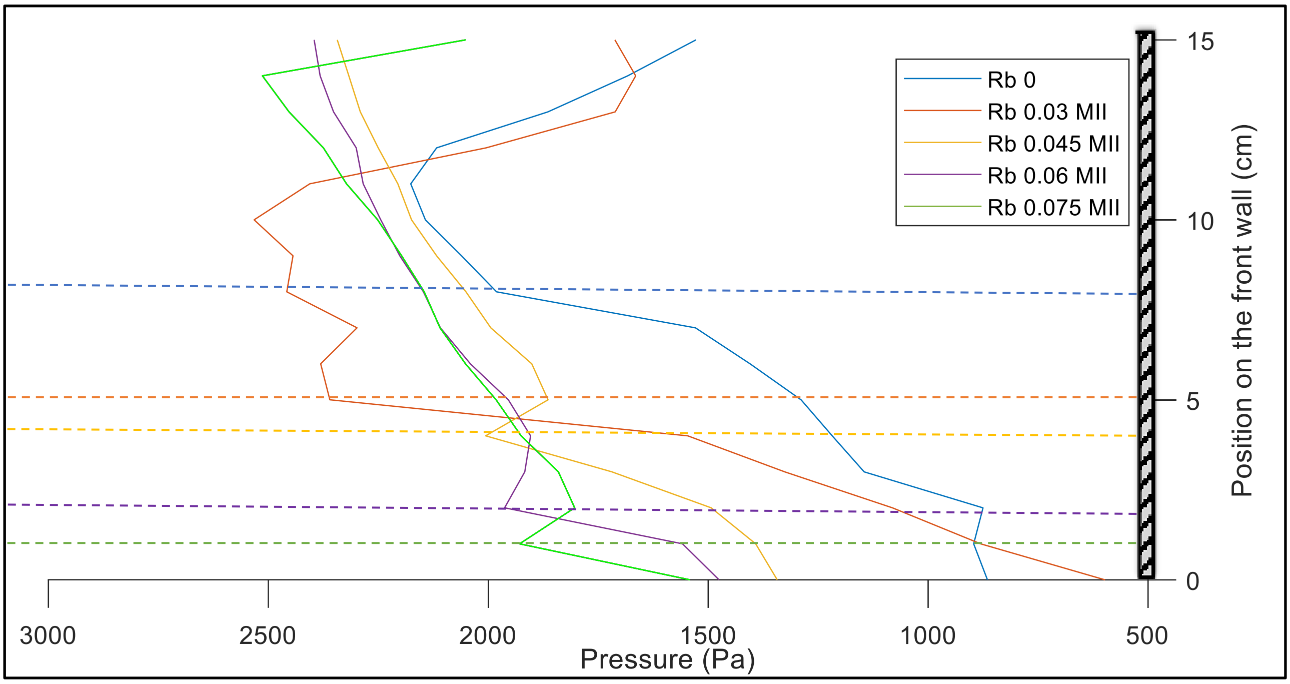

Figure 66. Horizontal pressure distribution at the moment of maximum horizontal force F_H for varying base freeboards R_b with method II. The horizontal dashed lines illustrate the height up to which the crown wall is protected by the armour layer for that freeboard.

The increasing pressure at the upper part of the vertical face could be connected with changing wave-structure interaction and overtopping as the freeboard increases. This can be observed in Figure 67. Compared to the case when the R_b is increased, with no or small R_b, larger volume of water overtops the crown wall, as the same wave encounters a lower crown wall height. That results in a larger water volume 'escaping' behind the crown wall. On the other hand, when the freeboard is increased this volume does not escape through overtopping but down rushes on the crown wall face instead, leading to higher pressures. That also has an impact on the entrapped air as can be observed in Figure 67.

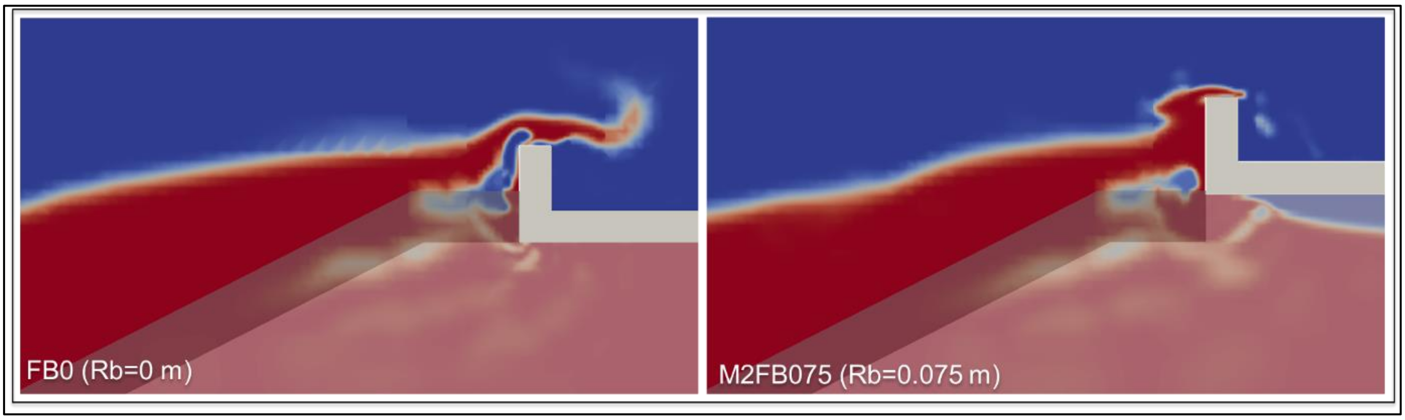

Figure 67. Wave-structure interaction at the moment of maximum horizontal force F_H for zero freeboard (FB0) and for the largest simulated freeboard with method II (test M2FB075).

The empirical methods of (Pedersen, 1996) and (Nørgaard et al., 2013) fail to predict the changes as they were formulated based on tests with zero freeboard. The reduction shown in the empirical methods (Figure 63) as R_b increases, result from the reduction of depth in Method I (increases the A_c or R_{ca} length in the formulas). For Method II it is the protected crown wall height $d_{c,prot}$ that is being reduced and is leading to reduced horizontal forces. These lengths in the formulas of (Pedersen, 1996) and (Nørgaard et al., 2013) were intended for changes in the armour layer or crown wall dimensions while the crown wall base is still at the SWL elevation. Because of that, they are not able to predict the change in loading due to freeboard changes accurately.

Vertical Forces

Concerning the vertical forces, in Figure 68 one can observe that the maximum vertical force F_V reduces as the base freeboard R_b increases for both methods. This is in agreement with the findings of (Bekker et al., 2018) and (Jacobsen et al., 2018). Moreover, it was expected as the wet base length X_c was also found to reduce (Figure 60), which reduces the integration area for the force, resulting in lower F_V.

For Method I, empirical formulas show a decrease of vertical force with increasing R_b, but still overestimate the forcing. On the other hand, the empirical methods fail to predict any change for increasing R_b with Method II. This is because these formulas were not designed for an increase of freeboard. The reason that there is a decrease in F_V with the empirical formulas for Method I is due to the decrease in water level, which changes the length of A_c (or R_{ca}) in the formulas. This does not change for Method II that has unchanged SWL resulting in no change in the predicted loading.

The calculation with Bekker's proposed reduction factor (as discussed in section 3.1) works only for Method I which it was designed for. As the water level in method II remains unchanged, the reduction factor takes a value of one, and the forces are calculated as in the method of (Nørgaard et al., 2013). For method I it shows an overall good agreement with the simulation results of Method I for which it was designed for. There is only a slight overestimation in the order of 10% for the smaller freeboards, while for case M1FB017 (largest freeboard) it predicts zero vertical force while the simulations result in a small force.

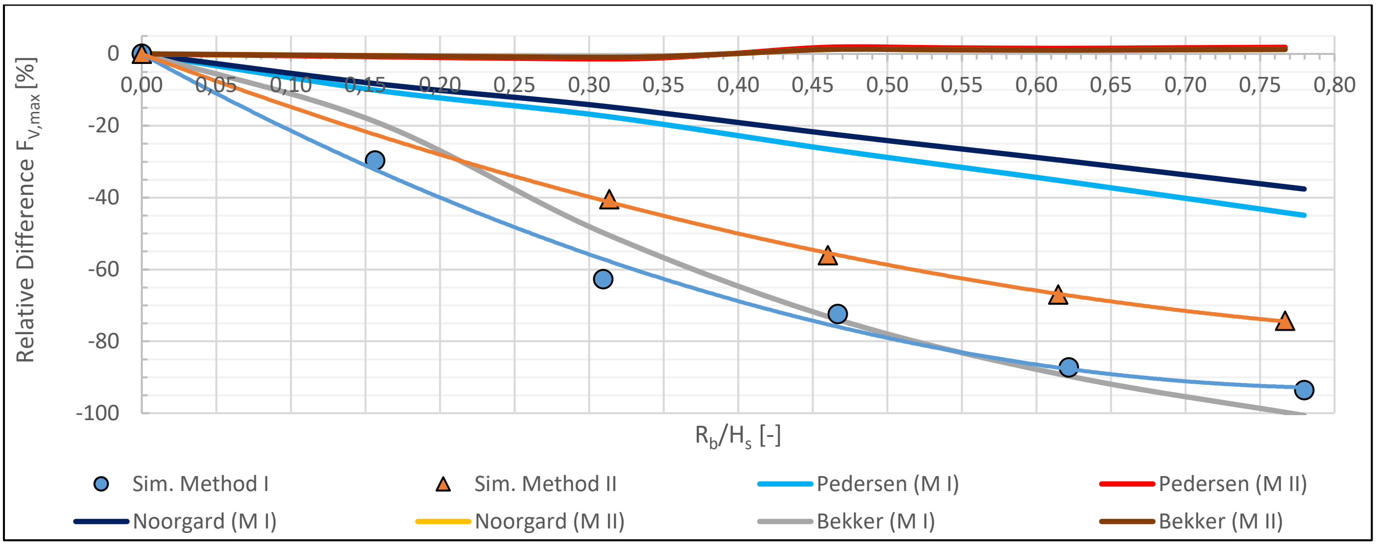

Figure 68. Relative difference of maximum vertical force F_V to the reference case for varying dimensionless base freeboard R_b/H_s with both methods. Includes simulation results and calculations with empirical methods.

Comparing the two methods, Method II results in higher vertical force in comparison to method I for all R_b values. One reason for that is the larger X_c for Method II (Figure 60). Another is that the magnitude of pressures is higher for Method II as well, as can be seen in uplift pressure distribution discussion that follows in section 6.3. This is because method II has a higher water level compared to method I, leading to a different reference level for the run-up (higher for method II). This results in a larger volume of water above the armour layer, as can be seen in the following Figure 69, which affects both the horizontal and vertical forces.

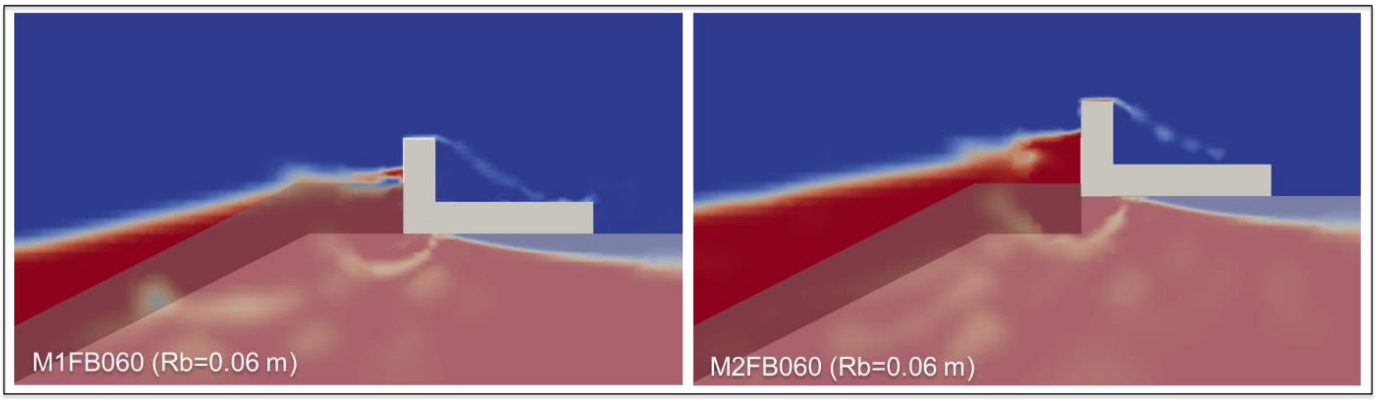

Figure 69. Wave-structure interaction at the moment of maximum vertical force F_V; (left) for base R_b freeboard 0.06 m with method I (test M1FB060) and (right) with method II (test M2FB060).

Relationship between Vertical and Horizontal Forces

In Figure 70 both the maximum F_H and F_V are plotted together. It is observed that for zero or small R_b the vertical forces dominate. However, as already discussed, as the base freeboard increases the horizontal force slowly increases and the vertical force decreases rapidly. This leads to a domination of the horizontal force for larger values of R_b. Comparing the two methods, one can observe that for method I this dominance of the horizontal force occurs for smaller R_b than in method II, as well as the difference between the magnitude of the two forces is larger in method I.

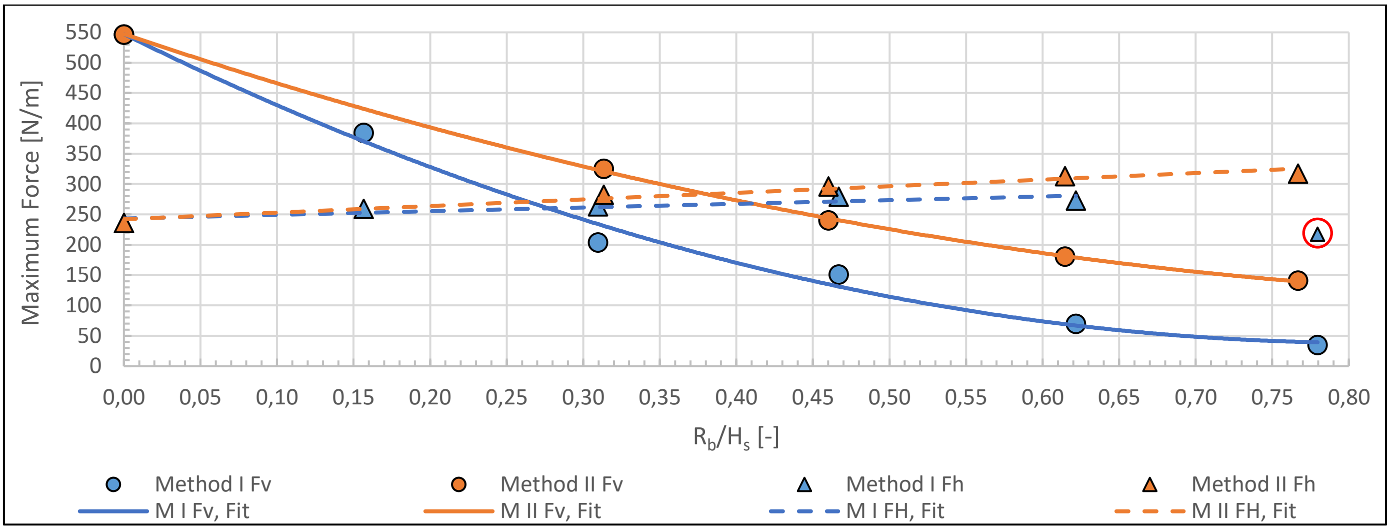

Figure 70. Simulated maximum vertical F_V and horizontal F_H forces against the dimensionless base freeboard R_b/H_s with both methods. Circled data point considered as an outlier.

Effect on critical weight

This paragraph focuses on the maximum critical weight W_c due to sliding, as calculated by equation 2.1. As previously discussed, the moment in time when the maximum W_c occurs is the critical condition and is not necessarily the same moment in time when the maximum F_V and F_H occur. In Figure 71, the relative difference of maximum W_c compared to the reference case is observed for increasing R_b using both methods. This is done by using the resulting F_V and F_H time signals that resulted from post-processing of the measured pressures into equation 2.1 and acquiring the maximum value of the W_c time signal. As explained in section 6.1, the maximum F_V and F_H do not occur at the same moment in time and this maximum value of W_c is at a moment in time either the same of one of the two maximum forces, or at a time between the two maxima. Additionally, the maximum W_c using empirical methods are plotted. As these methods assume the maximum F_V and F_H to occur simultaneously, these values are used in equation 2.1 to calculate W_c.

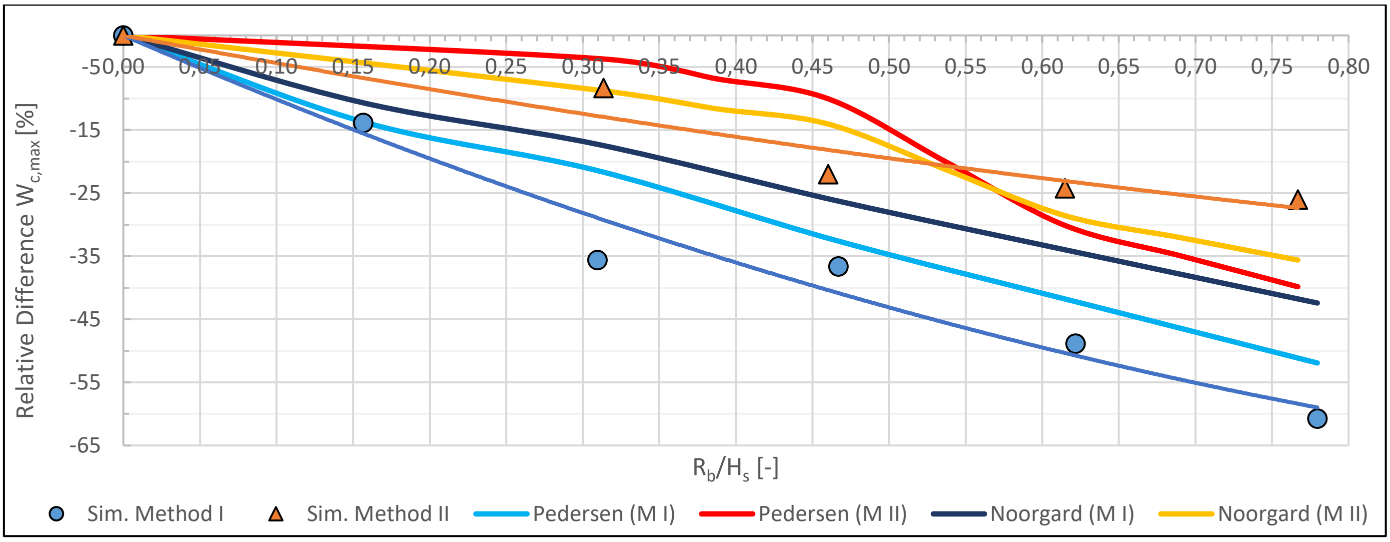

Figure 71. Relative difference of maximum critical weight W_c to the reference case (FB0) for varying dimensionless base freeboard R_b/H_s with both methods. Includes simulation results and calculations with empirical methods.

In Figure 71 is observed that W_c for method I is always smaller than the one for method II, which is expected as both the maximum F_V and F_H for method I are smaller than the ones for method II.

Moreover, as R_b increases the maximum W_c decreases. For the part where F_V is larger than F_H (small R_b values) this can be explained by the domination of F_V, which reduces with increasing R_b, in equation 2.1. However, as shown in Figure 70, F_H is higher for larger values of R_b, and as in equation 2.1 is divided by the friction factor which is smaller than 1, its influence becomes even greater. For that reason, it is expected for W_c to show an increasing trend for the large values of R_b, which however is not the case.

The reason that the maximum W_c is still influenced more from F_V rather than F_H can be understood by examining the time of occurrence of the maximum forces and maximum critical weights. It was found that the maximum W_c occurs either simultaneously with the maximum F_V (at that time F_H has a lower magnitude than its maximum) or at a moment closer to the time where the maximum F_V occurs than the time the maximum F_H occurs. As such, at the time of critical condition, F_V is closer to its maximum magnitude while F_H is not, resulting in a greater influence of the vertical force.

The empirical methods of (Pedersen, 1996) and (Nørgaard et al., 2013) that assume simultaneous occurrence of the maximum F_V and F_H, do not account for this time effect. Because of that they are influenced more by F_H. Thus, as explained in section 6.1 there is an overprediction for method I. For method II, as the empirical methods fail to predict any change on the vertical forcing (Figure 68) the trend followed is the same as that of the horizontal force. As that was found to constantly decrease for the empirical methods, while it increases for the simulated results, one can observe that the empirical methods start with overestimation, but for greater freeboards result in underestimation. That however is expected when observing the graphs of F_V and F_H (Figure 63 and Figure 68).

6.3. Shape of uplift pressure distribution for varying base freeboards.

As mentioned in section 3.1, (Bekker, 2017, Bekker et al., 2018) observed two uplift pressure distributions (shown in Figure 28) an S-shaped profile for small or zero R_b, where the base slab is wet in all its length, and a polynomial shaped profile for an increasing R_b, where X_c decreases. All of the currently used empirical methods assume a triangular distribution, unrelated to X_c. As previously discussed, the shape distribution greatly affects the vertical (uplift) force on the crown wall, as the area under the distribution curve is the pressure integration area for calculating the force. Also, it is the deciding factor for the point that the force is applied, which becomes important for the calculation of the overturning moment for the overturning failure criterion.

In the present study, the pressure distributions during the moment in time where the maximum W_c occurs where investigated. The cases examined were the ones detailed in section 5.4 for varying freeboards with the two different methods of increment. The results are presented in Figure 72. Similar trends with higher pressure magnitudes and slightly larger X_c were found at the time of maximum F_V.

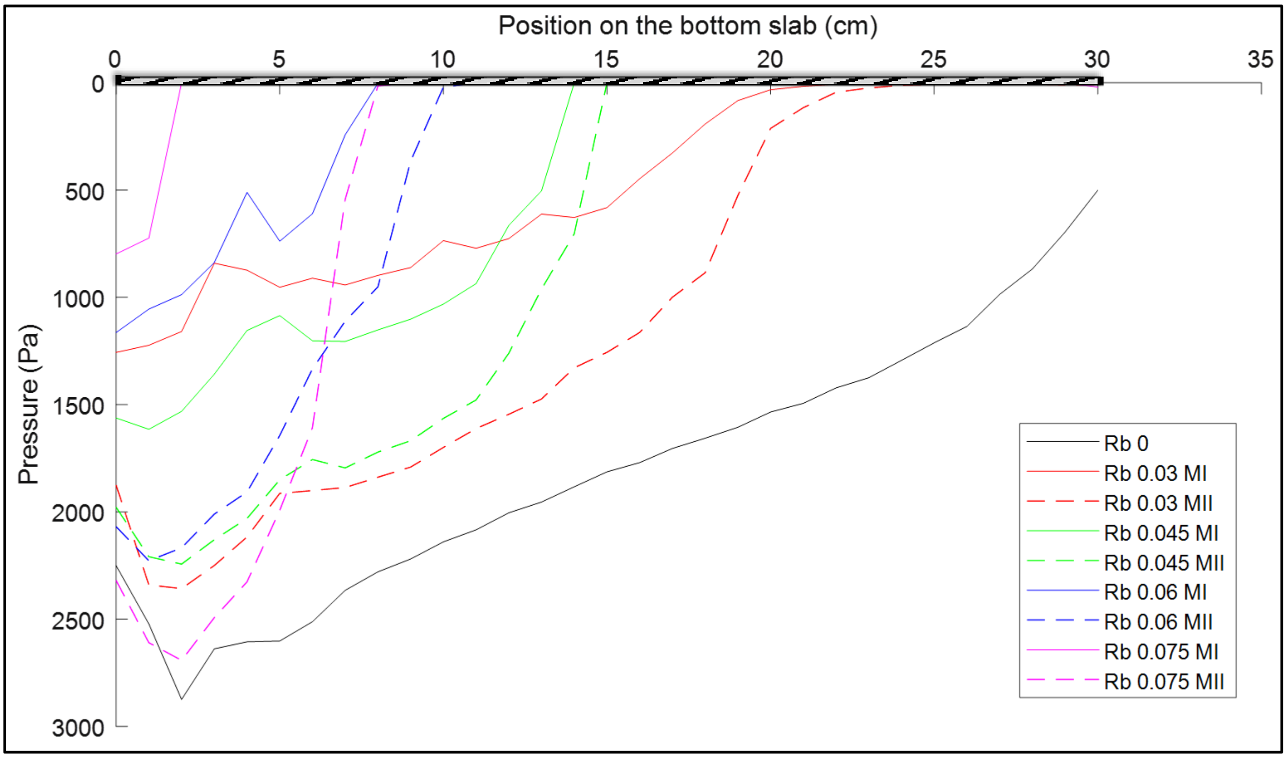

Figure 72. Uplift pressure distributions for various base freeboards R_b during maximum critical weight. Same colour represents same base freeboard. Solid line represents method I, while dashed line method II. Zero is the most seaward location, while 30 cm is the end of the bottom slab.

It was observed that for zero R_b the pressure distribution indeed followed an S-shaped profile as proposed by (Bekker, 2017, Bekker et al., 2018). There were however two notable differences. Firstly, as can be observed in Figure 73, the pressure has a peak not at the most seaward location of the bottom slab (as proposed by (Bekker, 2017, Bekker et al., 2018) and assumed by empirical methods) but at a location 2 cm inwards. That peak was also observed at that specific location for increased R_b with both methods (also in the following simulations with varying breakwater slopes). This peak could have been missed in the experiments of (Bekker, 2017) as there were only five pressure gauges used, with the first 4.1 cm inwards as shown in Figure 32. The peak is observed before that first pressure gauge of Bekker (as in the numerical experiment the bottom face of the crown wall is densely covered with pressure gauges), and as such could have been missed in the physical experiment.

The second difference as observed in Figure 73, is that the proposed shape by Bekker is fitted within the triangle of the previously assumed distribution (green dashed line under the red dashed line). Meaning that the pressure only becomes lower than previously assumed. The found distribution although S-shaped seems to become larger near its end than the previously assumed triangular distribution.

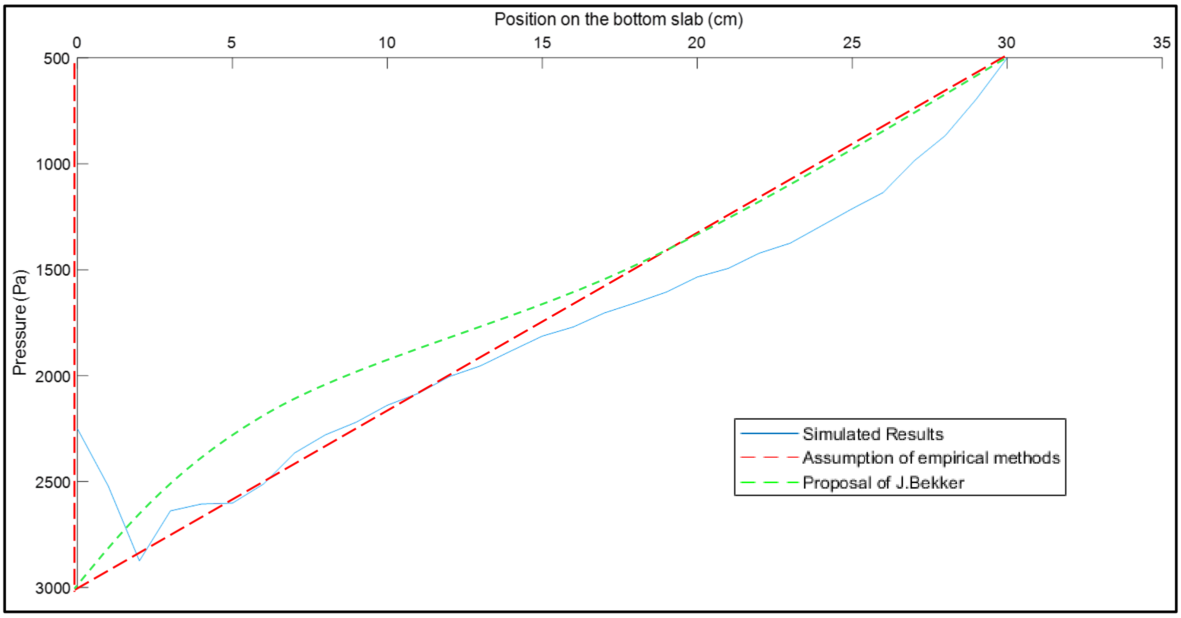

Figure 73. Uplift pressure distribution for reference base case (FB0). Zero base freeboard, 1:2 breakwater slope.

In most of the simulations the mentioned peak is followed by a steep decrease (reverse peak) at the location between 3 and 5 cm on the bottom slab. This effect can be the result of the air volume between the wave crest and trough that becomes entrapped the time when the crest reaches the vertical face of the crown wall. That space is then filled with a volume of water down rushing on the vertical face of the crown wall which, upon reaching the corner between the vertical and bottom faces, follows a circular motion and starts covering the bottom face. This is depicted in Figure 74, with the corresponding uplift pressure distribution in Figure 75.

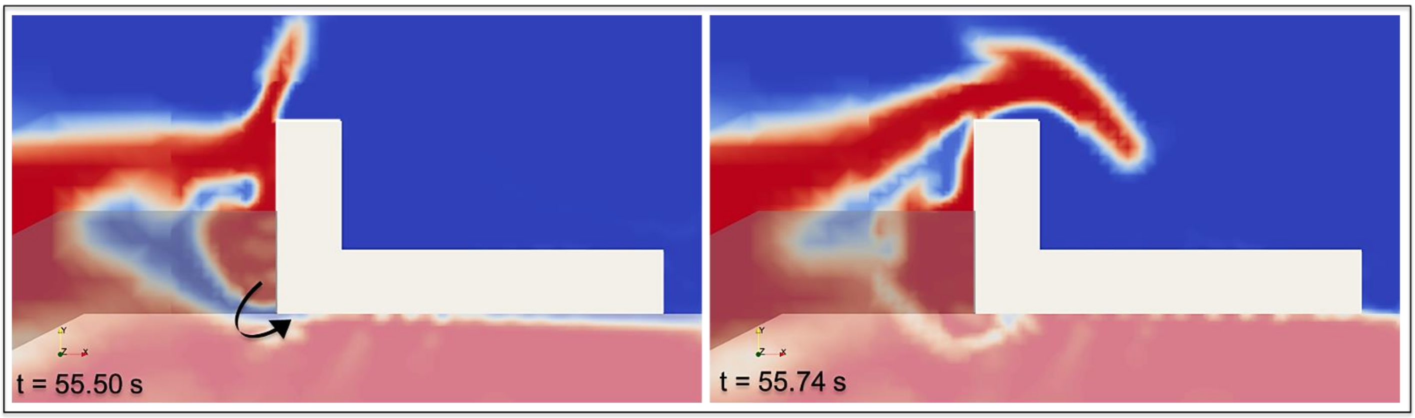

Figure 74. Wave impact on crown wall. Left: fraction of a second before moment of maximum W_c. Right: Time of maximum W_c. Case of 0.015 m base freeboard with method I (test M1FB015).

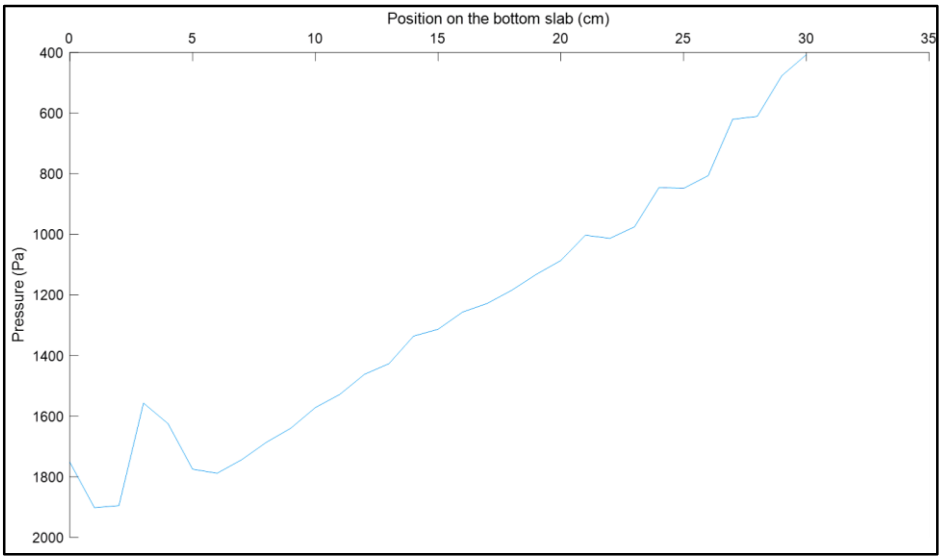

Figure 75. Uplift pressure distribution at the moment in time of maximum W_c. Case of 0.015 m base freeboard with method I (test M1FB015).

Following, it was observed that as R_b increases, firstly the distribution is limited to the wet base length X_c, similar to the proposal of (Bekker, 2017, Bekker et al., 2018). However, it was also observed that with the freeboard increasement the profile curve tends to reverse. For small freeboard R_b (0.015 m) it becomes almost a straight line (as seen in Figure 75), and as R_b increases the curve reverses. This contradicts the proposed distribution of (Bekker, 2017, Bekker et al., 2018), as the resulting profile has the opposite shape. This can be observed in Figure 76, where it also becomes apparent that the resulting area under the profile is significantly larger, which will result in a larger vertical force. However, no concrete conclusions can be drawn as the distributions proposed by (Bekker, 2017, Bekker et al., 2018) are based on a wider range of wave conditions in comparison with the findings of this study, where one wave condition is used. It is possible that different wave conditions will result in different uplift pressure distribution shapes.

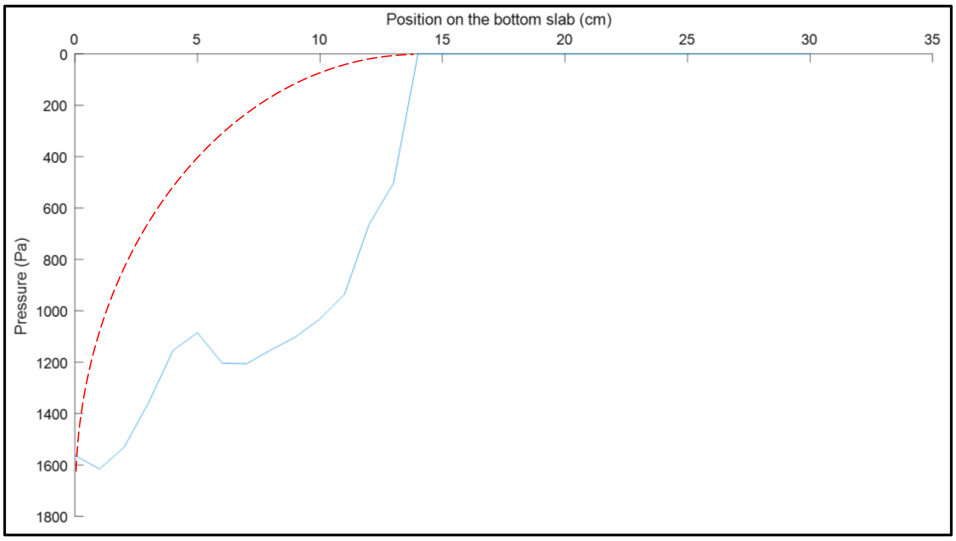

Figure 76. Uplift pressure distribution at the moment in time of maximum W_c. Case of R_b= 0.045 m with method I (test M1FB045). The red dashed line represents the proposed distribution by Bekker.

When comparing the two different methods of R_b increasement (comparison between solid and dashed lines of the same colour in Figure 72), one can observe that method II shows both a longer X_c and quite higher (1.5 to 2 times) peak pressures than method I. That results in a larger area and thus a higher F_V. Furthermore, it can be observed that this difference in X_c increases with increasing R_b. The difference is small for R_b= 0.03 m but becomes very significant for R_b = 0.075 m. The shapes of the distribution follow generally the same trend, from which can be concluded that the method of increasing the base freeboard has an impact on the magnitude of the pressure and force but is distributed in a similar manner along the bottom slab.

6.4. Time lag between horizontal and vertical forces.

As previously discussed, the maximum F_V and F_H do not appear at the same moment in time for each wave, but rather there is a time lag between their appearance (Bekker, 2017, Van Heemst, 2014, Pedersen, 1996). This time lag was examined during the interaction of the maximum wave of the time series for each case on the crown wall, which is also the wave for which the maximum W_c occurs. It was found that the maximum F_H always occurs first, with a time lag between 0.03 and 0.5 seconds before the occurrence of the maximum F_V. Because of the scale of the experiment, this corresponds to around 0.16 to 2.74 sec in the real world. This can be explained as the wave crest arrives first on the vertical face of the crown wall followed by the main "body" of the wave filling up the air volume underneath the crest, flowing through the porous medium and exerting pressure on the bottom face of the crown wall. This can also be visually observed in Figure 81 of the next section. Furthermore, there was no correlation found between the magnitude of the forcing and the length of the time lag.

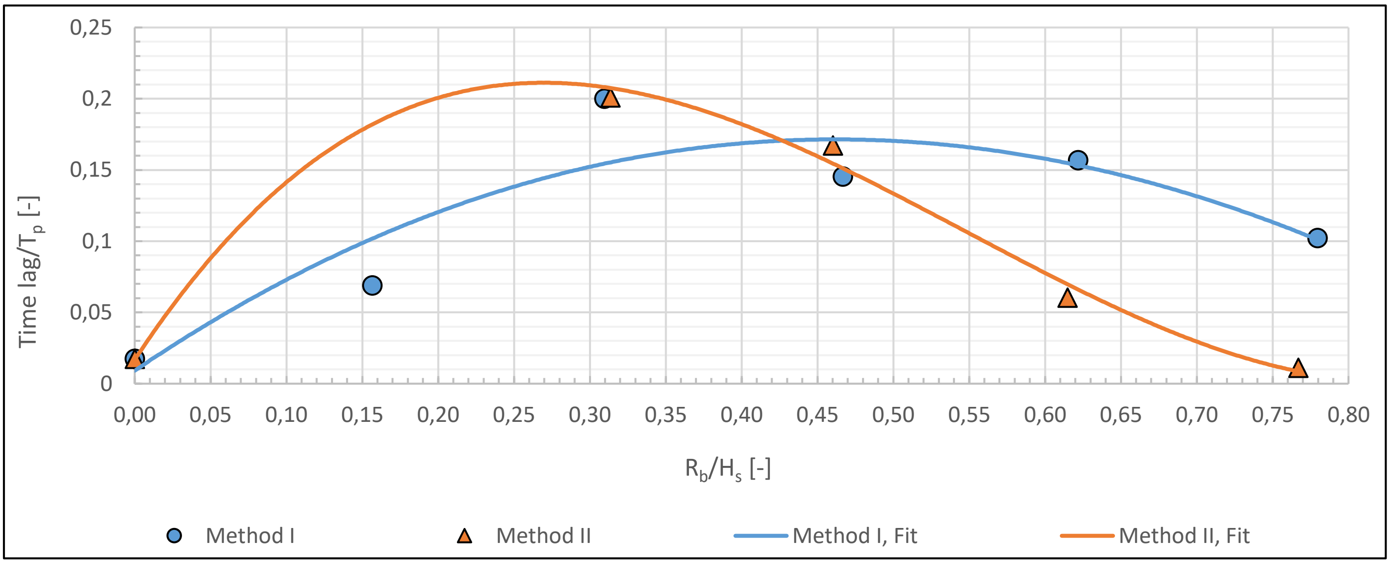

Figure 77. Dimensionless time lag between the occurrence of the maximum F_H and F_v, during the interaction between the largest wave and the crown wall for various dimensionless base freeboards R_b/H_s with both methods.

In Figure 77, the time between the occurrence of the horizontal and vertical force (time lag) is illustrated in a dimensionless manner, for various values of R_b with both of the investigated methods. One can observe that for small values of R_b the difference in the magnitudes of time lags between the two methods is fairly small, however for large R_b method I shows larger time lags than method II.

In Appendix Figure 1 and Appendix Figure 2 of Appendix B, one can observe that at the time either F_H or F_V reach their maximum value, their pairing force is much lower than its own maximum. This effect is observed to be stronger for Method I. Also, for larger R_b it is observed that the pairing force is closer to its maximum value.

In Figure 78, the dimensionless time lag is illustrated for varying breakwater slopes. Although the trend is not very clear and tests with more wave conditions should be implemented in order to acquire more data points, it appears that a gentler slope leads to longer time lag.

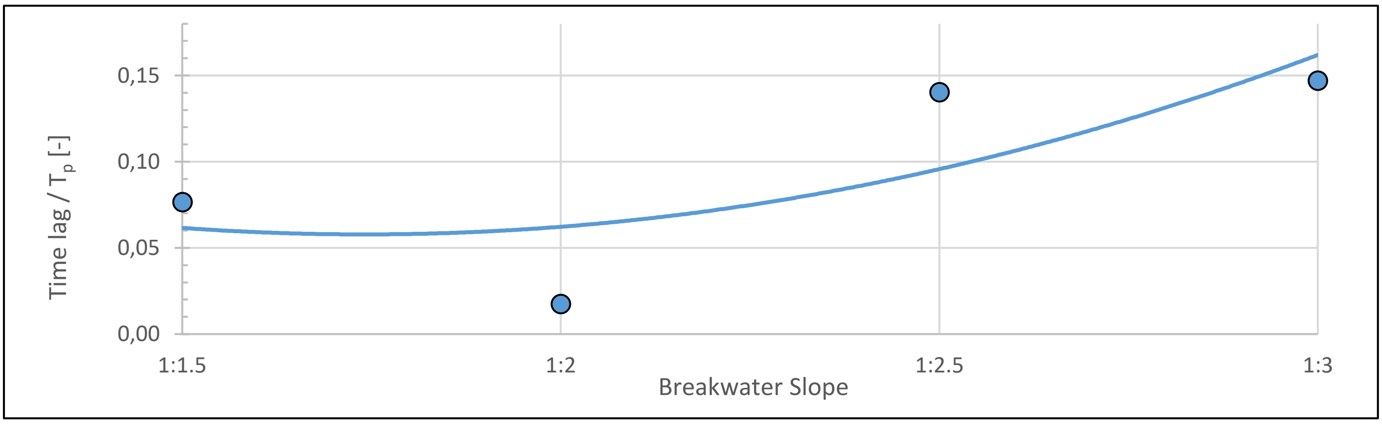

Figure 78. Dimensionless time lag between the occurrence of the maximum horizontal and vertical forces, during the interaction between the maximum wave and the crown wall for various breakwater slopes.

As in order to decide the stability of the crown wall, the forces exerted at a specific moment in time are of interest, and as the maxima do not appear simultaneously, the loading to the crown wall is thus reduced. As such, the crown wall which stabilizes by its own weight, can be designed lighter, using less material, and thus at less cost. As fore mentioned however, further studies are needed on the inertia effects and the response of the structure.

6.5. Effect of breakwater slope variations.

In this section the effects of varying breakwater slope angles are investigated. The slopes tested were 1:1.5, 1:2, 1:2.5 and 1:3. The base freeboard for all the cases is zero, to enable a comparison with empirical methods. The input wave conditions are kept constant as detailed in the previous chapters. In the following Table 25 the simulated cases ID along with the basic inputs are presented. All relative values in the graphs that follow are relative compared to their value for the reference base case FB0 (zero freeboard, 1:2 breakwater slope). The results are presented in Appendix Table 2 of Appendix A.

Table 25. Inputs for simulated cases for varying breakwater slope.

Case ID	SWL [m]	Base freeboard R_b [m]	Breakwater slope	H_s [m]	T_p [sec]
S15	0.65	0	1:1.5	0.10295	2.55
FB0	0.65	0	1:2	0.10295	2.55
S125	0.65	0	1:2.5	0.10295	2.55
S13	0.65	0	1:3	0.10295	2.55

It was observed that for all slope cases, the shape of the uplift pressure distribution during critical condition was similar. An example from the base (reference case) was shown in Figure 73, while the rest of the cases follow a similar distribution shape.

In Figure 79 the maximum F_V and F_H and in Figure 80 where the maximum W_c for the varying slopes are illustrated. It can be observed that a gentler breakwater slope results to a steep increase in F_V and as a consequence an increase to W_c as well. The horizontal force also shows a very slight increase.

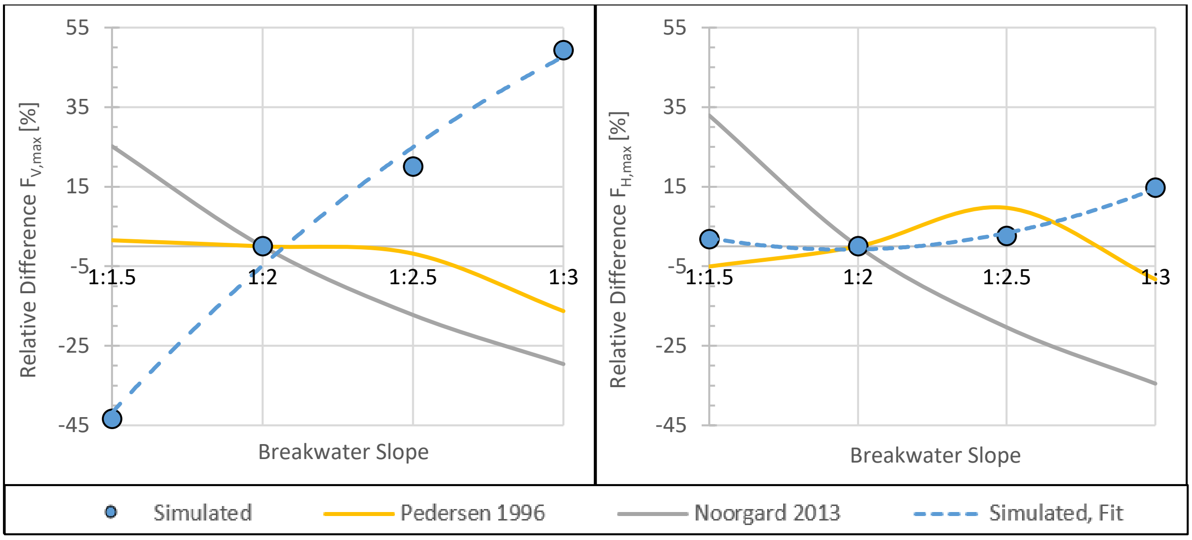

Figure 79. Left: Relative difference of maximum vertical force F_V to the reference case for varying breakwater slopes. Right: relative difference of maximum horizontal force F_H to the reference case for varying breakwater slopes.

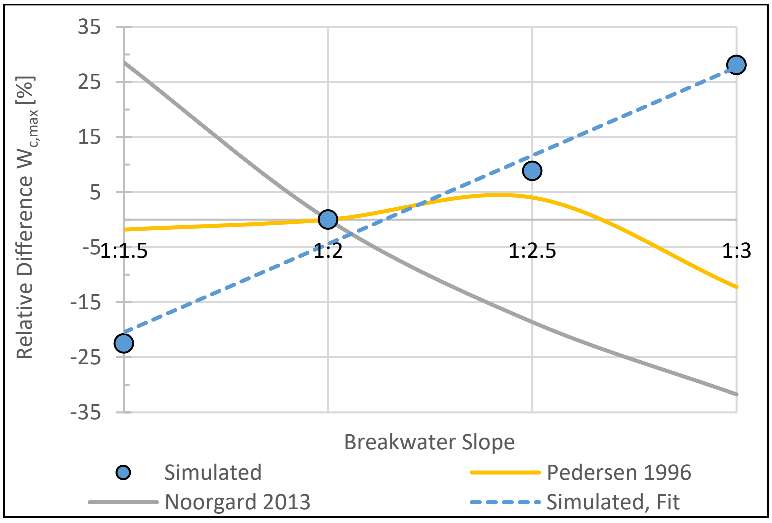

Figure 80. Relative difference of maximum critical weight W_c to the reference case for varying breakwater slopes.

In Appendix Table 2 one can observe that the breaker parameter ξ_m at the toe greatly reduces as the slope becomes gentler, changing the wave breaker type from surging to collapsing and then to plunging waves (the types of breaking waves were shown in Figure 10). This results in a reduction of run up and velocities on the breakwater slope, which in return are expected to result in lower loading on the crown wall. However, the opposite effect is observed on the loading, which in the previous figures was observed to increase.

Figure 81 illustrates the wave structure interaction for cases with three different breakwater slopes during the largest simulated wave. It is observed that in all cases the wave breaks on the crown wall face rather than the breakwater slope which is expected as the incoming wave is a low steepness swell wave. It is also observed that for gentler slopes the water surface near the structure is higher as the wave moves closer to the structure and the porous layers are filled with water before-during-and after the wave impact. On the contrary, for steeper slopes there is air in the porous layer before the crest reaches the crown wall. Meaning that there is larger internal set-up for gentler slopes. That is the cause for the steep increase in vertical forces.

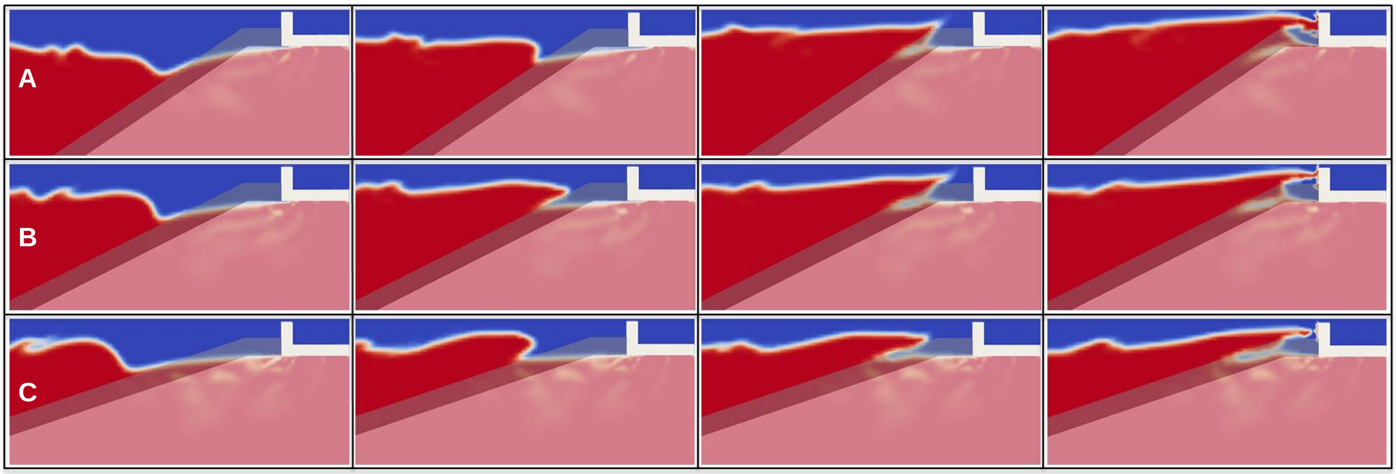

Figure 81. Simulated wave-structure interaction for various slopes (largest wave of time series) for A) slope 1:1.5 (test S15), B) slope 1:2 (test FB0) and C) slope 1:3 (test S13).

Except from the visual observations this is also quantified from the wave gauge measurements. In the following Figure 82, it is observed that close to the crown wall element, the internal setup inside the breakwater increases. For gentler slopes this increase is larger.

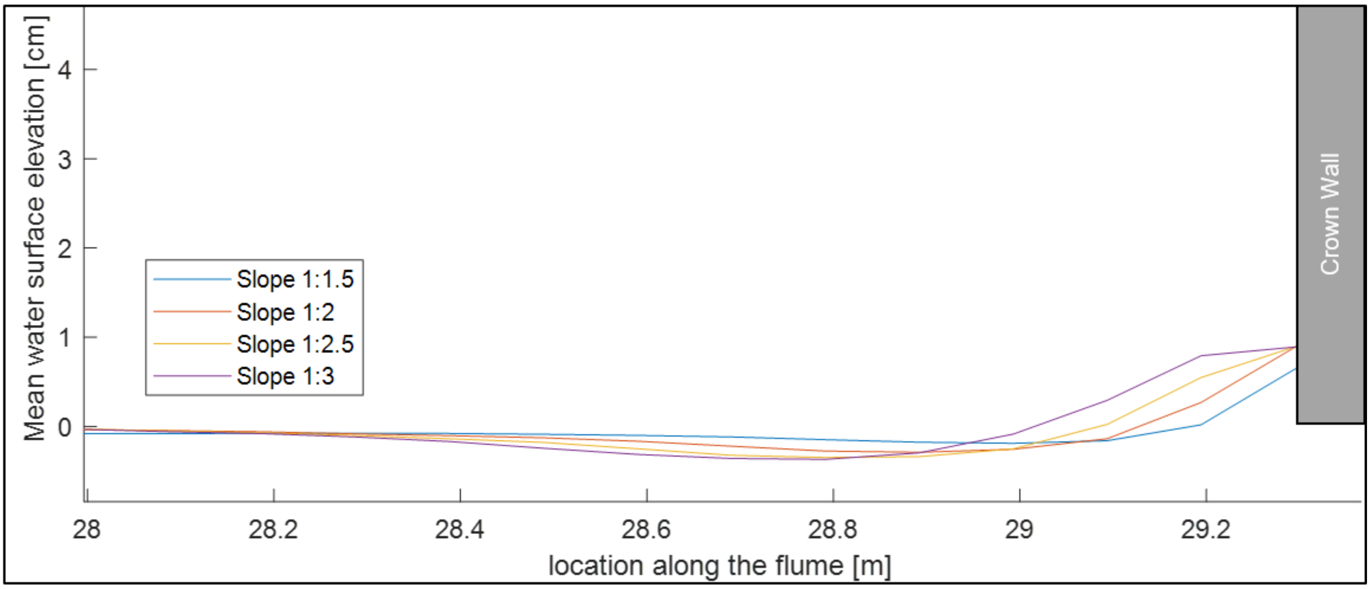

Figure 82. Mean water surface elevation (depth subtracted), from the location of the initial toe of the breakwater until the location of the crown wall, for various breakwater slopes.

The method of (Pedersen, 1996) was based on some breakwater slope variations (1:1.5, 1:2.5, 1:3.5) and because of that was expected to provide more accurate predictions. The large decrease of the loading for the slope of 1:3 is a result of a rapid decrease of run-up compared to the 1:2.5 slope. The increase of horizontal force for the 1:2.5 slope is a result of two changes. The one is the berm width of the armour layer in front of the crown wall B_a that is slightly reduced (third decimal) by the way the slope was changed and only the method of Pedersen takes that parameter into account. The second is an increase of the run-up wedge thickness y, because of the slope and calculated run-up change.

The method of (Nørgaard et al., 2013) was based on tests with only steep 1:1.5 breakwater slope and is not designed to take varying breakwater slopes into account. It predicts a continuous decrease of the loading due to the decrease of the run-up. Both of the methods do not take account the internal setup and as such give contrasting results with the simulated measurements.

7 Conclusions and Recommendations

This chapter draws the main conclusions from this thesis. In addition, recommendations for future studies are briefly presented.

7.1. Conclusions

This section summarizes the analysis discussed in chapter 6, first by presenting some general conclusions based on the results. Following, the research questions defined in section 4.2 are treated and answered.

General Conclusions

The benefits of using a numerical model instead of physical experiment become apparent as a better insight to details such as the wet length of the crown wall base, the uplift and horizontal pressure distribution shape and the flow through the porous structure can be gained. Shortcomings are the uncertainty of the agreement between the simulated results and reality and the long computation times.

Based on the simulation results, it is found that as the base freeboard is increased, the part of the base that becomes wet and the vertical force are reduced, while the horizontal force increases. The decrease of the vertical force agrees with previous research and is a result of the decreasing wet part of the base, as well as reduced pressure due to the larger distance between the still water level and the crown wall base. The horizontal force increase is a consequence of increasing pressure on the protected part of the vertical wall due to change in the volume of water that overtops the structure and the entrapped air. Especially for the approach of elevating the crown wall, it is mostly related to the increasing unprotected height of the vertical wall. This increase however contradicts an expected decrease, as well as results from previous research, undermining the reliability of the results.

Furthermore, the maximum critical weight (sliding criterion) is also reduced with increasing freeboard and was found to always occur for the largest simulated wave. The continuous reduction of the critical weight even though the horizontal force increases (for large freeboards becomes larger than the vertical force) is explained by the greater influence of the vertical force to it, due to timing.

It is concluded that the empirical methods of (Pedersen, 1996) and (Nørgaard et al., 2013) fail to predict the changes in loading for increasing freeboard.

1. What are the effects of different methods of increasing base freeboard on the crown wall loading and the base wet length?

It can be concluded that increasing the base freeboard by lowering the water level results in lower horizontal and vertical forces, as well as critical weight (sliding criterion) compared to elevating the crown wall element. The vertical forces are lower for two reasons. Firstly, because the first method shows a shorter wet base length which reduces the vertical pressure integration area. Secondly, because of lower vertical pressures for method one, related to different mechanisms of wave-structure interaction and run-up. The difference in horizontal forces is also related to this difference in run-up, but also to the unprotected (by the armour layer) length of the crown wall vertical face, which is greater in the case of the elevated crown wall.

The shapes of uplift pressure distributions for the two methods of freeboard increment were found to follow the same trend, with the first method displaying shorter wet base lengths and lower pressure peaks. These differences grow larger for increasing freeboard.

The proposed calculation method for the wet base length by J. Bekker was found to provide a slight underprediction compared to the simulated results. An overall good agreement was found between his proposed reduction coefficient for calculating the uplift pressures and the simulated results for increasing freeboard by lowering the water level.

2. What is the shape of the uplift pressure distribution during critical condition for varying freeboards and how is it compared to recent proposed distributions shapes?

The assumption that the uplift pressure reaches the rear end of the crown wall appears to be too conservative in situations with a freeboard, as the wet base length significantly decreases.

The profile shape was found to differ from the previous triangular assumption and from recent proposals. For zero base freeboard the profile is S-shaped. As the freeboard increases the shape converts into a reversed polynomial shape, as can be observed in the figures of section 6.3. Also, the peak pressure was found to be located slightly inwards and not at the most seaward end of the base slab, followed by a reverse peak. This is explained by the circular flow created at the corner between the front and bottom faces of the crown wall and the entrapped air.

The simulated cases are not sufficient to propose a generally applicable shape of the uplift pressure distributions, as only one wave condition was used.

3. What is the time difference between the occurrence of maximum horizontal and vertical forces during the interaction with the maximum wave?

It is concluded that a time lag between the maximum horizontal and vertical forces exists. The maximum horizontal force was found to occur 0.16 to 2.74 seconds prior to the maximum vertical force. This can be explained due to the wave propagation sequence and the time that the wave needs to flow through the porous medium. There was no correlation found between the magnitude of the forcing and the length of the time lag. Gentler breakwater slopes resulted in longer time lags. However, this correlation was not strong and more data points are required.

The proposed stability criteria of (CIRIA et al., 2007) where the maximum horizontal and vertical forces occur simultaneously was found to be too conservative, as the time lag reduces the critical weight (sliding criterion). This overestimation was found to usually be between 10 and 15% and in some cases over 20%.

Nonetheless, these findings are a result of only one wave condition and a specific geometry (varying only the base freeboard and breakwater slope) and further research is necessary.

4. What are the effects of breakwater slope variations on the horizontal and vertical forces, critical weight and uplift pressure distribution shape?

It is concluded that gentler breakwater slopes lead to an increase in vertical and horizontal forces, as well as critical weight (sliding criterion). The large increase was found for the vertical forces. This is presumably due to the larger internal set-up occurring for gentler slopes.

It was observed that for all slope cases, the shape of the uplift pressure distribution during critical condition was similar.

The empirical methods of (Pedersen, 1996) and (Nørgaard et al., 2013) produced contrasting results to the simulations as they include limited parameters and do not take into account the internal set-up.

Overall it is concluded that the available empirical methods currently used for designs tend to overestimate the results. All the simulated results from the present study, as well as previous research indicate the presence of time lag in the forcing, which was shown to have significant effect on sliding failure. Also, these methods were all based on tests with zero freeboard and although they do account for the water level and protected crown wall height, they do so for implementing changes in the geometry (as the tests they were based on) and not for a freeboard increment. Hence, for some cases they show no change for increasing freeboard, or a smaller change than the simulated results, which was also showcased in previous research. Only the method of (Bekker, 2017, Bekker et al., 2018) for calculating the uplift pressures in case of increasing freeboard led to predictions with sufficient accuracy, but is only applicable for lowering the water level approach.

It is however advisable to confirm the results with further research as the model used was not validated successfully. In the simulation used as a reference base case with zero freeboard, the vertical forces were significantly higher than the ones predicted from empirical methods or the physical experiment. It is suggested to validate the model with physical experiments enabling trusted quantifiable results.

More importantly, the numerical model predicted an unanticipated increase in the horizontal forcing for increasing freeboard which contradicts previous research. Especially for the approach of lowering the water level, a decrease of the horizontal force was expected due to reduced run-up. This was party explained due to the reduction of overtopping. It is possible that if the freeboard further increases, a threshold where there is no overtopping will be reached and then the horizontal forces reduce. Also, only one wave condition with swell waves breaking on the front wall was simulated. It is likely that waves breaking on the breakwater slope, where only the run-up reaches the crown wall, will showcase a different behaviour. Thus, additional investigation into the applicability of the numerical model is recommended. A first step towards that would be simulating a wider range of freeboards and varying wave conditions to examine if the numerical model results in the expected decrease of horizontal force.

7.2. Recommendations for future research

This section provides recommendations for further research on the stability of a crown wall on top of a rubble mound breakwater. It is suggested to vary more parameters, which were kept constant in the present study.

1. *Wave Conditions*

A spectrum specified by only one wave height, peak period and gamma factor was used in the present study. Future research where the wave height and period are varied is recommended. This becomes increasingly important in the case of time lag investigations and breakwater slope parametrization, as well as for uplift pressure distributions where the data points were limited in the present study.

2. *Breakwater Permeability / Layer Porosity*

It is recommended to conduct tests with parametrization of the layer porosity, the armour type, the number of filter layers and the width of the layers. These parameters were kept constant in the present research, however during the calibration and validation effort where the porosity was varied, significant effects on the loading were observed.

3. *Berm Width (B_a)*

The berm width is one of the important geometric parameters which was kept constant in the present study. Variations of the berm width are expected to have significant effects.

4. *Crown Wall Height*

It is suggested to examine the effects of varying crown wall height which was kept constant in this study. Other than affecting the horizontal force and overtopping, it could also impact the vertical forces by changing the wave-structure interaction.

5. *Method of freeboard increment*

Two methods of increasing the base freeboard (R_b) were investigated in the present study. However, there are other approaches available for future research. One example is increasing R_b by scaling up the size of the whole breakwater structure. Another is elevating the crown wall similarly to method II of the present research but reducing the vertical wall height equally. This will result in a constant total height of the structure but is expected to reduce the horizontal forces.

6. *Time Lag*

Further investigation is also needed on specifying the parameters that influence the time lag between horizontal and vertical forces. Additionally, research is needed on the dynamic response of the crown wall to the time lag in loading.

7. *Wave Breaking*

In the present study only swell waves that always broke on crown wall face were simulated. The literature review suggested that there are different effects when waves break on the crown wall and when they break on the breakwater slope. Hence it is interesting to investigate the effects of waves breaking on the breakwater slope.

8. *NewWave theory*

To acquire the 0.1% forces with high accuracy a large number of waves needs to be simulated, which however results in very long computation times. As the present study concluded that the critical condition occurs during the interaction with the largest simulated wave, one could simulate only one wave group corresponding to the statistically largest (extreme) wave occurring in a very large number of waves and investigate its effects. This can be done by using the NewWave theory proposed by (Tromans et al., 1991) that provides a realistic deterministic description of the largest waves in a random sea and is an alternative to regular wave theories. It can efficiently generate targeted waves at a prescribed time and location, thus greatly reducing the computation time. However, it should be applied for deep water conditions.

Appendices

Appendix A: Simulation Results

Appendix Table 1. Results from base freeboard variation investigation.

Case ID	SWL [m]	Base freeboard R_b [m]	X_c for $W_{c,max}$ [cm]	X_c for $F_{V,max}$ [cm]	$W_{c,max}$ [N/m]	$F_{H,max}$ [N/m]	$F_{V,max}$ [N/m]	$F_{H,Pedersen}$ [N/m]	$F_{V,Pedersen}$ [N/m]	$F_{H,Nørgaard}$ [N/m]	$F_{V,Nørgaard}$ [N/m]	$F_{V,Bekker}$ [N/m]
FB0	0.65	0	30	30	744.16	235.84	546.30	191.88	249.02	171.43	296.82	296.82
M1FB015	0.635	0.015	30	30	641.11	259.12	384.21	158.83	223.91	147.76	272.25	240.84
M1FB030	0.620	0.030	22	25	479.27	263.33	203.55	142.96	206.01	135.80	253.60	148.98
M1FB045	0.605	0.045	14	14	471.77	279.35	150.72	118.67	182.04	118.07	229.98	77.32
M1FB060	0.590	0.060	8	9	380.55	272.65	69.72	98.58	160.35	102.58	208.22	30.68
M1FB075	0.575	0.075	2	5	292.31	217.35	34.94	79.18	137.14	87.98	185.21	0.00
M2FB030	0.650	0.030	23	26	681.99	282.54	325.24	180.28	245.60	138.91	294.01	294.01
M2FB045	0.650	0.045	15	15	580.51	296.23	240.10	150.45	253.57	113.28	300.54	300.54
M2FB060	0.650	0.060	11	12	563.80	312.97	180.31	75.00	252.82	56.56	299.92	299.92
M2FB075	0.650	0.075	9	8	550.80	317.00	140.78	37.61	253.57	28.32	300.54	300.54

Appendix Table 2. Results from breakwater slope variation investigation.

Case ID	Slope	ξ_m [-]	X_c for $W_{c,max}$ [cm]	$F_{H,max}$ [N]	$F_{V,max}$ [N]	$W_{c,max}$ [N]	$F_{H,Pedersen}$ [N]	$F_{V,Pedersen}$ [N]	$F_{H,Nørgaard}$ [N]	$F_{V,Nørgaard}$ [N]
S15	1:1.5	5.44	30	240.13	309.13	576.88	182.17	252.82	227.83	371.52
FB0	1:2	4.10	30	235.84	546.30	744.16	191.88	249.02	171.43	296.82
S125	1:2.5	3.30	30	241.94	655.80	810.00	210.47	244.46	136.53	245.63
S13	1:3	2.76	30	270.66	815.47	953.05	175.98	208.47	112.28	208.96

Appendix B: Analysis Additional Graphs

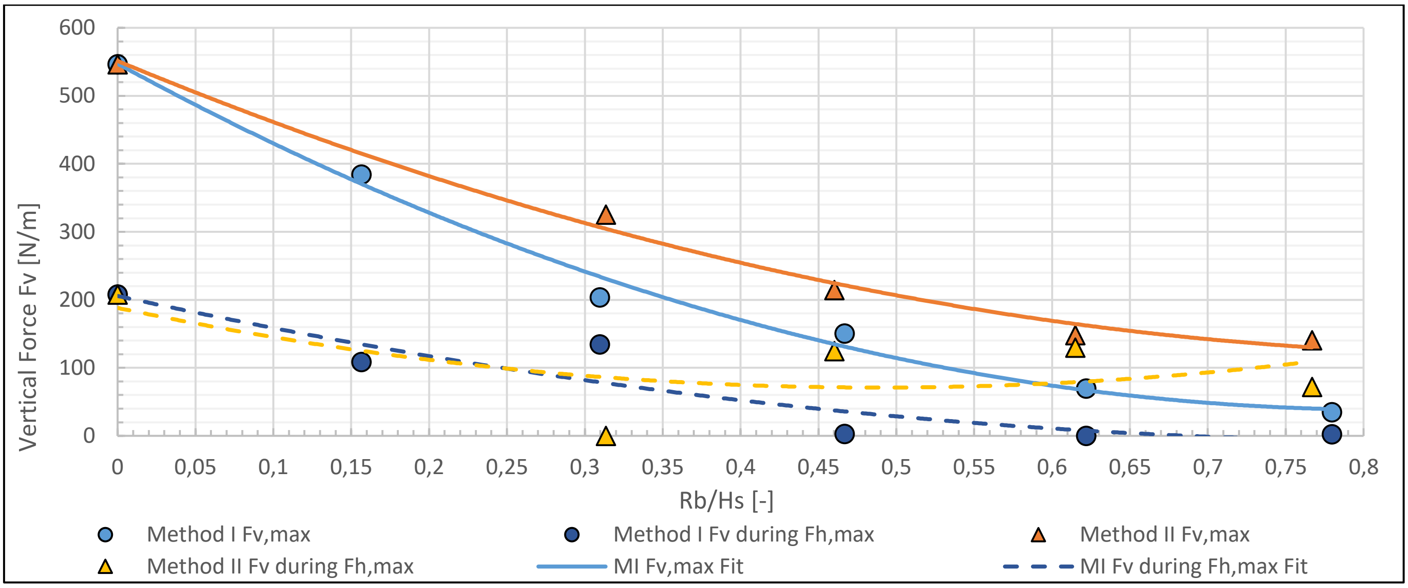

Appendix Figure 1. Vertical force F_V, at the time where its maximum occurs and at the time the maximum horizontal force F_H occurs, for various dimensionless base freeboards R_b/H_s with both methods.

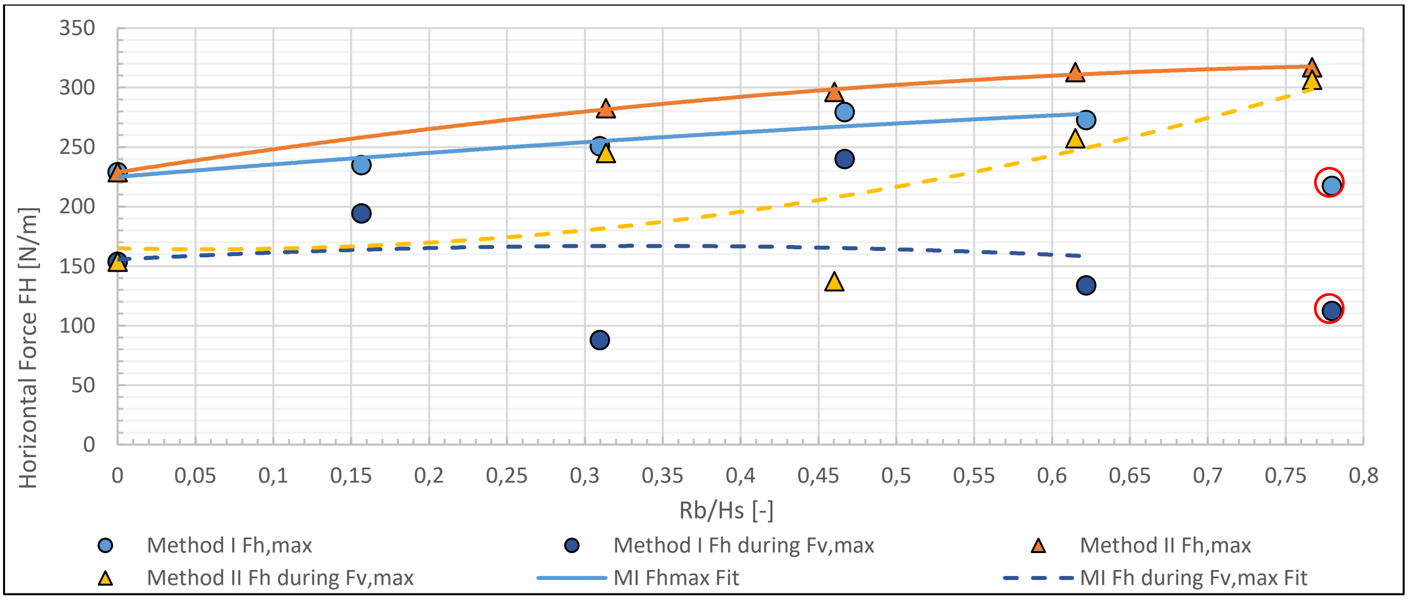

Appendix Figure 2. Horizontal force F_H, at the time where its maximum occurs and at the time the maximum vertical force F_V occurs, for various dimensionless base freeboards R_b/H_s with both methods. Circled data considered outliers.

Bibliography

BATTJES, J. A. & GROENENDIJK, H. W. 2000. Wave height distributions on shallow foreshores. *Coastal Engineering,* 40**,** 161-182.

BEKKER, J. F. 2017. Experimental research into the effect of freeboard on the stability of a crown wall on a rubble mound breakwater.

BEKKER, J. F., HOFLAND, B. & SMITH, G. M. 2018. EXPERIMENTS ON THE EFFECT OF FREEBOARD ON THE STABILITY OF A BREAKWATER CROWN WALL.

BERENGUER, J. & BAONZA, A. 2006. Rubble mound breakwater crown wall design. (in Spanish). *Proceeding of the National Conference of the Port and Coastal Technical Association, Algeciras, Spain*.

BOSBOOM, J. & STIVE, M. J. F. 2015. *Coastal Dynamics I,* Delft University of Technology, Keeghwaterstraat 42, 2628 CA Delft, The Netherlands, Delft Academic Press (VSSD).

BRADBURY, A. P., ALLSOP, N. W. H. & STEPHENS, R. V. 1988. Hydraulic Performance of Breakwater Crown Walls. *Report No SR 146.* HR Wallingford: HR Wallingford.

BRITISH STANDARDS INSTITUTION 1991. BRITISH STANDARD: Maritime structures - Part 7: Guide to the design and construction of breakwaters. *In:* COMMITTEE, C. E. A. B. S. P. & CSB/17, T. C. (eds.) *BS 6349, Maritime Structures.* British Standards Institution: British Standards Institution.

BURCHARTH, H. F., FRIGAARD, P., UZCANGA, J., BERENGUER, J. M., MADRIGAL, B. G. & VILLANUEVA, J. 1995. Design of ciervana breakwater. *Proc. Conf. Coastal Structures and Breakwaters*.

CAMUS, P. B. & FLORES, G. J. 2004a. WAVE FORCES ON CROWN WALLS: EVALUATION OF EXISTING EMPIRICAL FORMULATIONS. *Coastal Engineering,* 4**,** 4087-4099.

CAMUS, P. B. & FLORES, G. J. 2004b. WAVE FORCES ON CROWN WALLS: EVALUATION OF EXISTING EMPIRICAL FORMULATIONS. *Coastal Engineering,* 4**,** 4087-4099.

CHEN, L. F., ZANG, J., HILLIS, A. J., MORGAN, G. C. J. & PLUMMER, A. R. 2014. Numerical investigation of wave–structure interaction using OpenFOAM. *Ocean Engineering,* 88**,** 91-109.

CIRIA, CUR & CETMEF 2007. Rock Manual, The use of rock in hydraulic engineering.

DE WAAL, J. P., TONJES, P. & J., V. D. M. 1996. Overtopping of sea defences. *Coastal Engineering***,** 2216-2229.

DENTALE, F., REALE, F., DI LEO, A. & CARRATELLI, E. P. 2017. A CFD approach to rubble mound breakwater design. *International Journal of Naval Architecture and Ocean Engineering,* 10**,** 644-650.

ELSAFTI, H. & OUMERACI, H. 2017. Analysis and classification of stepwise failure of monolithic breakwaters. *Coastal Engineering,* 121**,** 221-239.

ENGSIG-KARUP, A. P., BINGHAM, H. B. & LINDBERG, O. 2009. An efficient flexible-order model for 3D nonlinear water waves. *Journal of Computational Physics,* 228**,** 2100-2118.

GREENSHIELDS, C. 2018. *OpenFOAM v6 User Guide: 5.3 Mesh generation with blockMesh* [Online]. cfd.direct.com: CFD Direct Ltd. Available: https://cfd.direct/openfoam/user-guide/v6-blockmesh/ [Accessed 01/06/2019 2019].

GUANCHE, R., ITURRIOZ, A. & LOSADA, I. J. 2015. Hybrid modeling of pore pressure damping in rubble mound breakwaters. *Coastal Engineering,* 99**,** 82-95.

GÜNBACK, A. L. 1985. Damage of tripoli harbor north west breakwater. *P. Bruun (Ed.), Design and Cosntruction of Mounds for Breakwaters and Coastal protection, Elsevier***,** 676-695.

GÜNBACK, A. R. & ERGIN, A. 1983. Damage and repair of antalya harbour breakwater. *Proc. Conf. Coastal Structures, Alexandria, Egypt*.

GÜNBACK, A. R. & GÖCKE , T. 1984. Wave screen stability of rubble mound Breakwaters. *Proceedings of the International Symposium on Maritime Structures in the Mediterranean Sea, Athens, Greece***,** 2999-2112.

HAYATDAVOODI, M., SEIFFERT, B. & ERTEKIN, R. C. 2014. Experiments and computations of solitary-wave forces on a coastal-bridge deck. Part II: Deck with girders. *Coastal Engineering,* 88**,** 210-228.

HIGUERA, P., LARA, J. L. & LOSADA, I. J. 2012. Realistic wave generation and active wave absorption for Navier–Stokes models Application to OpenFOAM. *Coastal Engineering,* 71**,** 102-118.

HIGUERA, P., LARA, J. L. & LOSADA, I. J. 2014a. Three-dimensional interaction of waves and porous coastal structures using OpenFOAM®. Part I: Formulation and validation. *Coastal Engineering,* 83**,** 243-258.

HIGUERA, P., LARA, J. L. & LOSADA, I. J. 2014b. Three-dimensional interaction of waves and porous coastal structures using OpenFOAM®. Part II: Application. *Coastal Engineering,* 83**,** 259-270.

HU, Z. Z., GREAVES, D. & RABY, A. 2016. Numerical wave tank study of extreme waves and wave-structure interaction using OpenFoam®. *Ocean Engineering,* 126**,** 329-342.

INGRAM, D. M., GAO, F., CAUSON, D. M., MINGHAM, C. G. & TROCH, P. 2004. NUMERICAL WAVE FLUME SIMULATIONS OF SEAWALL OVERTOPPING. *Coastal Engineering,* 4**,** 4560-4572.

IRIBARREN, R. & NOGALES, C. 1954. Obras marítimas: Oleaje y Diques. *Editorial Dossat Madrid, Spain (in Spanish).*

JACOBSEN, N. G., FUHRMAN, D. R. & FREDSØE, J. 2012. A wave generation toolbox for the open-source CFD library: OpenFoam®. *International Journal for Numerical Methods in Fluids,* 70**,** 1073-1088.

JACOBSEN, N. G., VAN GENT, M. R. A., CAPEL, A. & BORSBOOM, M. 2018. Numerical prediction of integrated wave loads on crest walls on top of rubble mound structures. *Coastal Engineering,* 142**,** 110-124.

JACOBSEN, N. G., VAN GENT, M. R. A. & FREDSØE, J. 2017. Numerical modelling of the erosion and deposition of sand inside a filter layer. *Coastal Engineering,* 120**,** 47-63.

JACOBSEN, N. G., VAN GENT, M. R. A. & WOLTERS, G. 2015. Numerical analysis of the interaction of irregular waves with two dimensional permeable coastal structures. *Coastal Engineering,* 102**,** 13-29.

JENSEN, B., CHRISTENSEN, E. D. & JACOBSEN, N. G. 2014a. SIMULATION OF EXTREME EVENTS OF OBLIQUE WAVE INTERACTION WITH POROUS BREAKWATER STRUCTURES. *Coastal Engineering Proceedings,* 1**,** 1.

JENSEN, B., JACOBSEN, N. G. & CHRISTENSEN, E. D. 2014b. Investigations on the porous media equations and resistance coefficients for coastal structures. *Coastal Engineering,* 84**,** 56-72.

JENSEN, O. J. 1984a. A monograph on rubble mound breakwaters. *Danish Hydraulic Institute (DHI)*.

JENSEN, O. J. 1984b. A Monograph on RubbleMound Breakwaters.

LOSADA, I. J., LARA, J. L. & DEL JESUS, M. 2016. Modeling the Interaction of Water Waves with Porous Coastal Structures. *Journal of Waterway, Port, Coastal, and Ocean Engineering,* 142.

MARITIME, A. 2017. *Completion of breakwaters for Portarlington harbour redevelopment project* [Online]. AW Maritime. Available: https://www.awmaritime.com/completion-of-breakwaters-for-portarlington-harbour-redevelopment-project [Accessed].

MARTIN, F. L. 1999. Experimental study of wave forces on rubble mound breakwater crown walls. *PIANC,* bulletin 102**,** 5-17.

MARTIN, F. L., LOSADA, M. A. & MEDINA, R. 1999. Wave loads on rubble mound breakwater crown walls. *Coastal Engineering,* 37**,** 149--174.

MARTIN, F. L., VIDAL, C., LOSADA, M. A. & MEDINA, R. 1995. Un metodo para el calculo de las acciones del oleaje sobre los espaldones de los diques rompeolas. *Ingenieria del agua,* 3**,** 37-52.

MOLINES, J., HERRERA, M. P. & MEDINA, J. R. 2018. Estimations of wave forces on crown walls based on wave overtopping rates. *Coastal Engineering,* 132**,** 50-62.

MOLINES, J. L. 2016. *Wave overtopping and crown wall stability of cube and Cubipod-armored mound breakwaters.* Universitat Politectina De Valencia.

NEGRO VALDECANTOS, V., LÓPEZ GUTIÉRREZ, J. S. & POLVORINOS FLORS, J. I. 2013. Comparative study of breakwater crown wall – calculation methods. *Proceedings of the Institution of Civil Engineers - Maritime Engineering,* 166**,** 25-41.

NØRGAARD, J. Q. H., ANDERSEN, T. L. & BURCHARTH, H. F. 2013. Wave loads on rubble mound breakwater crown walls in deep and shallow water wave conditions. *Coastal Engineering,* 80**,** 137-147.

PAULSEN, B. T., BREDMOSE, H. & BINGHAM, H. B. 2014. An efficient domain decomposition strategy for wave loads on surface piercing circular cylinders. *Coastal Engineering,* 86**,** 57-76.

PEDERSEN, J. 1996. Wave Forces and Overtopping on Crown Walls of Rubble Mound Breakwaters: an Experimental Study. *Aalborg: Aalborg Universitetsforlag,* No. 12.

RANSLEY, E. J., GREAVES, D., RABY, A., SIMMONDS, D. & HANN, M. 2019. Survivability of wave energy converters using CFD | Elsevier Enhanced Reader.

TROMANS, P. S., ANATURK, A. R. & HAGEMEIJER, P. 1991. A new model for the kinematics of large ocean waves - application as a design wave.

VAN DEN BOS, J. P. & VERHAGEN, H. J. 2018. Breakwater design. Delft University of Technology.

VAN DER MEER, J. W. & STAM, C.-J. M. 1992. Wave Runup on Smooth and Rock Slopes of Coastal Structures. *Journal of Waterway, Port, Coastal, and Ocean Engineering,* 118.

VAN HEEMST, C. 2014. Stability of a Crown Wall on a Breakwater: A refinement of existing design formulae.

WINDT, C., DAVIDSON, J., SCHMITT, P. & RINGWOOD, J. 2019. On the Assessment of Numerical Wave Makers in CFD Simulations. *Journal of Marine Science and Engineering,* 7.

WU, Y., CHEN, Y., BAHUGUNI, A., LU, X. & KUMAR, P. 2015. Study of Wave in deck loading on offshore structures during extreme events. Singapore: Lloyd's Register: Institute if High Performance Computing.

ZELT, J. A. & SKJELBREIA, J. E. 1992. ESTIMATING INCIDENT AND REFLECTED WAVE FIELDS USING AN ARBITRARY NUMBER OF WAVE GAUGES. *Coastal Engineering Proceedings,* 1.

ZHANG, X. 2018. Multi-model method for simulating 2D Surface-Piercing Wave-Structure Interactions. City, University of London Institutional Repository: City, University of London.